Final Report

Report on

Impact of Climate Change on Runoff and Sediment Yield for Puthimari River- A Major Tributary of River Brahmaputra

By

Dr. Swapnali Barman

Scientist 'C'

National Institute of Hydrology

North Eastern Regional Centre

Guwahati-781006

Summary of the Project

Project Title	**:**	**Impact of Climate Change on Runoff and Sediment Yield for Puthimari River- A Major Tributary of River Brahmaputra**

Type of Study	:	Internal
Date of Start	:	November 2018
Date of Completion	:	December 2021
Duration of the project	:	3 year (36 months)

PI and Co-PI of the project	:	PI: Dr. Swapnali Barman, Scientist- C Co-PI: 1. Dr. J.V. Tyagi, Scientist- G 2. Er. Waikhom Rahul Singh, Scientist - B

ACKNOWLEDGEMENT

I would like to express my deep sense of gratitude to **Dr. Jaivir Tyagi**, Director, National Institute of Hydrology, Roorkee for his immense help, kind support and encouragement towards the successful completion of the project.

I wish to record my deep gratitude to **Dr. Sharad Kumar Jain**, former Director, National Institute of Hydrology, Roorkee for his encouragement in taking up this project and his valuable comments.

I also express my sincere thanks to **Dr. A.K. Lohani**, Scientist 'G' and coordinator of North Eastern Regional Centre, Guwahati for his insightful comments in carrying out my work.

My Sincere thanks to **Mr. Waikhom Rahul Singh**, Scientist 'B', North Eastern Regional Centre, Guwahati, National Institute of Hydrology for his immense help in various stages of the project.

I am also thankful to **Dr. S.K. Sharma**, Scientist 'C' and **Mr. G. Tirkey**, Scientist 'B' of North Eastern Regional Centre, Guwahati, National Institute of Hydrology for their suggestions during the project work.

I am grateful to Central Water Commission and Water Resources Department, Govt. of Assam for providing the necessary data required for the study.

Swapnali Barman

ABSTRACT

The river Brahmaputra is one of the most heavily sediment-charged large rivers in the world along with its heavy discharge. Its heavy sediment load at the valley downstream is attributed to the fact that the river gradient is very steep at the upstream which becomes almost flat before entering into the plains of Assam. The Puthimari is a north bank tributaries of Brahmaputra that contributes a large part of sediment to the mainstream. This study aims at determining impact of climate change on both discharge and sediment yield of Puthimari river.

Climate change impact on precipitation and temperature has been analyzed using five different Coupled Model Intercomparison Project 5 (CMIP5) Global Climate Models (GCMs) under both RCP4.5 and RCP8.5. Historical period has been taken from 1970-2005, and the future rainfall and temperature has been analyzed for three different time periods each of 25 years duration viz., 2025-49, 2050-74 and 2075-99. It has been observed that both rainfall and temperature under RCP8.5 will be more compared to that under RCP4.5 and the historical period. There is also a possibility of decrease of rainfall in the monsoon season towards the end of the century. The study indicates that the average maximum, minimum and mean temperature over the basin will rise by 1.13-2.49°C, 1.3-2.64°C and 1.21-2.6°C respectively from 2025-99 compared to the historical period under RCP 4.5. Again, these temperatures will increase by 2.68-3.89°C, 2.85-4.74°C and 2.76-4.53°C under RCP8.5 towards the end of the century. The linear trend analysis of maximum, minimum and mean temperature indicates rising trends in future over the basin.

Land use/land cover (LULC) maps for the basin have been prepared using supervised classification technique and a change detection analyses has been carried out. It has been seen that the rural settlement and water bodies in the basin increased by 42.70% and 30.31% from 1999 to 2019. However, dense vegetation, silted water and cropland decreased by 9.24%, 27.47% and 28.10% during these two decades. The future LULC for 2035, 2065 and 2085 were created using CA Markov model taking 1999 and 2019 maps as the base maps.

To understand the impact of future climate change on discharge of Puthimari, a Soil and Water Assessment Tool (SWAT) model was set up. The model was run for three different conditions; first, change in both climate and LULC were taken into consideration, second, the future discharge was analysed keeping the LULC fixed and taking into consideration the change in climate, and, in the third condition, the climate was kept constant and impact of change in LULC on discharge had been analysed. Also, a coupled SWAT-ANN approach was developed to analyse the impact of climate change on future sediment yield of Puthimari river.

Table of Contents

List of Figures

List of Tables

CHAPTER-1

INTRODUCTION

1.1 General

With an average annual discharge of 19,830 m^3/s, the River Brahmaputra ranks fourth among the large rivers of the world (Goswami 1998). Brahmaputra is a trans-Himalayan River as it rises in south Tibet from the glaciers of Mount Kailash at an elevation of about 5150 m above sea level (a.s.l) at 30°31´N and 82°10´E (Dhar and Nandargi, 2000). The Brahmaputra River basin with an approximate area of 651,334 sq.km., covers four countries: China (50.5%), India (33.6%), Bangladesh (8.1%) and Bhutan (7.8%) (IUCN, 2014). Its basin in India is shared by Arunachal Pradesh (41.88%), Assam (36.33%), Nagaland (5.57%), Meghalaya (6.10%), Sikkim (3.75%) and West Bengal (6.47%) (Singh et al. 2004). The basin lies between 23°N to 32°N latitude and 82°E to 97°5´E longitude. The Brahmaputra basin is highly influenced by monsoon rainfall. Most part of the runoff of the Brahmaputra is because of the heavy rainfall of 510-640cm in the Abor and Mishmi hills in Arunachal Pradesh and 250-510cm in the Brahmaputra plains (Murthy, 1981).

Along with discharge, the Brahmaputra is also one of the most heavily sediment-charged large rivers in the world. It flows through a seismically active region, which has the effect of causing it to carry one of the highest sediment loads in the world. The river carries an average annual suspended load of 400 million metric tonnes at Pandu at an average daily rate of nearly two million metric tonnes in the rainy season (May to October) accounting for more than 95% of the annual suspended load.

During its course, the river Brahmaputra receives 22 major tributaries in Tibet, 33 in India and 3 in Bangladesh. The northern and southern tributaries differ considerably in their hydro-geomorphological characteristics owing to different geological, physiographic and climatic conditions. The north bank tributaries generally flow in shallow braided channels, have steep slopes, carry a heavy silt charge and are flashy in character. South bank tributaries on the other hand have a flatter gradient, deep meandering channels with bed and bank materials composed of alluvial soils and are marked by relatively low sediment load. Hence, it is important to study the tributaries which in turn affect the total sediment yield and discharge of the Brahmaputra River. For the present study, Puthimari river, a north bank tributary of Brahmaputra has been chosen to study its impact on discharge and sediment yield to the Brahmaputra. River Puthimari

originates in the Tethyan Himalaya, a part of eastern Himalaya in Bhutan at an altitude of 3750 m (27°26´55´´N latitudes and 91°55´34´´ E lngitudes) and flows north to south through the Nalbari, Kamrup, Darrang, Baksa and Odalguri districts of Assam and debouches into the Brahmaputra river near Barsulia village, 7.6 km downstream from Hajo in Assam, India (26°14´52´´N latitudes and 91°26´55´´ E longitudes). The Puthimari basin falls between 26°10´50´´N to 27°20´27´´N and 91°25´57´´E to 91°56´12´´E. The basin is extended in north-south direction from the high Tethiyan Himalayas to the flat plains of the River Brahmaputra in the state of Assam, India. As this basin is highly influenced by the monsoon rainfall, the climate change that results in variation in intensity of the monsoon, will affect both high and low flows leading to increased flooding and variability of available water both in space and time in the basin. Not only the precipitation, the change in LULC that has been taken place in the Puthimari basin also influences the change in runoff and sediment yield of the river. Fohrer et al. (2001) mentioned that surface runoff is highly affected by LULC changes over a watershed. Researchers have investigated the relationship between climate, land use and hydrological processes and their studies showed that stream flow generation capacity is also dependent on vegetation type (Dwarakish and Ganasri, 2015). The rapid growth in population has led to change in land use in terms of deforestation for improving the agricultural production. This leads to decrease in infiltration rate and increase in surface runoff. However, Ozturk et al. (2013) reported that influence of climate variability is more significant on surface hydrology than the land use change.

Global climate change has substantially increased the atmospheric concentration of carbon dioxide and other trace gases over the last century. It is expected that the concentration of carbon dioxide will be double by the middle or latter part of the next century (Kamga, 2001). It is obvious that, global warming caused by increased atmospheric concentration of carbon dioxide and other trace gases will alter the radiation balance of the atmosphere. This in turn will cause increases in temperature and changes in precipitation pattern and other climatic variables (Changchun et al. 2008). Higher greenhouse gas concentrations have trapped more thermal radiation and consequently warmed the planet (IPCC, 2007). In its Fifth Assessment Report, the Intergovernmental Panel on Climate Change reported that averaged combined land and sea surface temperature warmed between 0.65°C and 1.06°C from 1880 to 2012 (IPCC, 2013). Climate change is altering the earth's hydrologic cycle to various degree. Climate change affects hydrology mainly through changes in precipitation, temperature and evaporation and it subsequently influences the temporal-spatial distribution of runoff and sediment as well as pattern of runoff and sediment transport. As the Brahmaputra Basin is

highly influenced by the monsoon rainfall, the climate change that results in variation in intensity of the monsoon, will affect both high and low flows leading to increased flooding and variability of available water both in space and time (Postel et al. 1996) in the basin. Climate models are the primary tool to evaluate the projected future response of the atmosphere-land-ocean system to changing atmospheric composition (MacCracken et al. 2003). To study the impact of climate change at regional scale, the General Circulation Models (GCMs) are the most adapted tool which describes the atmospheric process by mathematical equations. The Coupled Model Inter-Comparison Phase 5 (CMIP 5) supplies daily data from more than 40 GCMs with different spatial resolutions from around the world (Rupp et al. 2013; Rehman et al. 2018). The data from these models are forced by the current projections of atmospheric conditions supplied by the fifth assessment report (AR5) of Intergovernmental Panel on Climate Change (IPCC) (Guilbert 2016). The advantage of CMIP5 over CMIP3 is that, these models have higher spatial resolutions and have better simulation ability of some climate features (Knutti and Sedlavcek 2012). The climate simulations of CMIP5 models in AR5 have been done according to representative concentration pathways (RCPs; Moss et al. 2010) that include a set of greenhouse gas emission, aerosols and land use change scenarios.

There are various hydrologic models ranging from lumped conceptual model to physically based distributed models which are in use worldwide, for flow forecasting of rivers based on meteorological data and catchment characteristics (Lorup et al. 1998). The physically based models take into consideration the physical characteristics of a watershed whereas the semi-distributed and fully-distributed models are capable of representing the spatial heterogeneity of the watershed (Dwarakish and Ganasri 2015). Integration of land use models with the rainfall-runoff models provides quantitative information about the land use changes on hydrological output. Also, different land uses in different sub-watersheds yield different hydrological output (Lin et al. 2009). Hydrological models provide an alternative approach for better understanding of sediment transport and deposition processes by overland flow and allow reasonable prediction and forecasting. Hence, sediment yield modeling has been increasingly used to evaluate the impacts of variables controlling sediment dynamics at the basin scale (Chakrapani, 2005). Numerous studies around the world have employed SWAT for different purposes. SWAT model provides satisfactory statistics on stream flow and sediment yield across a range of scales. The model requires several input data to simulate catchment hydrologic processes, and these include a digital elevation model (DEM), LULC data, soil types, and different daily weather data, including details of precipitation, maximum and minimum air temperatures, solar radiation, wind speed, and relative humidity. SWAT has

received international acceptance as a robust interdisciplinary catchment-scale modelling tool. However, its application in arid and semi-arid areas is still challenging due to the unavailability of flow data for model calibration and validation procedures (Mengistu et al. 2019)

1.2 Objectives of the Study

Most studies focused on the impact of precipitation on runoff and have rarely investigated the impact of precipitation on sediment yield. In fact, high sediment content is an important and unique characteristic of the tributaries of Brahmaputra. It is thus imperative to consider sediment when studying the water resources problems of these rivers.

Keeping these facts in mind. The present study has been proposed with the following objectives:

1. Future Rainfall and temperature trend analysis over Puthimari River Basin using different CMIP5 Models
2. Land use/land cover change detection study of Puthimari River Basins from 1999 to 2019 using Remote Sensing and GIS techniques.
3. Prediction of future LULC changes using CA-Markov Model.
4. To analyze the impact of climate change on future runoff using Soil and Water Assessment Tool (SWAT).
5. To analyze impact of climate change on future sediment yield of Puthimari River using a SWAT-ANN based hybrid approach.

1.3 Research Questions

1. How climate change affects future precipitation and temperature over the Puthimari basin?
2. How the land use/land cover over the basin changes in future?
3. How climate change and change in land use/land cover impact future discharge for the Puthimari river?
4. How climate change impacts future sediment yield for the Puthimari watershed?

CHAPTER-2

REVIEW OF LITERATURE

2.1 Climate change and its significance

Accelerated change in climate is expected to have major impact on the future sustainability of the earth (McMullen and Jabbour 2009). The main driving force is the increase in earth's temperature as a result of human activities which included greenhouse gas emissions. According to Intergovernmental Panel on Climate Change (IPCC), there is a possibility of temperature increase of 1.1ºC to 6.4ºC by 2100, due to which storms and floods will get affected and lead to rise in sea level because of the thermal expansion of the oceans and the melting of ice sheets and glaciers (IPCC, 2007a).

Global climate models (GCMs) have been valuable tools for assessing climate change and produce climate projections (Ramesh and Goswami, 2014). The Coupled Model Intercomparison Project 5 (CMIP5) has provided numerous GCMs, which have more complicated mechanisms than before, and incorporate carbon cycle models and a dynamic vegetation module (Taylor et al. 2012). Many studies have found that the CMIP5 models perform better than the CMIP3 ones, have a smaller bias, and an overall improved capability of simulating climate change (Sun et al. 2015; Meher et al. 2017). Many studies have been conducted to assess the performance of precipitation simulations of the CMIP5 GCMs using various methods in different regions (Kumar et al. 2013; Kadel et al. 2018; Ruan et al. 2018). Fu et al. (2013) evaluated the performance of 25 GCMs using a score-based method in southeastern Australia. Das et al. (2018) adopted a Multiple Imputation Chained Equation technique to cope with the limited data availability and poor data quality in the Western Himalayan Region. Li et al. (2019) used the technique for order preference by similarity to ideal solution model to assess 31 GCMs in mainland Southeast Asia. In the fifth assessment report (AR5) of Intergovernmental Panel on Climate Change (IPCC), climate simulations have done for 21st century according to representative concentration pathways (RCPs) based on four greenhouse gas concentration trajectories (Demirel and Moradkhani, 2016). RCPs provide a quantitative depiction of concentrations of atmospheric pollutants over time ensuing from human activities along with their radiative forcing in 2100. There are four pathways to a rigorous mitigation scenario (RCP2.6), two intermediate (RCP 4.5 and RCP 6.0) and one with

very high GHG emissions (RCP8.5). The numbers with each RCP indicate the forcing for each RCP (Wayne, 2013).

2.2 Climate change and temperature

Climate, in a broad sense, is the statistical mean and variability of relevant variables such as precipitation, temperature, humidity, atmospheric pressure, albedo that constitute weather and climate over a period of time ranging from months to thousands or millions of years (IPCC, 2008). In the present century, there has been a lot of discussions going on between world leaders and climate experts about the global climate change (Toprak et al. 2013). Various scientific assessment in the past demonstrated that earth's climate has been changed on both global and regional scales since the start of industrial era. Accelerated change in climate is expected to have major impact on the future sustainability of the earth (Stern 2006; McMullen and Jabbour 2009). The change in the global environment due to climate change may lead to environmental disasters (Zarandi et al. 2017). Increase in anthropogenic emissions of gases (e.g., carbon dioxide, methane) into the atmosphere, and an enhanced greenhouse effect are the major driving forces behind the accelerated global warming that has taken place over the last century (IPCC, 2007a,b). Global warming will alter the radiation balance of the atmosphere. This in turn will cause increase in average temperature of the earth and changes in precipitation pattern and other climatic variables (Changchun et al. 2008). Higher greenhouse gas concentrations have trapped more thermal radiation and consequently warmed the planet (IPCC 2007). Climate change projection study is important to assess its impact and to take proper management strategies (Rehman et al. 2018). In its Fifth Assessment Report, the Intergovernmental Panel on Climate Change reported that average combined land and sea surface temperature warmed between 0.65°C and 1.06°C from 1880 to 2012 (IPCC 2013). IPCC (2013) also reported that during the period from 1951 to 2010, the number of warm days and nights has increased, and number of cold days and nights has decreased across the globe. The increasing trend of temperature will accelerate more towards the end of 21st century and the temperature may increase by 5.5^{o}C (Mahmood and Babel 2014; Stocker et al. 2013). Steffen et al. (2018) indicated an increase in global average temperature by 4-5^{o}C compared to the pre-industrial era that will lead to rise in the sea level by 10-60m.

In context of India, the vast population of the country depends on sectors such as agriculture, forestry, animal husbandry and fisheries for their livelihood. The production of these sectors is very sensitive to the change in climate which may come in the form of fall in precipitation and rise in temperature. Sathaye et al. (2006) mentioned a report from IPCC which projects the

increase of global mean temperature between 1.4^{o}C and 5.8^{o}C by 2100. The study stated that the impact of this unprecedented increase in global temperature would be severe in the tropical areas including India. Kumar et al. (1994) found the overall maximum temperature over India increased at the rate of 0.6^{o}C per 100 years and attributed this to be the sole reason for increasing the mean temperatures over India during 1901 to 1987. Kothawale and Kumar (2005) analysed the surface temperature trends over India during the period 1901 to 2003 and found that the mean annual temperature has increased at the rate of 0.05^{o}C per decade. Similarly, Pant and Kumar (1997) also found a significant warming trend of 0.57^{o}C per 100 years over India. During the years from 1891 to 2009, 23 numbers of large-scale droughts have occurred in India where the frequency of droughts is increasing, posing a grave threat to agriculture and food security (Kumar and Gautam, 2014). The seasonal and annual temperature over India has increased significantly during the period 1901-2007 with increase in mean temperature by 0.003^{o}C /year (Mondal et al. 2015). The Centre for Climate Change Research-Indian Institute of Tropical Meteorology (2017) reported significant warming trends in northwest, eastern and western Himalayan region, and relatively less significant warming trends in the southern part of the country during the period 1981-2017.

North-eastern region of India is one of the most vulnerable parts to climate change that impacts the hydrology and water resources of the region. Using the India Meteorological Department (IMD) gridded data, Dash et al. (2012) analysed the annual mean temperature, and annual minimum and maximum temperature over northeast India. They showed that during the period 1971 to 2005, the annual mean temperature possessed a significant increasing trend. Annual minimum temperature significantly increased at the rate of 0.04^{o}C/year while the annual maximum temperature does not show significant trend. Dutta (2014) showed that the average temperature over North-eastern part of India will be 2^{o}C higher in 2050 as compared to the temperature records from 1950-2000. Jain et al. (2013) found that maximum, minimum and mean temperature over northeast India during the period 1901 to 2003 has increased in all the seasons viz. monsoon, pre-monsoon, post-monsoon and winter. There has been an increase in maximum temperature in northeast India over a time span of 107 years (Mondal et al. 2015).

2.3 Impact of climate change on precipitation, runoff and sediment yield

One of the major impacts of climate change is variation in rainfall pattern which directly or indirectly affects the regional water sources which are rain fed/recharged. The precipitation is expected to increase under global warming at high latitudes and in the vicinity of the equator, but decreases in the subtropics (Watterson and Whetton 2011). Increase in precipitation can

be attributed to the high amounts of atmospheric moisture accumulated as a result of warming climate (Shiu et al. 2012). Dore (2005) indicated that the wet areas have become wetter and dry and arid areas have become drier. Donat et al. (2016) identified a significant increase in extreme daily precipitation for the past six decades although the changes in total precipitation were inconsistent. Globally the number of extreme rainfall events have significantly increased over the last three decades (Lehmann et al. 2015). In the context of India's precipitation pattern, Mohapatra et al. (2018) observed a weak decreasing trend in ISMR, based on linear trend analysis of 113 years of ISMR data. They observed decreasing trends in ISMR over northeast India and increasing trends in northwest India over the last two decades. Ghosh et al. (2016) observed significantly decreasing trends across south, northeast and northwest India during 1951-2004. Mukherjee et al. (2018) observed a substantial increase in the frequency of extreme precipitation over southern and central India post 1982 and Guhathakarta et al. (2015) observed a similar trend over the monsoon core region of India during 1951-2000.

As atmosphere warms up, one of the most possible alarming consequences of climate warming would be the change in streamflows (Jones 2011). Climate change has the potential to significantly alter the river flow. With doubling of the CO_2 concentration, global mean runoff may increase by 5% (Betts et al. 2007). Future climate change will increase water stress in some parts of the world and increase river discharge in others (Arnell 2004). Simultaneous increase in precipitation and evaporation may produce no change in the runoff even though both these parameters change (Stonevicius et al. 2016). Again, combination of the increase in temperature and variation in precipitation will result in a significant change of the runoff (Mousavi et al. 2018). Both climate and land use change are important drivers of changes in watershed hydrology and hence, distinguishing effects of land use changes and concurrent climate variability poses a particular challenge (Tollan 2002). Ozturk et al. (2013) stated that the influence of climatic variability is more significant on surface hydrology than the land use change. Legesse et al. (2003) assessed the sensitivity of water resources to the change in climate and land use in a semi-arid to sub-humid basin using a physically based semi-distributed model. Their climate scenario study revealed that the hydrologic system was more reactive to an increase in rainfall than to a decrease in rainfall. Li et al. (2009) and Ozturk et al. (2013) stated that the influence of climatic variability is more significant on surface hydrology than the land use change.

Sediment yield is defined as the total sediment outflow from a watershed or drainage basin. It includes both bed material and suspended materials. Sediment yield is a function of the amount of absolute or gross erosion in the watershed and the efficiency of the stream system to transport

eroded materials out of the watershed (Glymph et al. 1954). The sediment load of a river is sensitive to both climate change and a wide range of human activities within its drainage basin. These factors could influence sediment mobilization and transfer through actions like clearing of land, agricultural development, mineral extraction, urbanization and infrastructure development, dam and reservoir construction, and soil conservation and sediment control programs (Walling 2008). While researchers have highlighted the significant potential of climate change in increasing global soil erosion rates and possibly, consequent, increasing the amount of suspended sediment flux in rivers, the actual response of suspended sediment flux in a particular place varies because it is also highly affected by the physical characteristics of the catchment and human activities in it (Zhang and Nearing 2005).

2.4 Rainfall-runoff and sediment yield modelling

Modelling of rainfall-runoff process is very complicated due to spatial and temporal variability of topographical characteristics, rainfall pattern and the number of parameters to be derived during the calibration (Nandakumar and Mein, 1997).

Hydrological models can also be classified as conceptual, empirical and physical models. Empirical models establish the relationship between rainfall and runoff based on the hydro-mateorological data and contain no physical transformation function to relate input to output (Sarkar and Kumar 2012). The main constraint of the empirical models is the non-consideration of physical processes such as sub-surface flow, surface runoff and infiltration in the catchment. Conceptual models are simplifications of the complex process of runoff generation in a catchment. Viviroli et al. (2009) introduced precipitation-runoff-evapotranspiration HRU model, a semi-distributed hydrological model that implements a conceptual process-oriented approach. Valent et al. (2012) used lumped conceptual model, Hron rainfall-runoff model to predict runoff. The results suggested that the model have uncertainties with respect to conceptualization of complex runoff generation process. The physically based distributed models on the other hand are able to represent the spatial variability of land surface characteristics such as topographic elevation, slope, aspect, vegetation, soil and climatic parameters like precipitation, temperature and evapotranspiration (Akbari and Singh 2012).
Artificial neural network (ANN) is a soft computing technique composed of densely interconnected processing nodes which has the ability to extract and store the information from the few patterns (data) in training through learning. The ANN model can identify the non-linear relationship between runoff and rainfall, even though it cannot represent the physical process of the catchment. Gaume and Gosset (2003) compared feed forward ANN model with

a linear model and a conceptual model. They found that the conceptual model outperformed the linear and the ANN model. Maria et al. (2004) compared ANN and Box and Jenkins techniques and found that ANN is better than the Box and Jenkins model. Only a few studies (Tayfur 2002; Cigizoglu 2004) focused on ANN-event based sediment yield modelling and sediment concentration. Sediment yield modeling has been increasingly used to evaluate the impacts of variables controlling sediment dynamics at the basin scale (Chakrapani 2005). The Soil and Water Assessment Tool (SWAT) model was developed by US Department of Agriculture- Agriculture Research Service (USDA-ARS). It is a conceptual model that functions on a continuous time step. Numerous studies around the world have employed SWAT for different purposes. Most published research has concluded that the SWAT model can satisfactorily estimate sediment yield (e.g. Cheng et al.2007; Hao et al.2004; Yesuf et al. 2015), although some studies have resulted in unsatisfactory results (Srivastava et al. 2006; Uzeika, et al. 2012).

2.5 Land use/land cover change detection study

Land use/land cover assessment is an important parameter for meaningful planning of land resource management (Rawat and Kumar 2015). The rapid development of satellite remote sensing techniques helps in preparation of accurate land use/land cover maps which in turn helps in monitoring changes at regular intervals of time.

Pandy and Nathawat (2006) carried out a study on land use/land cover mapping of Panchkula, Ambala and Yamunanger districs, Hangana state in India. They observed that the development of land use and land cover in these districts is mainly due to heterogeneous climate and physiographic conditions. Bhagawat (2011) presented the change analysis based on the statistics extracted from four land use/land cover maps of the Kathmandu Metropolitan using GIS. According to him, land use statistics and transition matrices are important information to analyze the changes of land use. Landsat-TM images represent valuable and continuous records of the earth's surface and is also a wealth of information for identifying and monitoring changes in manmade and physical environments (Chander et al. 2009). To map and monitor land cover changes in the seven-country Twin Cities of Metropolitan Area of Minnesota, Yuan et al. (2005) developed a methodology using multi-temporal Landsat TM data. A post-classification method with maximum likelihood classifier algorithm was adopted by Adepoju et al. (2006) to examine the land use/land cover changes that have taken place in Lagos for the last two decades due to rapid urbanization. The freely available MODIS data can also be used efficiently to study land use/land cover with greater thematic, spatial and temporal detail. Giri and Jenkins

(2005) prepared land cover database of Greater Mesoamerica using MODIS 500m resolution satellite data. Usman et al. (2015) used MODIS data of 250m spatial resolution for preparation of land use maps of the Lower Chenab canal irrigated region of Pakistan from 2005 to 2012. The land use/land cover change detection indicated that wheat and rice have less volatility of change in comparison with both rabi and kharif fodders. They also concluded that MODIS products are quite useful to discriminate different land use/land cover classes.

Like in other parts of the world, in India also, various scholars have done researches on land use/land cover analysis. Sarma and Kushwaha (2005) worked on the impact of coal mining on land use/land cover in Jaintia hills districtof Meghalaya, India using Landsat data of 1975, 1987, 1999 and 2005. Visual interpretation technique has been used to prepare the land use/land cover maps. Kuldeep and Kamlesh (2011) studied the land use/land cover change detection in the Dehradun valley, India between 2000 and 2009 using Landsat (ETM+, TM, MSS), LISSIII, SRTM and digital SOI topographic maps. Mehta et al. (2012) presented an integrated approach of remote sensing and GIS for land use/land cover study of arid environment of Kutch region in Gujarat from 1999 to 2009. Sharma et al. (2012) introduced land consumption rate (LCR) and land absorption coefficient (LAC) for quantitative assessment of changes in Bhagalpur city of Bihar, India between the years 1976 and 2008.

CHAPTER-3
MATERIAL AND METHODOLOGY

3.1 Material used in the study

Remote Sensing Data:

LANDSAT data: Cloud free LANDSAT data of 30m resolution have been used in the study for the year 1999, 2009 and 2019.

Digital Elevation Model (DEM): Advanced Spaceborne Thermal Emission and Reflection Radiometer Global Digital Elevation Model (ASTER GDEM) of 30m resolution has been used in the study.

Hydro-meteorological data:

Precipitation data: Downscaled rainfall data available at 25km x 25km spatial resolution from five different CMIP5 models for RCP4.5 and RCP8.5 have been used in this study. Table 3.1 gives the spatial resolutions of the selected CMIP5 models:

Table 3.1: Resolutions of the selected CMIP5 models

Sl. No.	Model Name	Grid	
		Latitude	Longitude
1.	CCSM4	0.9424	1.25
2.	INMCM4	1.5	2
3.	MIROC5	1.4008	1.40625
4.	MPI-ESM-MR	1.8653	1.875
5.	MRI-CGCM3	1.12148	1.125

IMD daily rainfall data available at 0.25°x0.25 ° spatial resolution from 1996-2012 have been used for SWAT model.

Temperature data: Downscaled daily maximum and minimum temperature data available at 25km x 25km spatial resolution from five CMIP5 models (Table 3.1) for RCP4.5 and RCP8.5 have been used in this study.

Also, IMD 1° daily max and min temperature from 1996-2012 have been used in SWAT model.

Wind speed, solar radiation and relative humidity are simulated in ArcSWAT using weather generator for the Indian region.

Discharge and Sediment data: Daily observed discharge and sediment data from 1999 to 2010 have been collected from Water Resources Department, Govt. of Assam.

Soil Map: NBSSLUP soil map and NRCS soil map have been used to prepare the soil map of the study area (Fig.3.1).

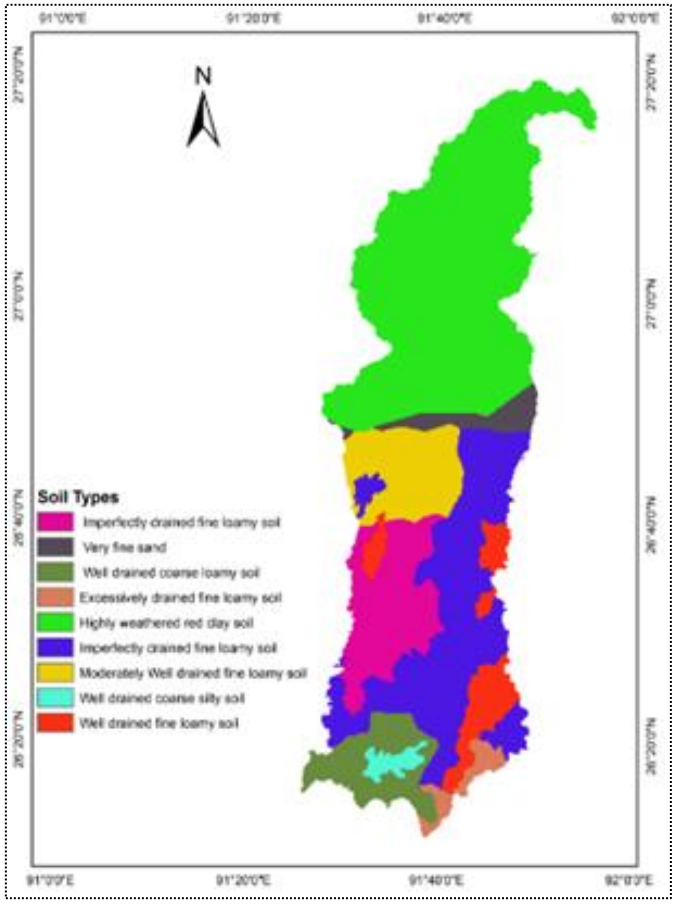

Fig.3.1: Soil Map of Puthimari Basin

3.2 Methodology

The flowchart for the methodology is shown in Fig. 3.2.

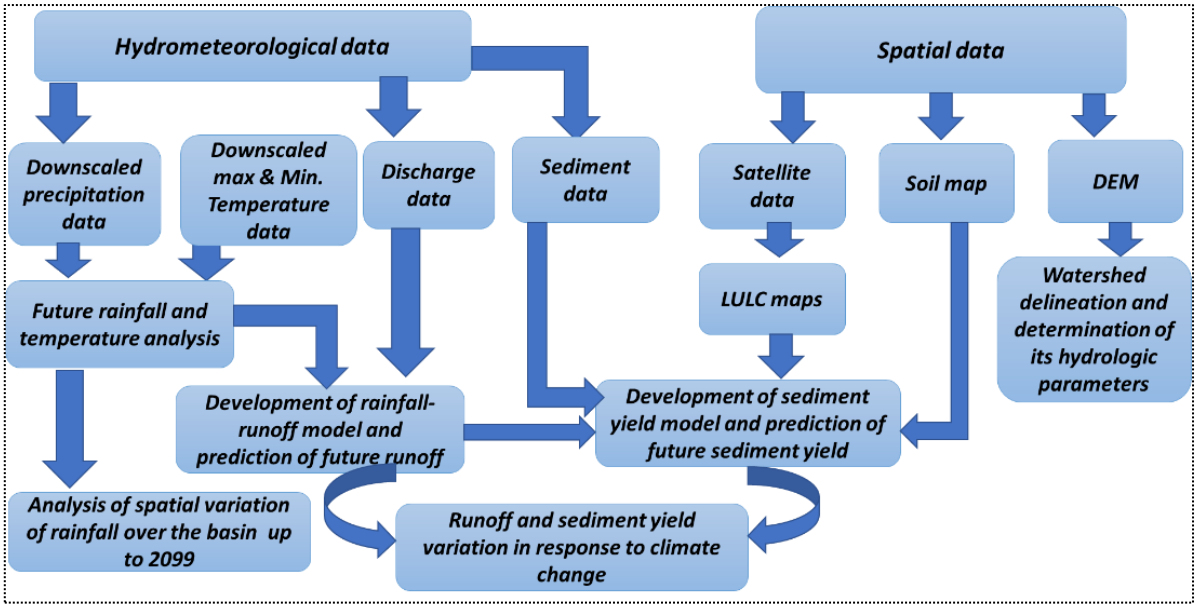

Fig. 3.2: Flowchart showing the methodology

3.2.1 Watershed delineation

ASTER GDEM of 30m resolution has been used to delineate the watershed in. Six different tiles were downloaded from Earth Explorer site. These tiles were then mosaiced and projected to UTM. The Puthimari basin falls in UTM Zone 46. The various maps generated in the process are flow direction map, flow accumulation map, stream network map and finally the delineated watershed.

3.2.2 Future Rainfall Trend Analysis over Puthimari River Basin

Bias corrected statistically downscaled daily rainfall data available at 25km x 25km spatial resolution have been downloaded from NASA Centre for Climate Simulation covering the catchment. After processing the data available at netCDF format, monthly variation of rainfall has been analyzed from 1970 to 2099 under RCP4.5 and RCP8.5. The analysis has been carried out for both historical and future time periods. The historical period has been considered from 1970 to 2005. The future period up to 2099 have been divided into three more time periods each of 25 years duration viz., 2025-49, 2050-74 and 2075-99. Maximum rainfall in each time period has been determined and accordingly percent change of maximum rainfall from one time period to another has been analyzed. For more detailed analysis, one complete year has been divided into four different seasons, Winter season comprising of January and February; summer season comprising of March, April, May; monsoon season from June to September,

and finally post-monsoon season comprising of October, November and December. The percent change in seasonal rainfall between two consecutive time periods have then been analyzed.

Mann-Kendall (M-K) (Mann 1945; Kendall 1975) non-parametric test which is used to identify trends in time series data have been carried out to understand the trends of monthly as well as seasonal rainfall over the basin from 1970 to 2099. The Z statistics have been analyzed to identify the nature of the trends.

The MK statistics 'S' is defined as,

$$S = \sum_{i=1}^{N-1} \sum_{j=i+1}^{N} \mathrm{sgn}(x_j - x_i) \quad (1)$$

Where, N is the number of data points. sgn θ is determined as

$$sgn(x_j - x_i) = \begin{cases} 1 \ if \ x_j - x_i > 0 \\ 0 \ if \ x_j - x_i = 1 \\ -1 \ if \ x_j - x_i < 1 \end{cases} \quad (2)$$

For $N \geq 10$, S is approximately normally distributed and the mean and the variance are given as,

$$E(S) = 0 \quad (3)$$

$$Var(S) = \frac{N(N-1)(2N+5) - \sum_{k=1}^{n} t_k(t_k-1)(2t_k+5)}{18} \quad (4)$$

Where, n is the number of tied groups, and t_k is the number of data points in the k^{th} tied group.

The standard Z statistics is then calculated as,

$$Z = \begin{cases} \frac{S-1}{\sqrt{Var(S)}} & if \ S > 0 \\ 0 & if \ S = 0 \\ \frac{S+1}{\sqrt{Var(S)}} & if \ S < 0 \end{cases} \quad (5)$$

The Z value is used to determine if a trend is statistically significant or not. A positive value of Z indicates an upward trend while a negative value of Z indicates a downward trend. If Z value lies between ±1.96, the null hypothesis of having no trend in the series cannot be rejected at 95% level of confidence.

Finally, a comparison has been made to check the difference in seasonal rainfall between RCP4.5 and RCP8.5 in same time period.

3.2.3 Future Temperature Analysis over Puthimari River Basin

Bias corrected statistically downscaled minimum and maximum daily surface air temperature for nine different CMIP5 climate models available at 25 km x 25 km spatial resolutions have been downloaded from the web portal of NASA Centre for Climate Simulation. The study has been conducted under RCP4.5 and RCP8.5. Change in temperature over Puthimari basin has been carried out in five different time periods as done for rainfall analysis. Both the maximum and minimum temperature variations have been observed for each month. The change in average maximum and minimum temperature from one time period to another as well as the years of occurrence of highest maximum and highest minimum temperature in each time period has been determined. Moreover, the variations in monthly mean temperature during different time periods have been analyzed for each model from which the warmest year having the highest mean temperature in each period has been found out. All these analyses were performed for RCP 4.5 and RCP 8.5 separately. A linear trend analysis of future projected maximum, minimum and mean temperature for the selected models has been performed to check the effect of the two selected scenarios on future temperature over the basin.

3.2.4 Land use/land cover (LULC) change detection study of the Puthimari river basin using remote sensing and GIS technique

Remote sensing and GIS techniques have been employed to delineate the watershed and to prepare the LULC maps of the study area. The watershed has been delineated using ASTER GDEM of 30m resolution in ArcGIS version 10.2.2 software. LANDSAT5-TM data of 30m resolution have been used for the years 1999 and 2009. For 2019, Landsat-8 data of 30m resolution has been considered. The LANDSAT data sets were imported in ERDAS Imagine version 2013 remote sensing software where the false color composite (FCC) images have been created. The LULC classification for different years has been carried out using supervised classification method with the maximum likelihood classifier algorithm. Different polygons have been digitized in the image for different LULC types to collect spectral signatures from the training sites which then are used for classification of all other pixels in an image. Five different LULC types have been considered in the study area viz., dense vegetation, surface water bodies, silted water, cropland and rural settlement. To perform the LULC change detection, a post-classification detection method has been taken into consideration. Classified

images of different years were compared in order to determine quantitative aspects of the changes for the periods from 1999 to 2019. In this regard, percent of total area covered by different classes have been compared in each year. The increase and decrease in area for each category of LULC were then determined and compiled for three different periods, 1999-2009, 2009-2019 and 1999-2019.

3.2.4.1 Future prediction of land use/land cover using CA Markov Model

The CA Markov model has been applied to determine the future LULC maps of 2035, 2065 and 2085. The following expression represents the CA model (Subedi et al. 2013; Ghosh et al. 2017; Tadese et al. 2021):

$$S(t, t+1) = f(S(t), N)$$

S(t+1) is the status of the system at time (t, t+1), N is the cellular field, and f is the transformation rule of cellular state in local space.

The equation for Markov chain model is expressed as,

$$S(t, t+1) = P_{ij} \times S(t)$$

Where, S(t) and S(t+1) are the LULC status of the system at time t and (t+1) respectively. P is the transition probability and P_{ij} is the transition probability matrix in a state i.e. the probability of changing from the state i to another state j which is determined as,

$$Pij = \begin{bmatrix} P_{11} & P_{12} & \cdots & P_{1n} \\ P_{21} & P_{22} & \cdots & P_{2n} \\ \cdots & \cdots & \cdots & \cdots \\ P_{n1} & P_{n2} & \cdots & P_{nn} \end{bmatrix}$$

Where, $0 \leq P_{ij} \leq 1$ and $\sum_{j=1}^{N} P_{ij} = 1$, $(i, j = 1,2,3 \ldots . . n)$

Markov model is weak in predicting the spatial pattern of changes in LULC classes though it gives better quantitative changes of the classes (Chandralal et al. 2009). The quantity of land that would change in a predicted date from the present is accurately given by the Markov chain model (Tedse et al. 2021). This process will result in the transition probability matrix that gives the probability of change of the LULC classes to every other class (Mishra et al. 2014).

3.2.5 Hydrological modeling using SWAT

Soil and Water Assessment Tool (SWAT) has been used to analyse the impact of climate change on discharge and sediment yield for the Puthimari river up to 2099.

3.2.5.1 The SWAT Model

The SWAT hydrological model is a continuous-time simulation, semi-distributed, river basin model and has been developed by the USDA Agricultural Research Service (ARS) (Arnold et al. 1998). It is a process-based model which is computationally efficient and also capable of continuous simulation over long periods (Arnold et al. 2012). Using the topographic, soil, land use and climate data as inputs, SWAT model simulates water, sediment, nutrient, pesticide and bacteria yields as output (Neitsch et al. 2011; Krysanova and White 2015). The water balance equation used in SWAT to simulate the hydrological processes is:

$$SW_t = SW_0 + \sum_{i=1}^{t} \left(R_{day} - Q_{surf} - W_{seep} - E_a - Q_{gw} \right)$$

Where,

SW_t is the humidity of soil (mm), SW_0 is the base humidity of soil (mm), t is the time (days), R_{day} is rainfall volume in mm, Q_{surf} is the surface runoff (mm), E_a is the evapotranspiration (mm), W_{seep} is the seepage of water from the soil into deeper layers, Q_{gw} is the underground runoff (mm).

3.2.5.2 SWAT Setup

ArcSWAT 2012, with an interface in ArcGIS, was used to setup the model in this work.

3.2.5.2.1 Streamflow definition

After creating a new SWAT project, the ASTER GDEM of 30m resolution has been imported to SWAT to begin the delineation process of the watershed. In the stream definition section, initial stream network and sub-basin outlets were defined. The streams can be defined on the basis of drainage area threshold or by importing predefined watershed boundaries and streams. After defining the streamflow, flow direction and flow accumulation have been determined.

3.2.5.2.2 Inlet and outlet definition

The NH crossing point, where the observed discharge for the Puthimari river is available, has been considered as the outlet point of the watershed and the watershed has been delineated. The entire basin has been divided into 9 sub-basins. Finally, the sub-basin parameters have been calculated and the topographic report was created.

3.2.5.2.3 Defining land use, soil and slope

The LULC maps prepared from Landsat data as well as the predicted LULC maps for 2035, 2065 and 2085, and the soil map have been used as input to the model. Also, the look up table for land use and soil have been prepared. The default land use of the SWAT model was linked to land use map through the look up table which was again linked to the land use map.

The SWAT's soil database that has been created using the physical attributes of the soil types has been linked to the soil map through the look up table which was again linked to the soil map and was given as input to the model.

Five categories of slope were defined (0–10%, 10–20%, 20-30%, 30-50% and >50%) to characterize the variety of the surface. The minimum threshold area of 10/5/5 [%] for land use/soil class/slope over the sub-basin area was used. After the overlay of the land-use, soil maps

and slope, the distributions of the Hydrological Response Units (HRUs) were determined. HRU is the smallest element of the watershed that consists of landuse, slope and soil. Each HRU simulate the process based on the hydrological water balance equation including infiltration, percolation, lateral flow and evapotranspiration from the soil and return flowfromthe shallow aquifer. In this study, 94 numbers of HRUs have been created.

3.2.5.2.4 Defining climate database

The main climate data inputs required in the SWAT model are, rainfall, maximum and minimum temperature, solar radiation, wind speed and relative humidity. The IMD daily rainfall data available at 0.25°x0.25° spatial resolution, and IMD daily maximum and minimum temperature available at 1° resolution from 1996 to 2012 have been used as the observed climate data. Wind speed, solar radiation and relative humidity are simulated in ArcSWAT using weather generator for the Indian region. The historical and future daily rainfall, and maximum and minimum temperature for the five climate models have been fed as the input to the model to analyse the impact of climate change on discharge of the Puthimari river up to 2099. The model was set up with two year warm-up periods.

3.2.5.3 Model Calibration,Validation and Sensitivity Analysis

Sensitivity analysis and calibration of parameters of the SWAT model were carried out automatically in SWAT-CUP using the SUFI-2 algorithm. The parameters were calibrated

using the observed daily discharge; the process consists in adjusting them so that the daily simulations are as close as possible to the observations. The parameters were related to stream-flow assessment and include viz. r_CN2.mgt (curve number), v__ALPHA_BF.gw (base flow alfa factor), v__GW_DELAY.gw (groundwater delay time), v__GWQMN.gw (threshold depth of water in shallow aquifer required for return flow), v_SURLAG.bsn (lag time of surface runoff), r_SOL_Z.sol (Depth from the soil surface to bottom of the layer),), r_SOL_AWC.sol (soil available water capacity), r_SOL_K.sol (soil hydraulic conductivity), v_CH_N2.rte (manning roughness for the main channel), v_CH_K2.rte (effective hydraulic conductivity in main conductivity), v_OV_N.hru (Manning's n value for overland flow), r_SOL_BD.sol (Moist bulk density), v_EPCO.hru (Plant uptake compensation factor), v_ESCO.hru (soil evaporation compensation factor), v_RCHRG_DP.gw (Deep aquifer percolation fraction), r_SLSUBBSN.hru (Average slope length), v__GW_REVAP.gw (groundwater 'revap' coefficient) have been considered for model parameterization and calibration and validation process.

The input data series were divided into three phases: warm-up, calibration and validation. The period from 1999 to 2005 was chosen for model calibration, preceded by a three-year warming period (1996–1998). After calibration, the model was validated using daily streamflow from 2006 to 2010. The model efficiency was evaluated based on four statistics including Nash-Sutcliffe efficiency coefficient (NSE) which is a measure of predictive power of the model, percent bias (PBIAS) which is the average tendency of the simulated data to be larger or smaller than their observed counterparts, and coefficient of determination (R^2) which is a measure of the strength of the linear correlation between the predicted and observed values. A global sensitivity analysis was conducted to identify the most important influence parameters for streamflow simulation, which were adjusted during calibration. The effect of the parameters on the simulated streamflow was evaluated with p-value which determines the significance of the sensitivity and t-stat which provide a measure of sensitivity. The equations involved in determination of NSE, R^2 and PBIAS are,

$$NSE = 1 - \frac{\sum_{i=1}^{n}(O_i - P_i)^2}{\sum_{i=1}^{n}(O_i - \bar{O})^2}$$

$$R^2 = \frac{\sum_{i=1}^{n}(O_i - O)(P_i - \bar{P})}{\sqrt{\sum_{i=1}^{n}(O_i - \bar{O})^2}\sqrt{\sum_{i=1}^{n}(P_i - \bar{P})^2}}$$

$$PBIAS = \frac{\sum_{i=1}^{n}(O_i - P_i) * (100)}{\sum_{i=1}^{n} O_i}$$

where Oi is i^{th} observed streamflow; $\bar{O}$ is mean observed streamflow; Pi is i^{th} predicted streamflow and; P is mean predicted streamflow values and, n is the total number of observations.

Multiple regression system has been calculated to estimate the global sensitivity of streamflow parameters. The t-stat and p-value factors have been used to evaluate the sensitivity of the parameters in SWAT-CUP that provides measure of sensitivity (with absolute value go larger) and significance of sensitivity magnitude (close to zero).

3.2.6 Scenario based prediction of discharge

Three different scenarios have been considered in this study to determine the future runoff of the Puthimari river.

i. In the first scenario, change in both climate and LULC have been considered.

ii. In the second scenario, the LULC has been kept constant up to 2099 and the changed climate has been considered.

iii. In the third scenario, constant climate has been considered with changes in LULC.

3.2.7 Development of an ANN-SWAT Based Hybrid Model to Analyze Impact of Climate Change on Sediment Yield of River Puthimari

An Artificial Neural Network Model was developed to simulate the sediment yield of Puthimari river at its outlet. The daily rainfall, the SWAT simulated runoff and the observed sediment yield for the river have then been put as input to the ANN model. The ANN model was run using the time series analysis and this was carried out in MATLAB. The method selected in the present study is the non-linear autoregressive with External (Exogenous) Input (NARX) which predict series y(t) given d past values of y(t) and another series x(t) (Fig.3.3). The non-linear autoregressive network with exogenous inputs (NARX) is a recurrent dynamic network, with feedback connections enclosing several layers of the network. The NARX model is based on the linear ARX model, which is commonly used in time-series modeling. NARX networks can learn to predict one time series given past values of the same time series, the feedback input, and another time series, called the external or exogenous time series.

The standard NARX network is a two-layer feedforward network, with a sigmoid transfer function in the hidden layer and a linear transfer function in the output layer. This network also uses tapped delay lines to store previous values of the x(t) and y(t) sequences. In our study, y(t) is the sediment yield at the final outlet and x(t) are the rainfall and simulated runoff. Mathematically, it can be defined as,

$$y(t) = f(x(t-1), \ldots, x(t-d), y(t-1), \ldots y(t-d))$$

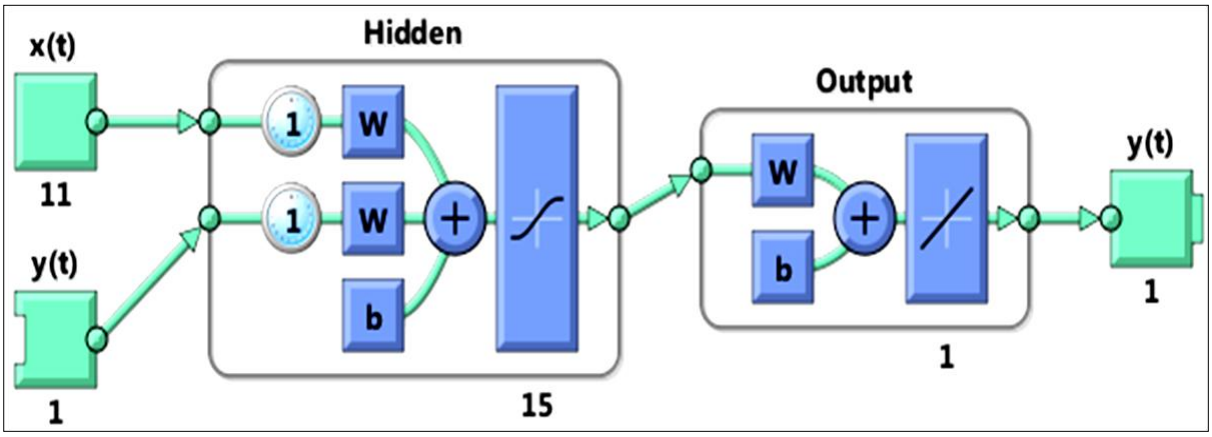

Fig.3.3: NARX neural network (open loop)

Prediction is a kind of dynamic filtering, in which past values of one or more time series are used to predict future values. Dynamic neural networks, which include tapped delay lines are used for non-linear filtering and prediction. There are three kinds of target time-steps: (i) Training time steps which are presented to the network during training, and the network is adjusted according to its error, (ii) Validation time steps which are used to measure network generalization, and to halt training when generalization stops improving and (iii) Testing time steps that have no effect on training and so provide an independent measure of network performance during and after training. In the present study, testing, training and validation were performed for the period 1999 to 2010 (up to which the observed sediment data are available). Out of the total data, 70% were selected for training and 15% each for validation and testing. The number of hidden layers selected was 15 and no. of delays selected was 1. The network was created and trained in open loop form. Open loop (single-step) is more efficient than closed loop (multi-step) training. Open loop allows us to supply the network with correct past outputs as we train it to produce the correct current outputs. After training, the network was converted to closed loop form for multi-step prediction up to 2099. Close loop Converts neural network open-loop feedback to closed loop. Fig.3.4 shows the NARX neural structure for closed loop. The *preparets* function available in MATLAB is used to prepare the input and

target time series data for network simulation or training. This function simplifies the normally complex and error prone task of reformatting input and target time series. It automatically shifts input and target time series as many steps as are needed to fill the initial input and layer delay states.

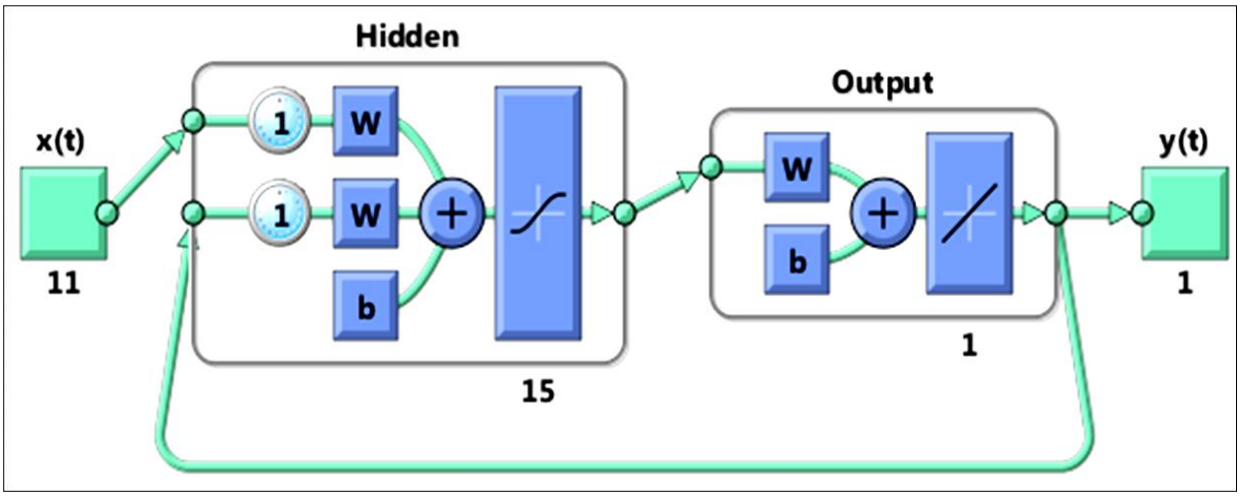

Fig. 3.4: NARX neural network (closed loop)

Here, in this study, the future sediment yield has been predicted for four different time steps viz. 2024-2049, 2050-2074 and 2075-2099.

CHAPTER- 4
RESULTS AND DISCUSSION

4.1 Watershed Delineation in ArcSWAT

Using the ASTERGDEM of 30m resolution, the Puthimari river basin has been delineated in ArcSWAT. Various maps viz., flow direction map, flow accumulation map, stream network map etc. were generated in the process of watershed delineation. Fig.4.1 gives the various maps generated in the process.

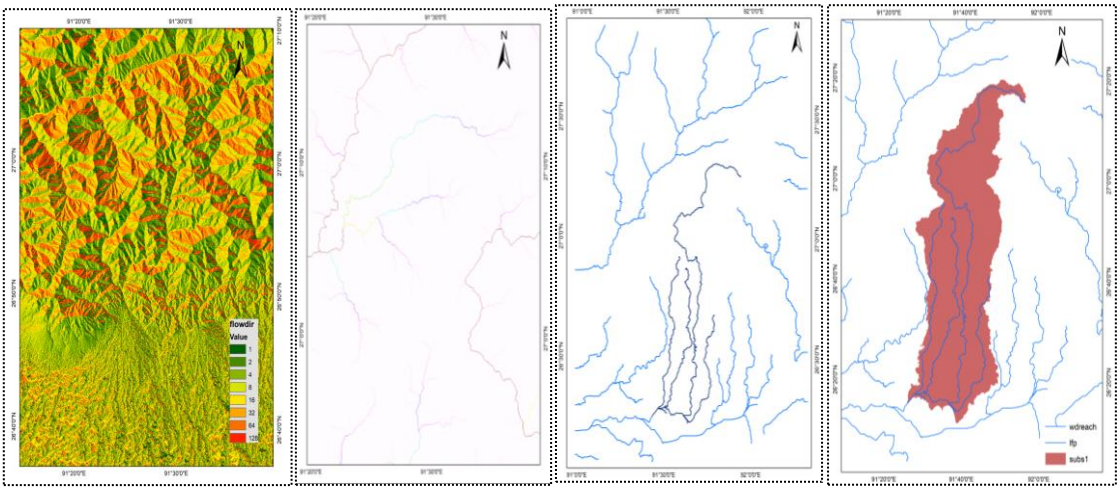

(a)Flow direction map (b) Flow accumulation(c) Stream network maP (c) Delineated Catchment

Fig.4.1: Maps generated during watershed delineation in ArcGIS

It has been found that the Puthimari catchment area is 3225.47 km^2. Its drainage density is 697.54 m/km^2, sinuosity is 1.728, total drainage length is 2567.93 km. The length of the Puthimari river is 214.02 Km.

4.2 Analysis of Future rainfall for Different Models for RCP 4.5 & RCP 8.5

4.2.1 Rainfall analysis for RCP4.5

The rainfall data from 1970 to 2099 for the climate models have been plotted to analyze the variation of monthly rainfall over the basin for RCP4.5 as shown in Fig.4.2. It is observed the maximum rainfall for most of the models occur in the months of June and July. Among all the

models, the highest rainfall of 653.88mm during 2050-74 is seen for MRICGCM3 in the month of July.

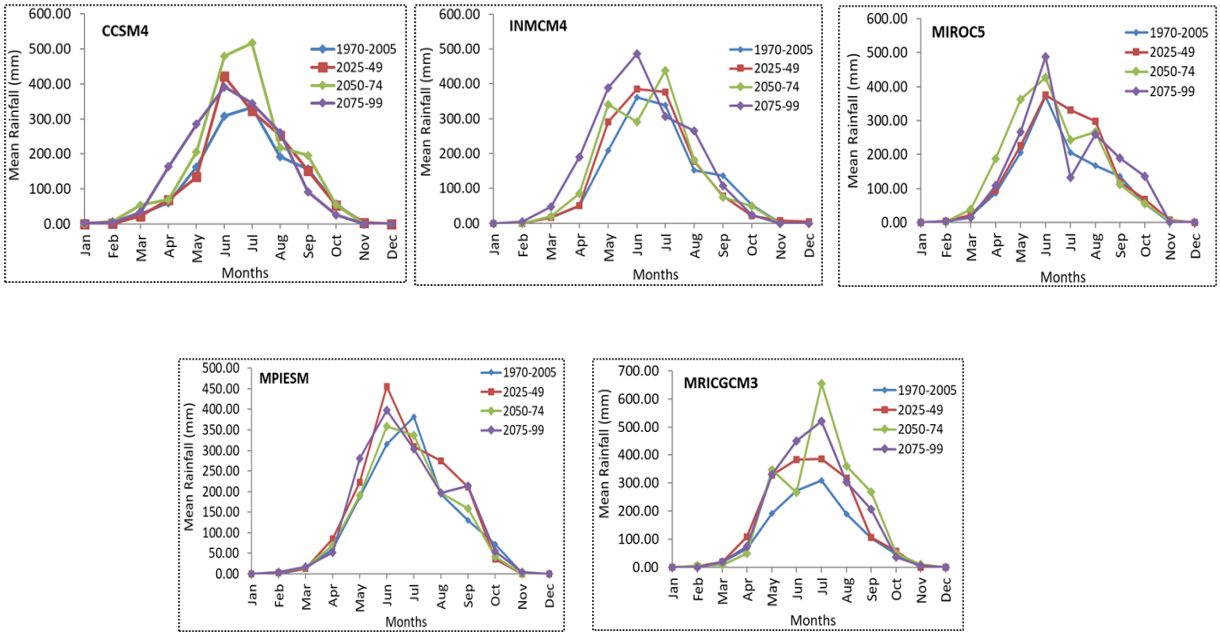

Fig. 4.2: Monthly rainfall variation of climate models under RCP4.5

Table 4.1 gives the months of occurrence of maximum rainfall for all the climate models. Maximum rainfall is also different in different time periods. The percent change of maximum rainfall from one time period to another has been determined as shown in Fig.4.3.

Table 4.1: Months of occurrence of maximum rainfall under RCP4.5.

Climate models	**1970-2005**	**2025-49**	**2050-74**	**2075-99**
CCSM4	July	June	July	June
INMCM4	June	June	July	June
MIROC5	June	June	June	June
MPIESM	July	June	June	June
MRICGCM3	July	July	July	July

The seasonal variation of rainfall due to climate change over the basin for four different seasons, winter, summer, monsoon and post-monsoon have also been analyzed. The average rainfall for these seasons during different time periods have been plotted as shown in Fig.4.3. As can be seen from the figure, during winter the average rainfall remains between 0-3.80mm. The models CCSM4, INMCM4, MIROC5 and MPIESM advocate an increase in winter rainfall towards the end of the century. Apart from winter season, considerable amount of rainfall can be seen for the other three seasons.

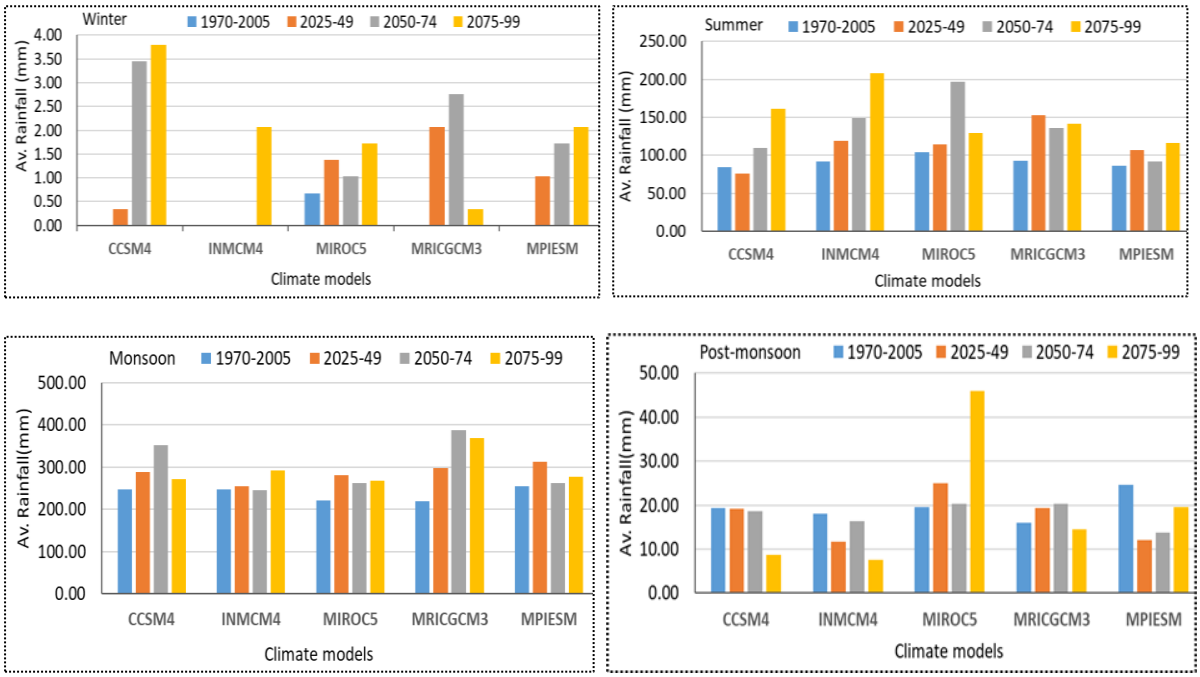

Fig.4.3: Seasonal average rainfall of the models for different time periods under RCP4.5

The corresponding plot depicting percent change in average rainfall from one time period to another for the seasons is given in Fig.4.4 except for the winter season where few of the models show no trace of rainfall for certain time periods.

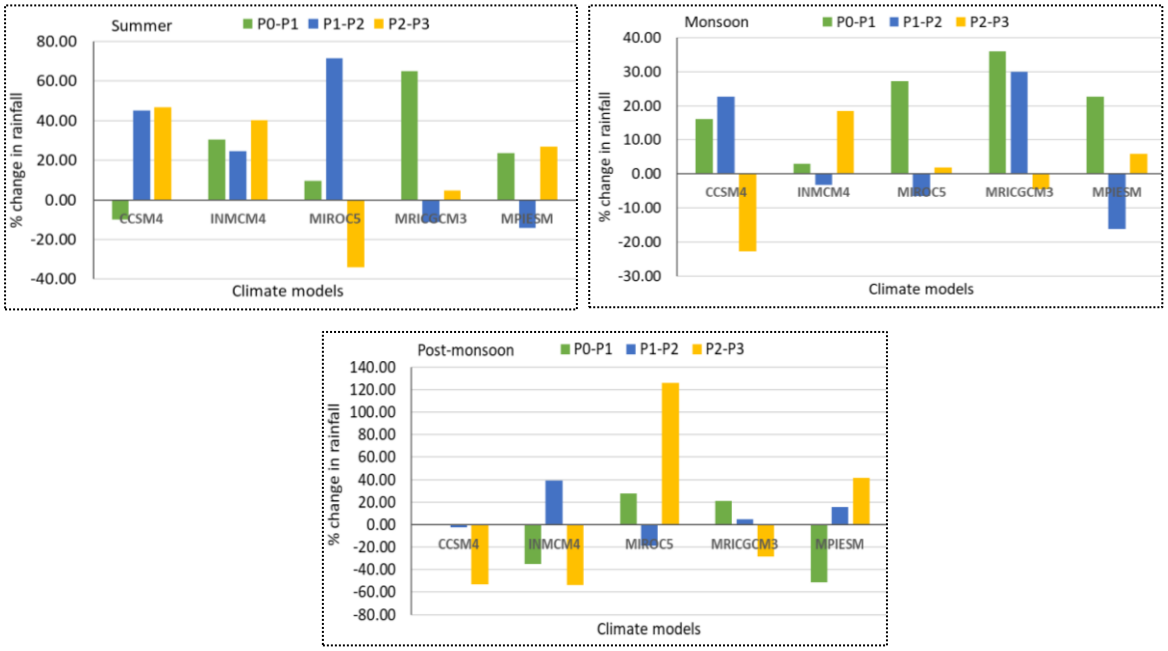

Fig.4.4: Percent change in average seasonal rainfall between different time periods under RCP4.5

In Fig. 4.4, P0, P1, P2 and P3 denote the time periods 1970-2005, 2025-49, 2050-74 and 2075-99 respectively. It is observed that except for CCSM4, increase in summer rainfall from P0 to P1can be seen for the remaining models. For CCSM4, INMCM4 and MIROC5, rainfall increase from P1 to P2, and decreases for the remaining models, the maximum increase being 71.63% (MIROC5) and the maximum decrease being 10% (MPIESM). For the last two time periods, i.e. from P2 to P3, except MIROC5, the rainfall increases for the other models with highest increase of 45% shown by CCSM4. For monsoon, INMCM4 shows the highest increase in rainfall by 18% from P0 to P1. In contrast, CCSM4, MRICGCM3 gives negative change between P2 and P3 depicting decrease in monsoon rainfall towards the end of the century. Also compared to P1, the rainfall will decrease in P2 for most of the models except CCSM4 and MRICGCM3. During post-monsoon, except MIROC5 and MPIESM, for other models, only decrease in rainfall can be observed towards 2099.

Mann-Kendall test has been performed for the models to determine the trends of rainfall in each time period. The nature of those trends was then identified by analyzing the Z statistics. Both monthly and seasonal trends have been identified for the models. For better visualization, the Z values have been plotted as heat maps as shown in Fig. 4.5 that denotes the trends of monthly rainfall for RCP4.5.

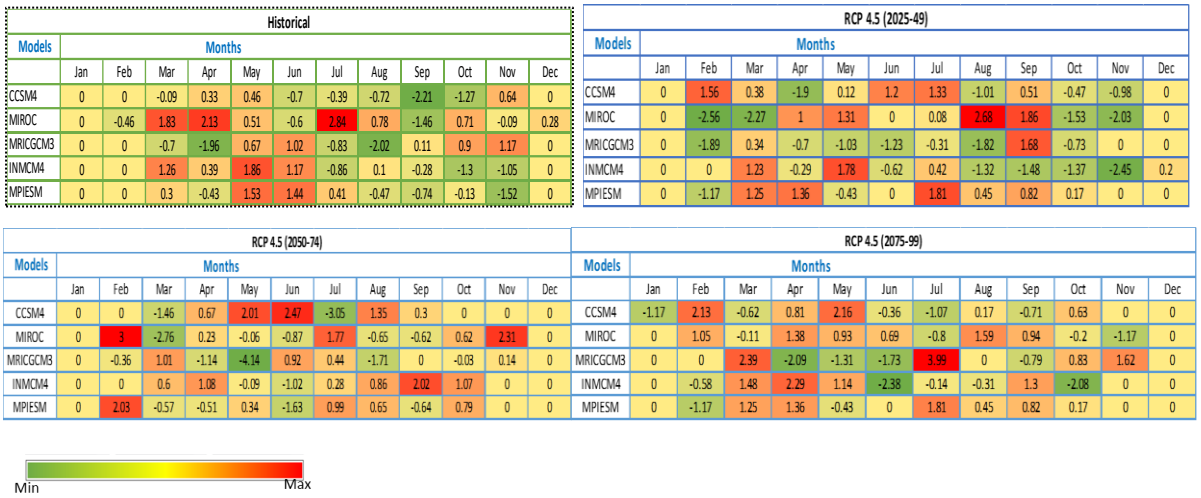

Fig.4.5: Heat map showing Z values of monthly rainfall of the climate models for RCP4.5

Under RCP4.5, the trends for January and December are insignificant. In January during 2075-99, decrease in rainfall for CCSM4 is observed. Notable decreasing trends in rainfall are observed during 2050-74 for MRICGCM3 in the month of May. The highest rising trend among all the models is observed for MRICGCM3 in the month of July during 2075-99

followed by MIROC5 in February during 2050-74. Only mild increasing and decreasing trends are observed for October and November for the models.

4.2.2 Rainfall analysis for RCP 8.5

Fig.4.6 gives the monthly rainfall variation of the models for different time periods under RCP8.5. Similar to RCP4.5, the maximum rainfall under RCP8.5 is also observed in the months of June and July for all the models during the different time periods. The months of maximum rainfall in each time period for the models are given in Table 4.2. Among all the models, the maximum rainfall of 785.20mm during 2075-99 is observed in the month of June for INMCM4 model. In almost all cases, the historical rainfall is less than the future predicted rainfall.

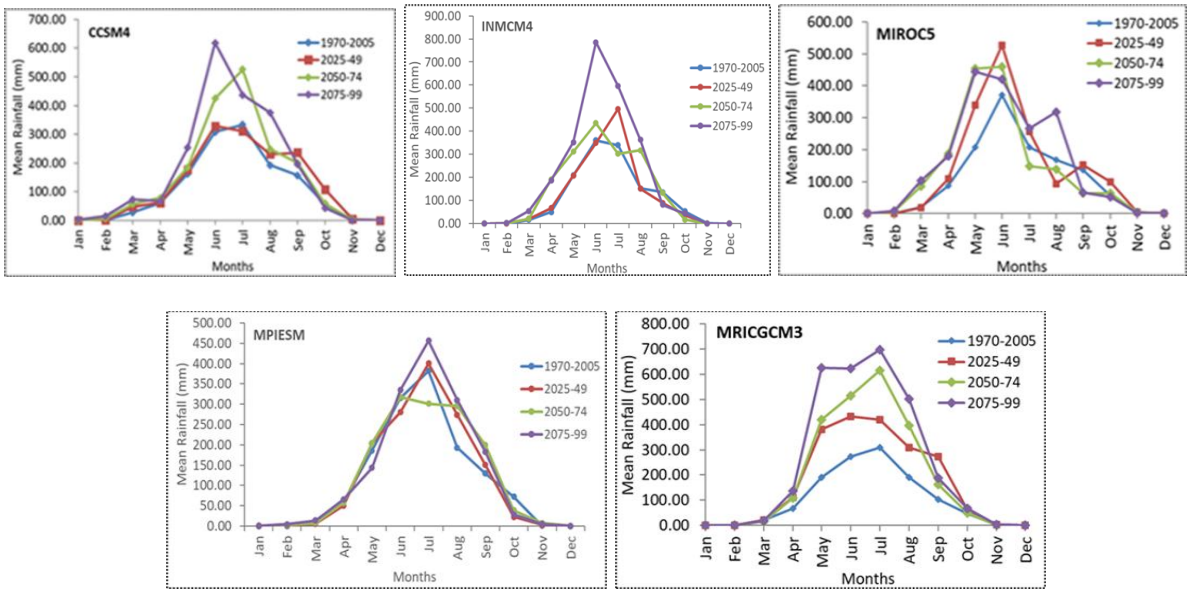

Fig. 4.6: Monthly rainfall variation of climate models under RCP8.5

Table 4.2: Months of occurrence of maximum rainfall under RCP8.5.

Climate models	1970-2005	2025-49	2050-74	2075-99
CCSM4	June	June	July	June
INMCM4	June	July	June	June
MIROC5	June	June	June	May
MRICGCM3	July	June	July	July
MPIESM	July	July	June	July

The seasonal average rainfall of the models for different time periods under RCP8.5 are as shown in Fig.4.7. As was seen in case of RCP4.5, under RCP8.5 too during winter few models

show no trace of rainfall for certain periods. However, rainfall will increase substantially during 2075-99 compared to its previous time periods.

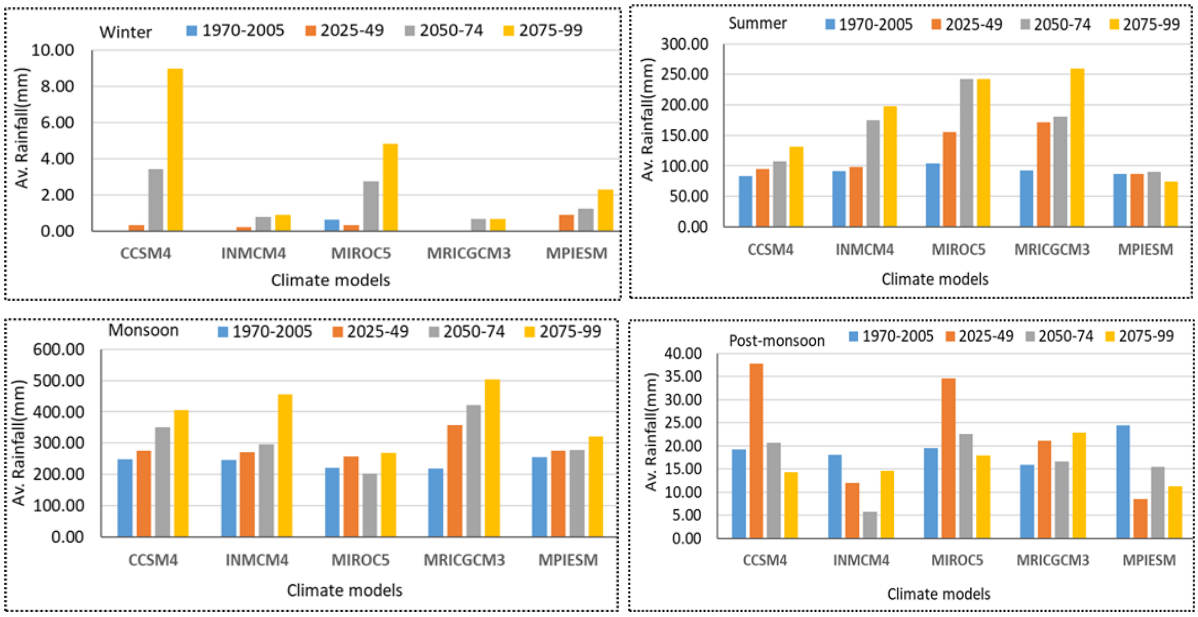

Fig.4.7: Seasonal average rainfall of the models for different time periods under RCP8.5

During this end period, out of all the models, CCSM4 gives the highest rainfall of 8.99mm followed by MIROC5 (4.84mm). Also, majority of the models show increase in winter rainfall during 2050-74. For the summer season, continuous increase of rainfall from 2025 to 2099 is witnessed by the models. Exception is MPIESM where more rainfall is observed during 2050-74 than the end period. Highest rainfall of 259.43mm among all the models is shown by MRICGCM3 during 2075-99 followed by MIROC5 during 2075-99(242.38mm) and 2050-74(242.15mm). Increase in rainfall towards the end of the century is observed for majority of the models in the monsoon season. The rainfall during monsoon season may increase to as high as 503.19mm during the end period as witnessed by MRICGCM3. For MIROC5 and MPIESM, 2025-49 rainfall is more than 2050-74. For the post-monsoon season, continuous decrease of rainfall from 2025-99 is seen for CCSM4 and MIROC5. For INMCM4 and MRICGCM3, rainfall first decreases from 2025-74 and then increases again during 2075-99. Reverse is the case for MPIESM, where rainfall first increases from 2025-74 and then decreases again during 2075-99.

The percent changes of seasonal rainfall from one time period to another for summer, monsoon and post-monsoon seasons are shown in Fig.4.8.

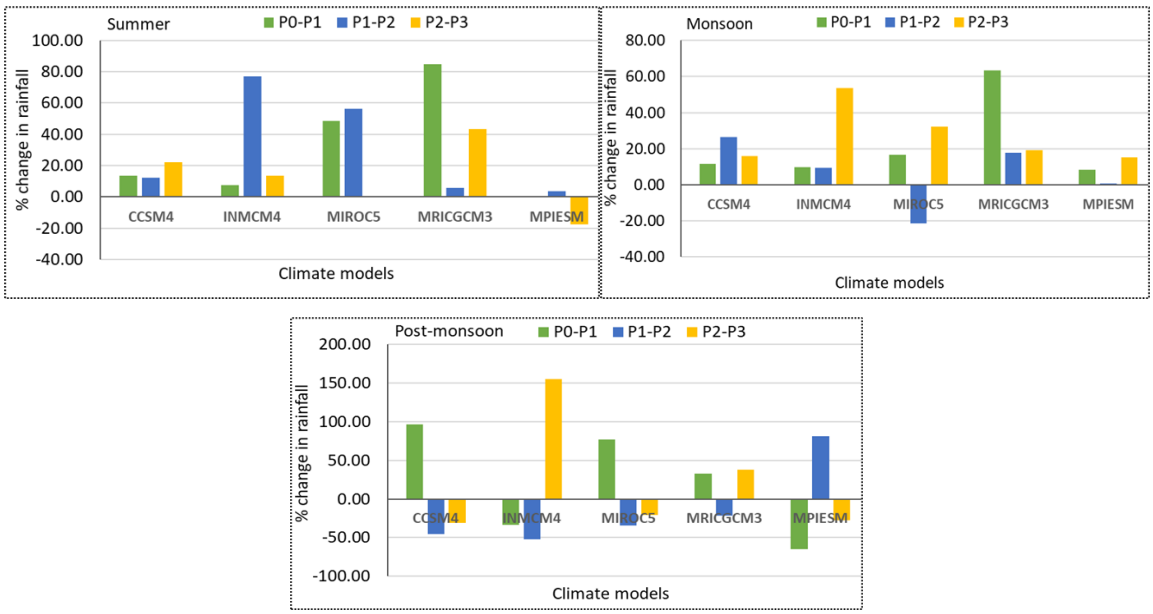

Fig. 4.8: Percent change in average seasonal rainfall between different time periods under RCP8.5

During summer, decrease in rainfall from P2 to P3 is seen for MPIESM where rainfall decreases by 17.41%. During the monsoon season, positive changes in rainfall between two time periods are seen for most of the models. In contrast, MIROC5 shows decrease in rainfall by 21.38% during P1-P2. For the post-monsoon season, except MPIESM, other models show decrease in rainfall from P1 to P2.

The Z statistics were then analyzed to understand the nature of the rainfall trends under RCP8.5. Fig.4.9 gives the heat map showing Z values of monthly rainfall for each model and for the different time periods.

Historical

Models	Months											
	Jan	Feb	Mar	Apr	May	Jun	Jul	Aug	Sep	Oct	Nov	Dec
CCSM4	0	0	-0.09	0.33	0.46	-0.7	-0.39	-0.72	-2.21	-1.27	0.64	0
MIROC	0	-0.46	1.83	2.13	0.51	-0.6	2.84	0.78	-1.46	0.71	-0.09	0.28
MRICGCM3	0	0	-0.7	-1.96	0.67	1.02	-0.83	-2.02	0.11	0.9	1.17	0
INMCM4	0	0	1.26	0.39	1.86	1.17	-0.86	0.1	-0.28	-1.3	-1.05	0
MPIESM	0	0	0.3	-0.43	1.53	1.44	0.41	-0.47	-0.74	-0.13	-1.52	0

RCP 8.5 (2025-49)

Models	Months											
	Jan	Feb	Mar	Apr	May	Jun	Jul	Aug	Sep	Oct	Nov	Dec
CCSM4	0	1.37	0.72	1.84	0.9	0.48	-1.89	-0.62	0.7	-0.33	-2.44	0
MIROC	0	-0.78	-0.17	0.83	2.58	0.36	0.74	0.26	-0.95	0.24	0.07	0
MRICGCM3	0	0	-0.6	-0.18	-1.48	0.03	0.56	0.03	0.14	0.36	1.75	0
INMCM4	0	0	1.23	-0.29	1.78	-0.62	0.42	-1.32	-1.48	-1.37	-2.45	0.2
MPIESM	0	-1.17	1.25	1.36	-0.43	0	1.81	0.45	0.82	0.17	0	0

RCP 8.5 (2050-74)

Models	Months											
	Jan	Feb	Mar	Apr	May	Jun	Jul	Aug	Sep	Oct	Nov	Dec
CCSM4	0	0.41	0.91	-1.7	-0.11	-0.39	1.36	2.39	-2.24	0.36	1.17	0
MIROC	0	0.39	-0.83	2.06	0.86	0.06	-1.09	0.17	-0.8	-0.59	1.47	0
MRICGCM3	0	-1.41	-0.84	2	1.76	0.78	-0.89	1.45	2.61	-0.22	0.78	0
INMCM4	0	0	0.6	1.08	-0.09	-1.02	0.28	0.86	2.02	1.07	0	0
MPIESM	0	2.03	-0.57	-0.51	0.34	-1.63	0.99	0.65	-0.64	0.79	0	0

RCP 8.5 (2075-99)

Models	Months											
	Jan	Feb	Mar	Apr	May	Jun	Jul	Aug	Sep	Oct	Nov	Dec
CCSM4	1.98	-0.41	-1.76	-1.07	0.65	-0.28	0.81	-0.69	1.74	1.91	0	0
MIROC	1.76	0.71	0.55	1.46	-0.47	0.34	1.01	-0.23	-0.62	0.08	1.17	0
MRICGCM3	0	-0.85	-0.52	2.85	-0.17	-1.73	-0.61	-1.19	-0.6	-1.67	0.07	0
INMCM4	0	-0.58	1.48	2.29	1.14	-2.38	-0.14	-0.31	1.3	-2.08	0	0
MPIESM	0	-1.17	1.25	1.36	-0.43	0	1.81	0.45	0.82	0.17	0	0

Fig. 4.9: Heat map showing Z values of monthly rainfall of the climate models for RCP8.5

From the figure it is evident that in the month of January CCSM4 and MIROC5 give positive trend of rainfall during 2075-99. Significant positive trends are given by CCSM4(2025-49) for the month of February. For the month of March, no steep positive trend can be seen in the future. Rather, more negative trends can be observed in March with significantly decreasing trends during 2075-99 by CCSM4. For the month of May, maximum rising trend is observed in MIROC5 during 2025-49 followed by MRICGCM3 during 2050-74. For other time periods, in the month of May, gentle rising/falling trends can be observed. The highest decreasing trend is seen during 2025-49 for MPIESM. From June to September, increasing trends during 2050-74 for CGCM3 in the month of September is most significant. For other periods, only gentle trends can be seen for the models. Negative trends for MPIESM (2025-49, July), INMCM4 (2075-99, August), CCSM4(2050-74, September) are also significant. In the month of November, for MIROC5 and MPIESM rising trends during the end period are observed. No trend is seen for the models in the month of December.

4.3 Analysis of Future temperature for Different Models for Different Time-Frames for RCP 4.5 & RCP 8.5

4.3.1 Temperature analysis for RCP4.5

Monthly average maximum and minimum temperature variations for five different models in each time period are represented graphically in Fig.4.10. Compared to the historical period, future warmer climate is observed for each of the model.

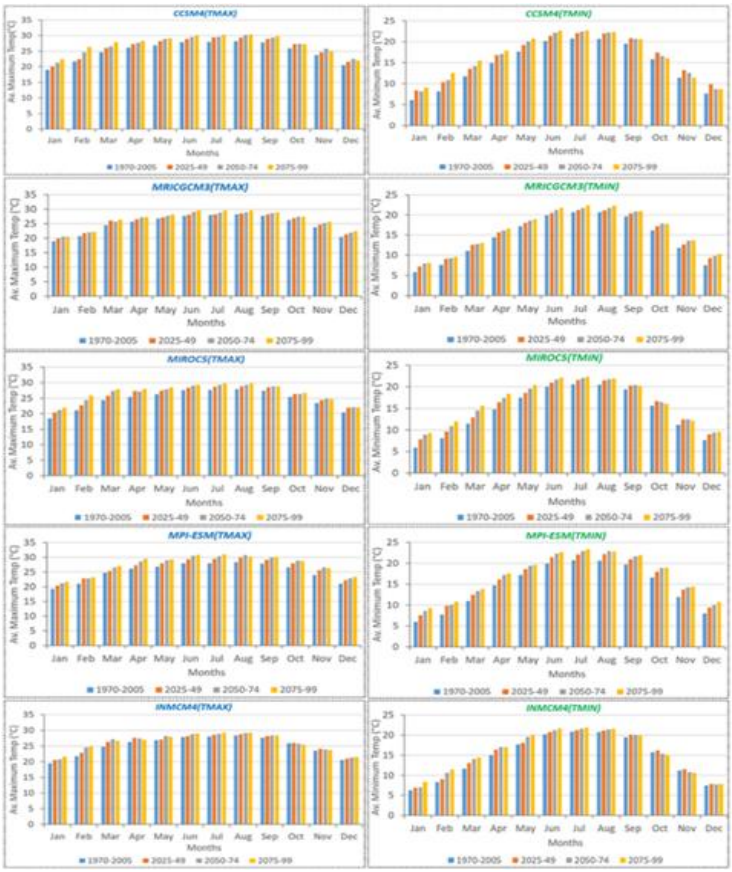

Fig.4.10: Monthly average maximum and minimum temperature for the climate models for RCP 4.5

Periodical analysis showed that both monthly maximum and minimum temperature rise continuously from 2025 to 2099 for most of the models. Exceptions are observed in certain models for few different months. For instance, in case of CCSM4, maximum temperature during 2075-99 decreases compared to the previous period in the months of November and December. Similarly, minimum temperature for this model as well as for INMCM4 show continuous decrease from 2025 to 2099 in September, October, November and December. For MRICGCM3 and MIRPC5, maximum temperature is less during 2050-74 compared the previous period 2025-49 in the month of March and April respectively. Also, minimum temperature for MIROC5 and maximum temperature for INMCM4 decreases continuously from 2025 to 2099 in the month of October. For most of the models, the highest maximum temperature is observed in the month of August except that during 2050-74, the maximum temperature will occur in the months of June and July respectively for MRICGCM3 and MIROC5. Also, during 2075-99, July will be the warmest month for MIROC5 and MPIESM. The highest maximum temperature will be between 28.5°C and 31.02°C for different models compared to historical period temperature of 27.89-28.36°C. The highest minimum

temperature for most of the models will occur in the month of July including the historical period except for MPIESM where the minimum temperature will be highest from 2025 to 2074 in the month of August. Compared to historical highest minimum temperature of 20.61-20.84°C, it is projected to increase to 21.2 23.34°C in future.

The year of occurrence of highest maximum and minimum temperature under RCP 4.5 in different time periods for the selected models are tabulated in Table 4.3.

Table 4.3: Years of occurrence of highest maximum and minimum temperature under RCP4.5

Climate models' Sl. No.	Highest Maximum Temperature (Temperature in °C)				Highest Minimum Temperature (Temperature in °C)			
	1970-2005	2025-49	2050-74	2075-99	1970-2005	2025-49	2050-74	2075-99
1.	1995 (*25.75*)	2038 (*26.88*)	2069 (*27.65*)	2088 (*27.94*)	2002 (*15.53*)	2038 (*16.71*)	2069 (*16.73*)	2099 (*17.32*)
2.	1979 (*23.95*)	2045 (*26.39*)	2074 (*27.04*)	2098 (*27.24*)	1996 (*15.12*)	2049 (*16.03*)	2072 (*16.54*)	2098 (*16.74*)
3.	1971 (*23.16*)	2034 (*26.63*)	2070 (*27.33*)	2087 (*27.50*)	1976 (*15.08*)	2049 (*16.44*)	2070 (*16.92*)	2085 (*17.36*)
4.	1987 (*25.96*)	2049 (*27.40*)	2056 (*28.08*)	2078 (*28.57*)	2003 (*15.22*)	2047 (*16.80*)	2061 (*17.75*)	2078 (*17.86*)
5.	1995 (*25.86*)	2042 (*26.61*)	2073 (*26.78*)	2099 (*27.42*)	1987 (*15.81*)	2033 (*15.88*)	2073 (*16.17*)	2099 (*17.05*)

In the historical period, the highest maximum temperature for the models varied between 23.16°C (MIROC5)-25.96°C (MPIESM) and it mostly occurred in between 1987 and 1995. Only MIROC5 showed the warmest year in 1971. The models indicate that during 2025-49, 2038, 2045, 2034, 2049 and 2042 will be the warmest year for models 1-5 respectively. The highest maximum temperature during this period ranges between 26.39°C (MRICGCM3)-27.40°C (MPIESM). During 2050-74, the maximum temperature range increases to 26.78°C (INMCM4) – 28.08°C (MPIESM) and occurs mostly after 2069 except MPIESM for which 2056 is observed as the warmest year. The highest maximum temperature for the models during the last period of the century is projected to rise between 27.24°C (MRICGCM3) and 28.57°C (MPIESM), and occurs after 2075. The highest minimum temperature under RCP 4.5 during 1970-2005 varied between 15.08-15.81°C and observed mostly after 1985. The range of

highest minimum temperature during 2025-49, 2050-74 and 2075-99 are observed to be in the range of 15.88°C (INMCM4, 2033) -16.80°C (MPIESM, 2047), 16.17°C (INMCM4, 2073)-17.75°C (MPIESM, 2061) and 16.74°C (MRICGCM3, 2098) -17.86°C (MPIESM, 2078) respectively.

Fig.4.11 shows the increase in average (a) maximum and (b) minimum temperature from one time period to another for RCP4.5. In the figure, P1, P2 and P3 denote the periods 2025-49, 2050-74 and 2075-99 respectively.

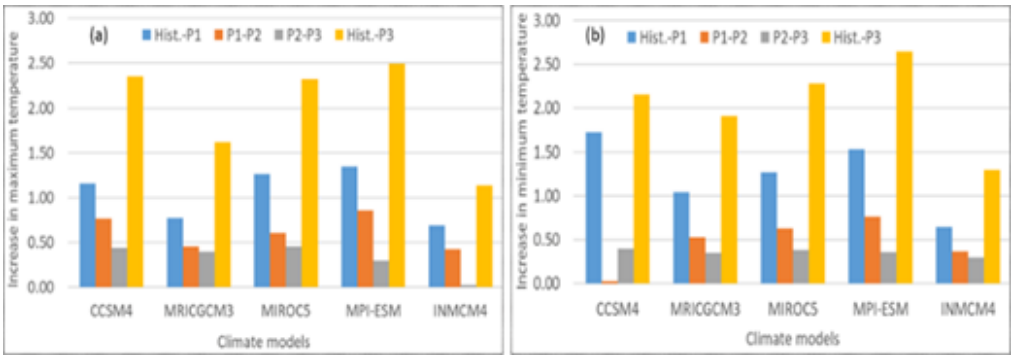

Fig.4.11: Increase in average maximum and minimum temperature from one time period to another for RCP 4.5

Increase in both maximum and minimum temperature is observed between two consecutive time periods for each model. The temperature difference decreases subsequently from P1 to P3 except for CCSM4 where the increase in average minimum temperature from P1 to P2 is less than that from P2 to P3. Compared to the historical period, the average maximum and minimum temperature over the basin are projected to increase by 1.13-2.49°C and 1.3-2.64°C respectively for the selected models towards the end of the century.

The mean temperature over the basin has also been analysed for the different climate models. Fig.4.12 gives the change in monthly mean temperature in different time periods for the models under RCP4.5.

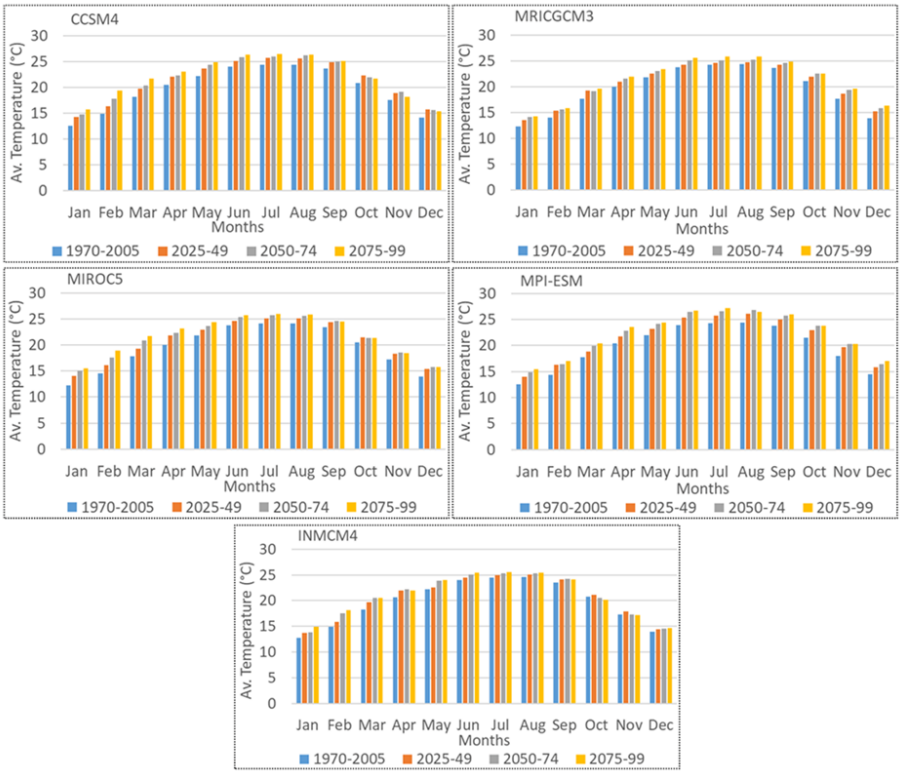

Fig.4.12: Mean monthly temperature variations for the models under RCP 4.5

Except for INMCM4, for rest of the models, there will be a continuous rise in temperature from 2025 to 2099 in each month. In case of INMCM4, gradual decrease in future temperature is observed for the months of October and November. Except for CCSM4 during 2025-49 and MIRPC5 during 2050-74 where the maximum mean temperature is seen in July, for all other models the temperature will be maximum in the month of August during 2025-49 and 2050-74. During 2075-99 however, the maximum temperature will shift to the month of July except for majority of the models. The maximum mean monthly temperature for the models will lie between 24.84°C -27.18°C compared to the historical period range of 24.21-24.54°C. The minimum mean temperature in all the time periods for the models are observed in the month of January.

Table 4.4 shows the years of occurrence of maximum mean temperature for different time periods under RCP4.5.

Table 4.4 Years of occurrence of maximum mean temperature for RCP 4.5

Sl. No.	Climate models	Maximum mean temperature (Temperature in °C)			
		1970-2005	2025-49	2050-74	2075-99
1.	CCSM4	2002 (*20.53*)	2038 (*21.79*)	2069 (*22.19*)	2087 (*22.44*)
2.	MRICGCM3	1979 (*19.33*)	2049 (*20.91*)	2074 (*21.74*)	2098 (*21.99*)
3.	MIROC5	1988 (*18.69*)	2049 (*21.41*)	2070 (*22.12*)	2099 (*22.37*)
4.	MPIESM	2004 (*20.49*)	2049 (*21.93*)	2061 (*22.74*)	2078 (*23.21*)
5.	INMCM4	1988 (*20.72*)	2033 (*21.23*)	2073 (*21.48*)	2099 (*22.23*)

During 2025-49, for models 2, 3 and 4, the warmest year be 2049, and for models 1 and 5, the warmest year are 2038 and 2033 respectively. The maximum mean temperature will remain between 20.91°C and 21.93°C. During 2050-74, for each model the maximum mean temperature (21.48-22.74°C) is observed in 2069, 2074, 2070, 2061 and 2073 respectively for models 1 to 5. In the end period, for models 3 and 5 maximum mean temperature is observed in 2099, while for models 1, 2 and 4 it is observed in 2087, 2098 and 2078 respectively. The maximum temperature lies between 21.99°C and 23.21°C.

Fig.4.13 gives the graphical representation of increase in mean temperature from one time period to another for RCP4.5.

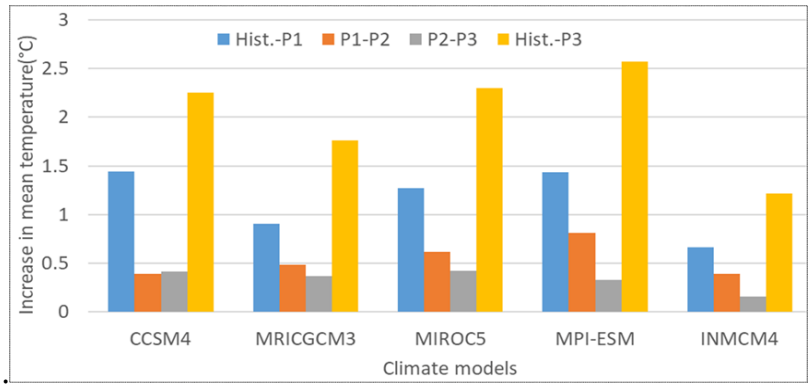

Fig.4.13: Increase in average mean temperature between different time periods for RCP 4.5

It is clear from the figure that for different models, mean temperature over the basin will rise by 1.21-2.6°C towards the end of the century as compared to the historical period. However, the increased value of temperature goes on diminishing between two consecutive time periods.

4.3.2 Temperature analysis for RCP 8.5

Similar analysis for future temperature has been carried out for RCP8.5. Fig.4.14 shows the monthly average maximum and minimum temperature for different time periods for the models under RCP8.5.

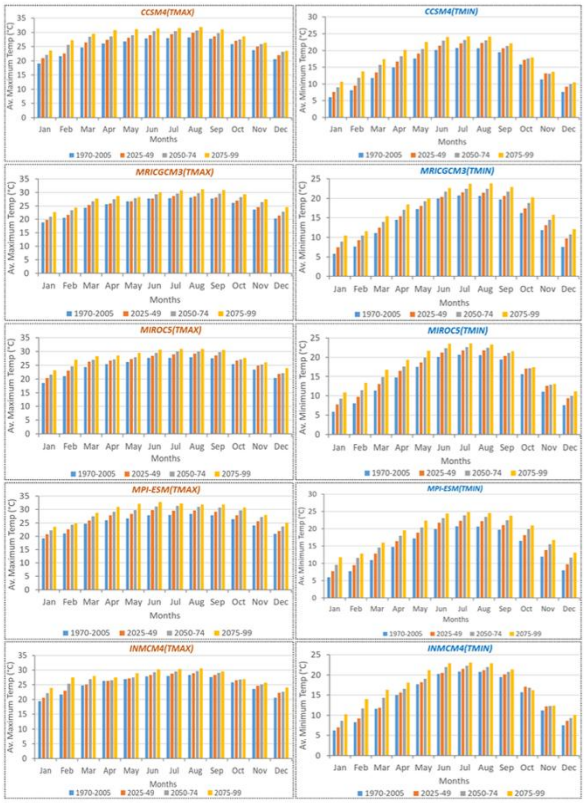

Fig.4.14: Monthly average maximum and minimum temperature for the climate models in each time period for RCP 8.5

Unlike RCP4.5, no exception can be seen in any of the models and for all of them temperature increases continuously from the historical period to the end of the century. For most of the models, the highest maximum and minimum temperature will be observed in the month of August and July respectively. Exceptions are for MRICGCM3 where highest maximum temperature during 2025-49 will occur in July, and for MPIESM it will occur in the months of June (2025-49) and July (2050-74). For CCSM4 during 2050-74, and for MRICGCM3 from 2050-99, the highest minimum temperature is observed in the month of August. The highest monthly maximum (minimum) temperature is observed between 28.63-32.77°C (21.50-24.85°C) compared to historical period temperature of 27.89-28.36°C (20.61-20.84°C).

The year of occurrence of highest maximum and minimum temperature for RCP 8.5 are as shown in Table 4.5.

Table 4.5: Years of occurrence of highest maximum and minimum temperature under RCP8.5

Climate models' Sl. No.	Highest Maximum Temperature (Temperature in °C)				Highest Minimum Temperature (Temperature in °C)			
	1970-2005	2025-49	2050-74	2075-99	1970-2005	2025-49	2050-74	2075-99
1.	1995 (*25.75*)	2047 (*26.96*)	2074 (*28.33*)	2096 (*30.14*)	2002 (*15.53*)	2048 (*16.65*)	2074 (*18.06*)	2099 (*19.27*)
2.	1979 (*23.95*)	2047 (*26.64*)	2072 (*27.86*)	2096 (*29.25*)	1996 (*15.12*)	2041 (*16.37*)	2072 (*17.63*)	2096 (*18.96*)
3.	1971 (*23.16*)	2041 (*26.76*)	2055 (*27.63*)	2098 (*29.07*)	1976 (*15.08*)	2044 (*16.53*)	2068 (*17.44*)	2098 (*18.83*)
4.	1987 (*25.96*)	2049 (*27.74*)	2071 (*28.96*)	2094 (*30.49*)	2003 (*15.22*)	2047 (*17.00*)	2073 (*18.87*)	2098 (*20.14*)
5.	1995 (*25.86*)	2047 (*26.47*)	2073 (*27.40*)	2099 (*28.78*)	1987 (*15.81*)	2046 (*16.24*)	2061 (*17.41*)	2099 (*18.77*)

It can be observed from Table 4.5 that during 2025-49, for RCP 8.5, the highest maximum temperature will occur between 2040-49 for all the models and maximum temperature lies between 26.47°C and 27.74°C. During the next time period from 2050-74, the highest maximum temperature is observed in range 27.40-28.96°C and occurs between 2070 and 2074 for the models except for MIROC5. During the last time period from 2075-99, the highest maximum temperature is observed between 2094-99 for the models. The highest maximum temperature in this period will lie between 28.78°C and 30.49°C. Again, the highest minimum temperature during 2025-49 (16.24-17°C) will occur in between 2040 and 2049. During 2050-74 (17.41-18.87°C) it occurs between 2060 and 2074. In the end period, highest minimum temperature in the range of 18.77-20.14°C is observed only after 2095 for all the models.

The increase in (a) maximum and (b) minimum temperature between two consecutive time periods for different models under RCP8.5 are shown in Fig.4.15. Compared to the historical period, the maximum temperature will increase by 2.68-3.89°C towards the end of the century.

The minimum temperature will increase by 2.85-4.74°C from 1970 to 2099. For each time period, both maximum and minimum temperature increases with different values of increased temperature compared to its previous time period.

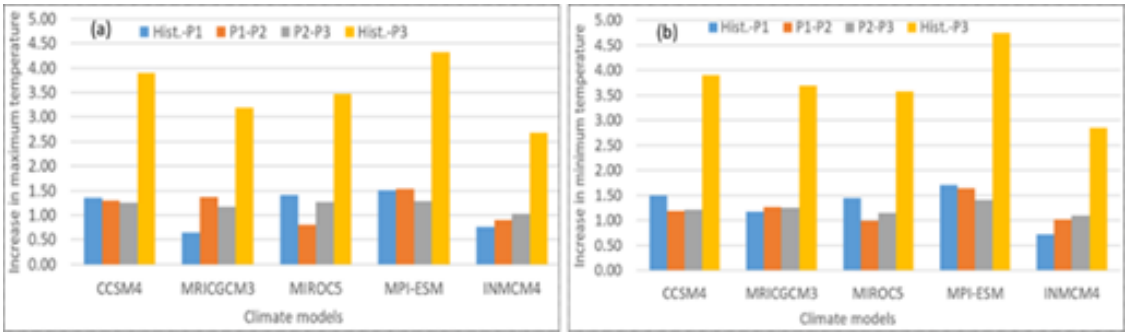

Fig.4.15: Increase in average maximum and minimum temperature from one time period to another for RCP 8.5

Fig.4.16 shows the monthly mean temperature in different time periods for the models under RCP8.5. For each month, all the models show continuous increase in temperature from 2025 to 2099. The maximum temperature in different time periods will occur mostly in the month of July and August for the models except that, for MPI-ESM during 2075-99, maximum temperature is observed in the month of June. The maximum mean monthly temperature from 2025 to 2099 will vary between 25.07-28.59°C for the models with the lowest and highest shown by MRICGCM3 and MPIESM respectively.

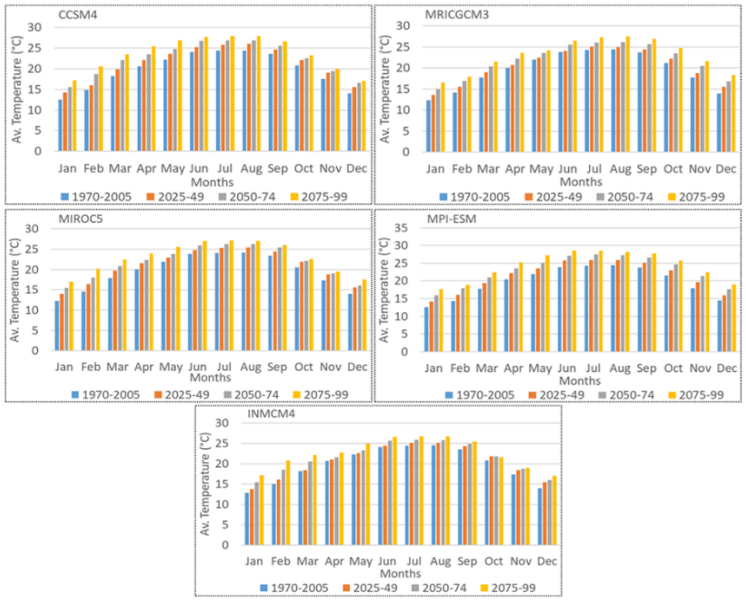

Fig.4.16: Mean monthly temperature variations for the models under RCP 8.5

Table4.6 gives the year for maximum mean temperature under RCP 8.5 for the models during different time periods.

Table 4.6: Years of occurrence of maximum mean temperature for RCP 8.5

Sl. No.	Climate models	Maximum mean temperature (Temperature in °C)			
		1970-2005	2025-49	2050-74	2075-99
1.	CCSM4	2002 (*20.53*)	2049 (*21.65*)	2074 (*23.19*)	2096 (*24.67*)
2.	MRICGCM3	1979 (*19.33*)	2047 (*21.29*)	2072 (*22.75*)	2096 (*24.11*)
3.	MIROC5	1988 (*18.69*)	2044 (*21.64*)	2072 (*22.44*)	2098 (*23.95*)
4.	MPIESM	2004 (*20.49*)	2047 (*22.32*)	2073 (*23.91*)	2098 (*25.27*)
5.	INMCM4	1988 (*20.72*)	2046 (*21.33*)	2073 (*22.33*)	2099 (*23.78*)

During 2025-49, the maximum mean temperature that lies between 21.33°C and 22.32°C is observed after 2043 for the models. For the next time period, maximum mean temperature of 22.33-23.91°C is observed after 2070. For the last period 2075-99, the maximum mean temperature occurs after 2095 with temperature ranging from 23.78°C to 25.27°C. It is also observed that during each time period, the maximum mean temperature is lowest for INMCM4 and highest for MPIESM. Fig.4.17 shows the graphical representation of increase in average mean temperature between two consecutive time periods under RCP 8.5.

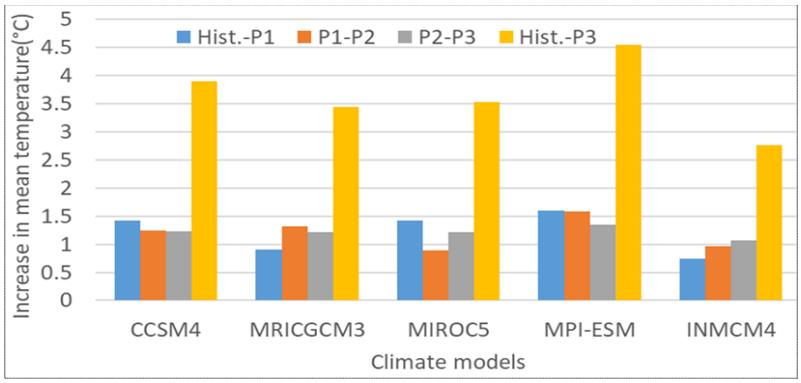

Fig.4.17: Increase in average mean temperature between different time periods for RCP 8.5

From historical to P1, P1 to P2 and P2 to P3, mean temperature will increase by 0.74-1.6°, 0.89-1.5° and 1.06-1.34° for the various models. Compared to the historical period, the mean temperature is projected to increase by 2.76-4.53° towards the end of the century.

4.3.3 Linear trend analysis of future temperature for RCP 4.5 and RCP 8.5

A linear trend analysis has been performed to check the trends of maximum, minimum and mean temperature from 2025 to 2099 under RCP 4.5 and RCP8.5 as shown in Fig.4.18.

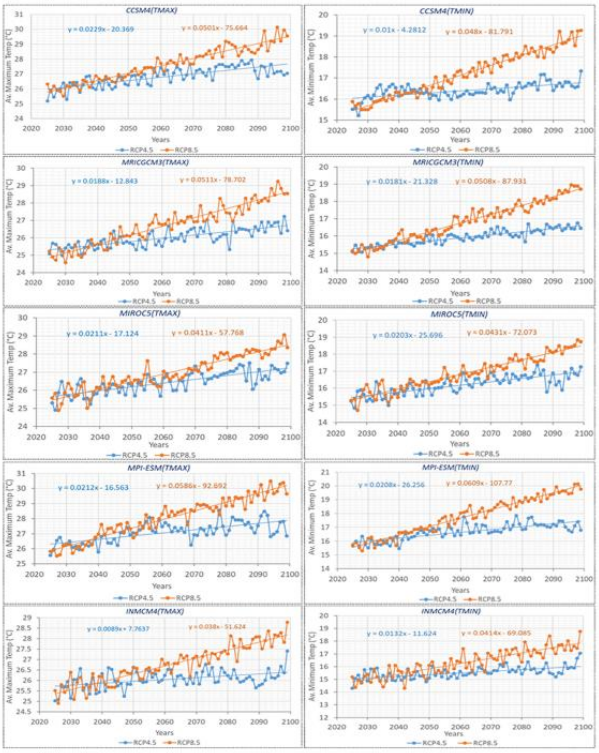

Fig.4.18: Linear trend analysis of future maximum and minimum temperature under RCP 4.5 and RCP 8.5

Rising trends of both maximum and minimum temperature is observed for all the models under both the RCPs with steeper trend under RCP8.5.

4.4 Land use/land cover change detection study

The LULC maps prepared for Puthimari basin for the year 1999, 2009 and 2019 are shown in Fig.4.19.

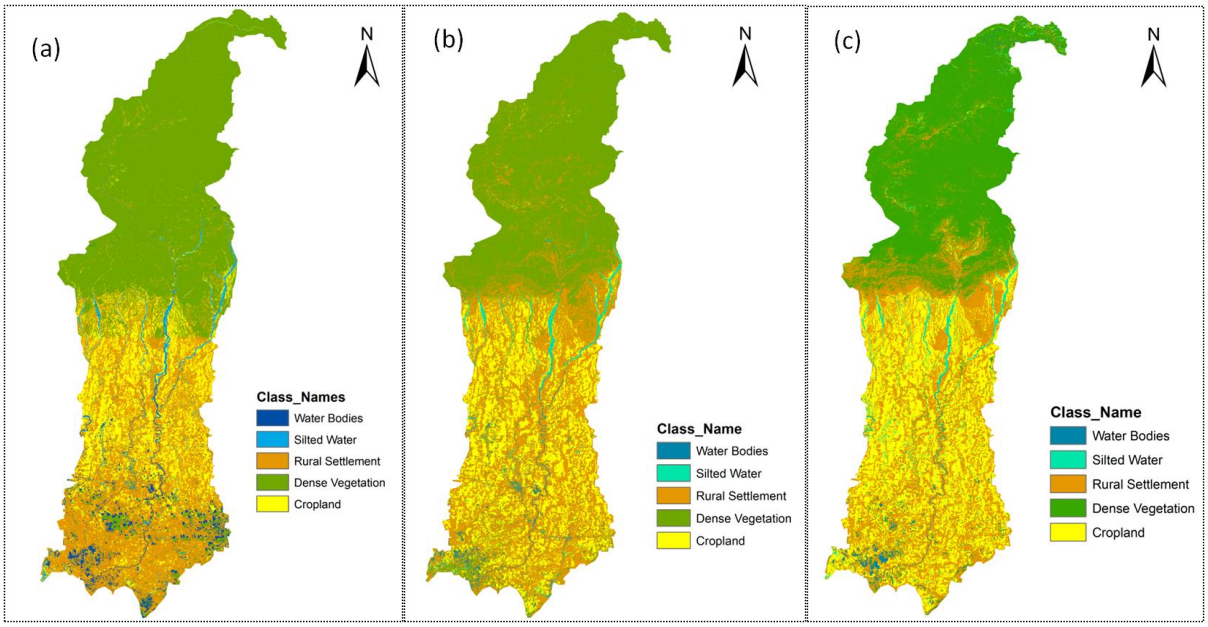

Fig.4.19: LULC maps of Puthimari basin for (a)1999, (b)2009 and (c)2019

The areas covered by different LULC classes from 1999 to 2019 are given in Table 4.7.

Table 4.7: Area covered by different LULC classes in Puthimari basin from 1999 to 2019

LULC Class	Area covered in Km^2		
	1999	2009	2019
Dense vegetation	1520.49	1458.96	1380.00
Water bodies	44.69	50.18	58.23
Crop land	752.09	659.74	540.74
Rural settlement	837.70	992.06	1195.37
Silted water	70.50	64.52	51.13

Throughout the study period that covers two decades from 1999 to 2019, compared to the other classes, dense vegetation has been observed to cover the maximum area that mainly occupies the northern part of the catchment that falls mostly in Bhutan and part of Assam state in India followed by rural settlement, crop land, silted water and water bodies. Based on the total catchment area, the percent of total basin area covered by each LULC class has been determined. Fig.4.20 shows the pie diagrams depicting the percent of total area covered by each LULC class. Fig.4.21 shows the Pie diagrams giving year wise percent of total area covered by each LULC class in Puthimari river basin from 1999 to 2019.

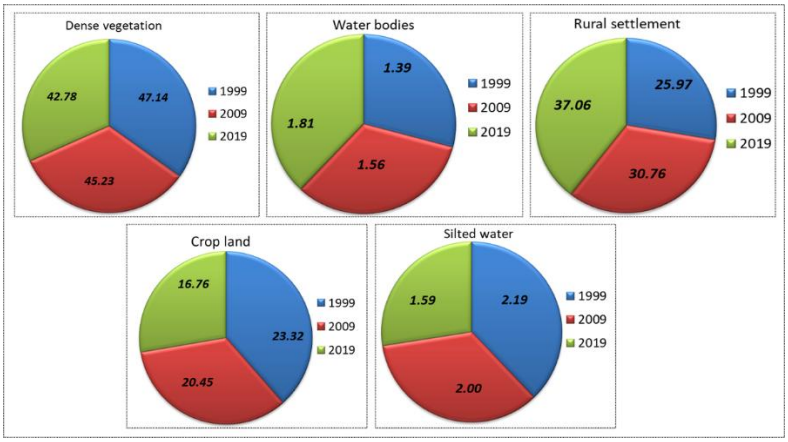

Fig.4.20: Pie diagrams depicting the percent of total area covered by each LULC class

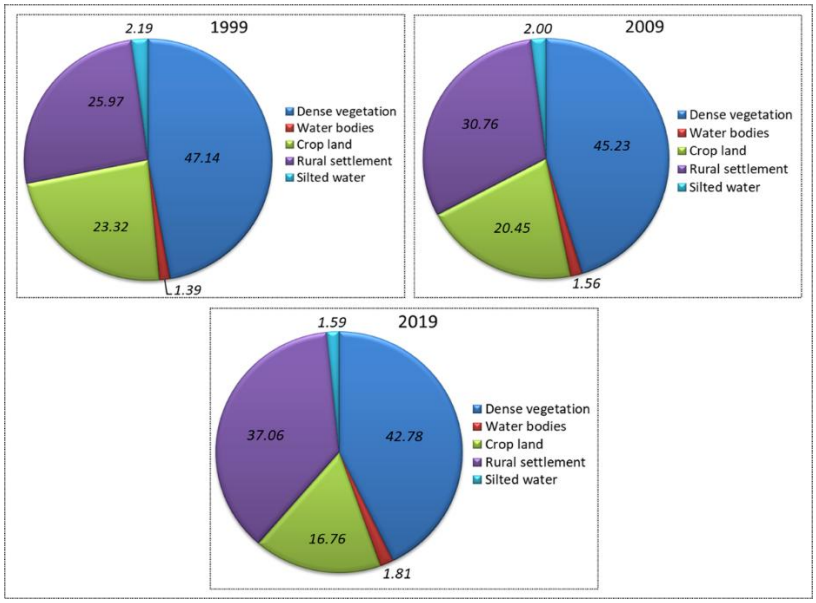

Fig.4.21: Pie diagrams giving year wise percent of total area covered by each LULC class

The percentages for dense vegetation, silted water and crop lands were found to be 47.14%, 2.19% and 23.32% respectively in the year 1999. After one decade i.e. in 2009, the area covered by these three classes decreased to 45.23%, 2.00% and 20.45%. A further decrease to 42.78%, 1.59% and 16.76% could be seen after one more decade i.e. in 2019. A gradual decrease in area covered by these three classes is an evident that the decreased land has been occupied by some other land use classes. The other two classes considered in the study i.e. rural settlement and water bodies have been increasing in terms of area from 1999 through 2009 to 2019. In 1999, 1.39% and 25.97% of total area respectively were covered by water bodies and rural settlement that increased to 1.56% and 30.76% in 2009. These then further increased to 1.81% and 37.06% in 2019. The percent changes in different classes during the time periods have been calculated as shown in Table 4.8.

Table 4.8: Percent changes for different LULC classes during different time periods

Time period	*Percent change in LULC classes (%)*				
	Dense vegetation	Water bodies	Crop land	Rural settlement	Silted water
1999-2009	-4.05	12.29	-12.28	18.43	-8.47
2009-2019	-5.41	16.04	-18.04	20.49	-20.76
1999-2019	-9.24	30.31	-28.10	42.70	-27.47

These then are graphically represented as bar diagrams in Fig.4.22(a), (b) and (c) respectively for 1999-2009, 2009-2019 and 1999-2019. During the first decade from 1999 to 2009, rural settlement increased the maximum by 18.43% in contrast to maximum decrease in crop land by 12.28%. Also, dense vegetation and silted water decreased by 4.05% and 8.47% respectively and water bodies increased by 12.29%. Moving to the next decade from 2009 to 2019, again the rural settlement and water bodies increased by 20.49% and 16.04% respectively leading to 5.41%, 18.04% and 20.76% decrease in dense vegetation, crop land and silted water. Again, when the two-decade period has been considered altogether from 1999 to 2019, overall increase in rural settlement and water bodies in the basin are by 42.70% and 30.31% respectively. area covered by dense vegetation, crop land and silted water have been decreased by 9.14%, 28.10% and 27.47% respectively.

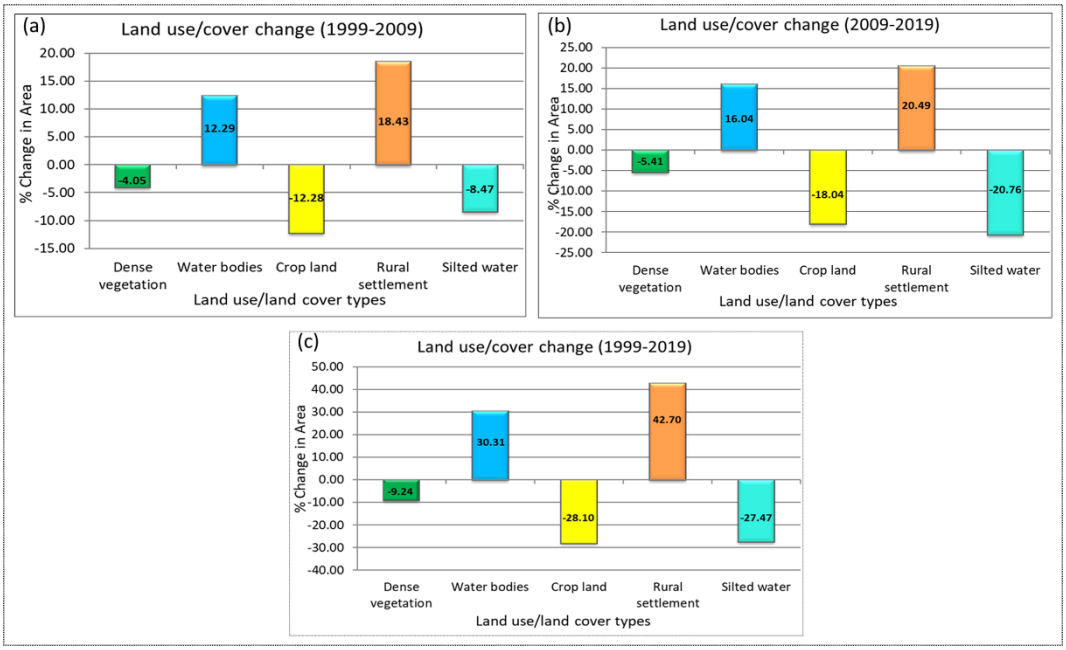

Fig.4.22: Graphical representation of LULC changes during (a)1999-2009, (b) 2009-2019 and (c) 1999-2019

From the result, the continuos decrease in crop land and dense vegetation can be attributed to increase in rural settlement. Significant population growth and migration of people from nearby places to the basin is the reason behind decrease in vegetation cover. As much of the area started to be covered by human settlement, the area covered by agricultural crop land in turn started decreasing.

4.4.1 prediction of LULC using CA-MARKOV Model

Based on the available LULC images, the future LULC of 2035, 2065 and 2085 have been predicted using CA-Markov model. The transition probability matrices have been created using the Markov Model. The Markov transition area file and transition suitability image collection have been incorporated in the model for future prediction.

The change analysis carried out in the land change modeler between the base years 1999 and 2019 are shown in Fig. 4.23.

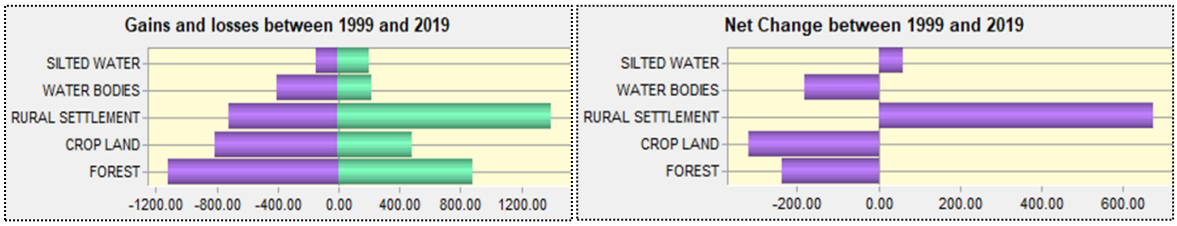

Fig.4.23: Change analysis in LCM between 1999 and 2019

From the figure, it is clear that apart from rural settlement and silted water, other LULC classes decrease in area during 1999 and 2019. Contribution to net change in individual LULC is shown in Fig. 4.24.

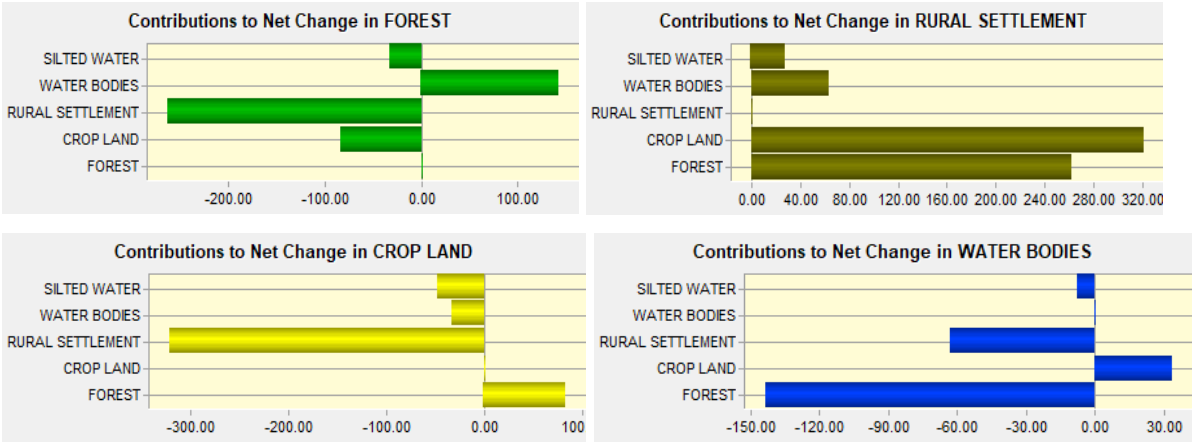

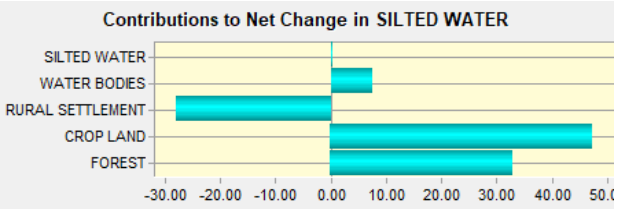

Fig.4.24: Contribution to net change in different LULC class

The exchange and spatial trends of change between different classes during 1999-2019 are given in Fig. 4.25 and Fig.4.26 respectively.

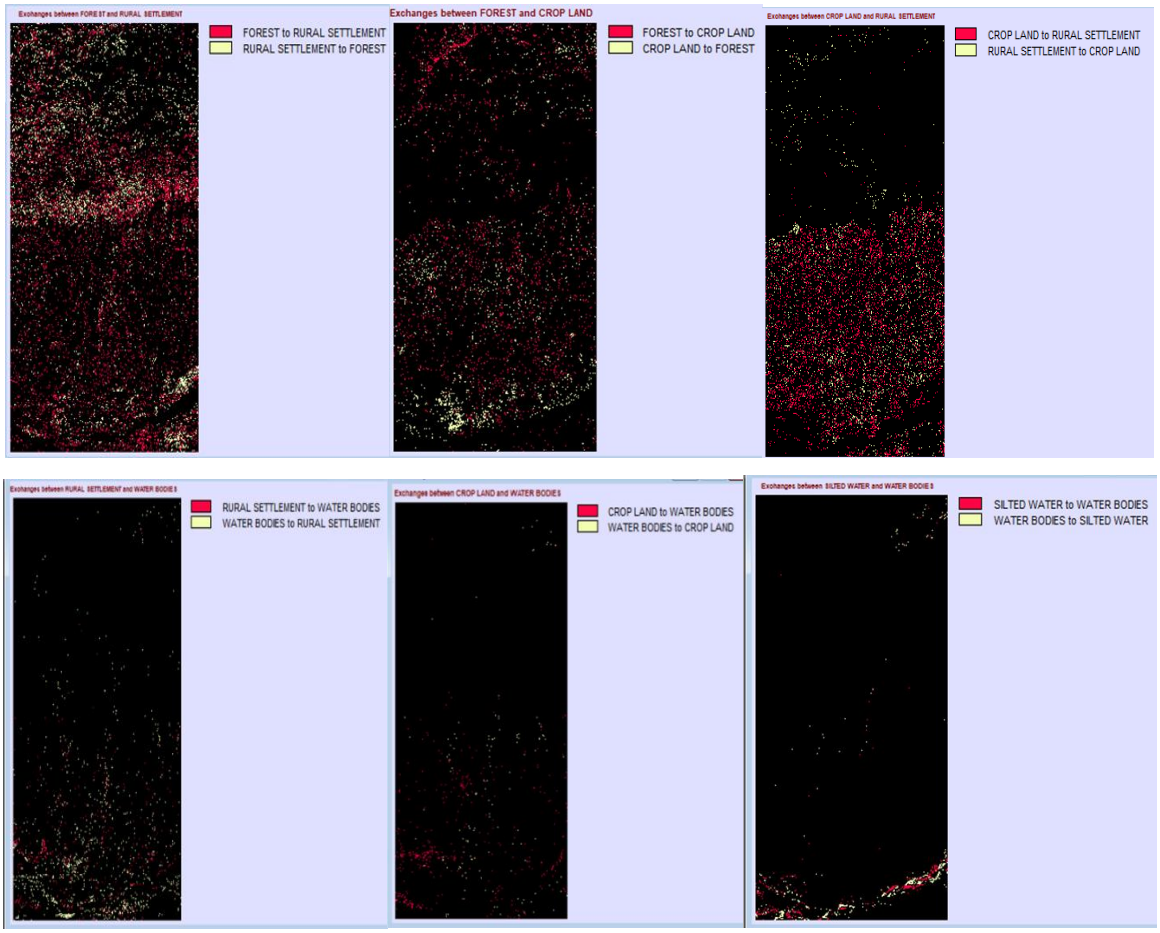

Fig.4.25: Exchange between different classes during 1999-2019

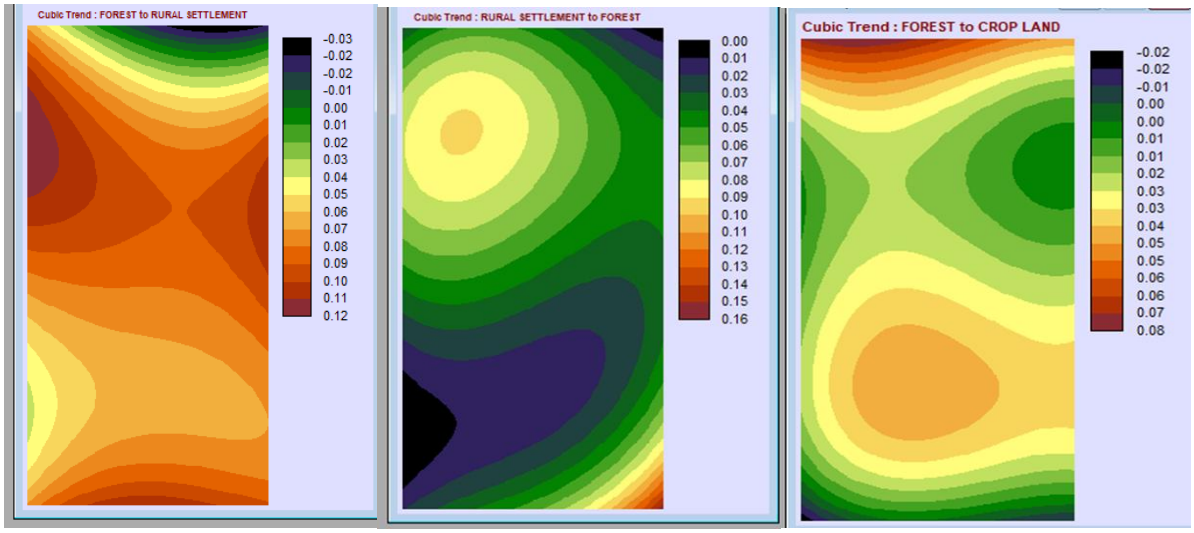
Cubic Trend : FOREST to RURAL SETTLEMENT
-0.03
-0.02
-0.02
-0.01
0.00
0.01
0.02
0.03
0.04
0.05
0.06
0.07
0.08
0.09
0.10
0.11
0.12
Cubic Trend : RURAL SETTLEMENT to FOREST
0.00
0.01
0.02
0.03
0.04
0.05
0.06
0.07
0.08
0.09
0.10
0.11
0.12
0.13
0.14
0.15
0.16
Cubic Trend : FOREST to CROP LAND
-0.02
-0.02
-0.01
0.00
0.00
0.01
0.01
0.02
0.03
0.03
0.04
0.05
0.05
0.06
0.06
0.07
0.08

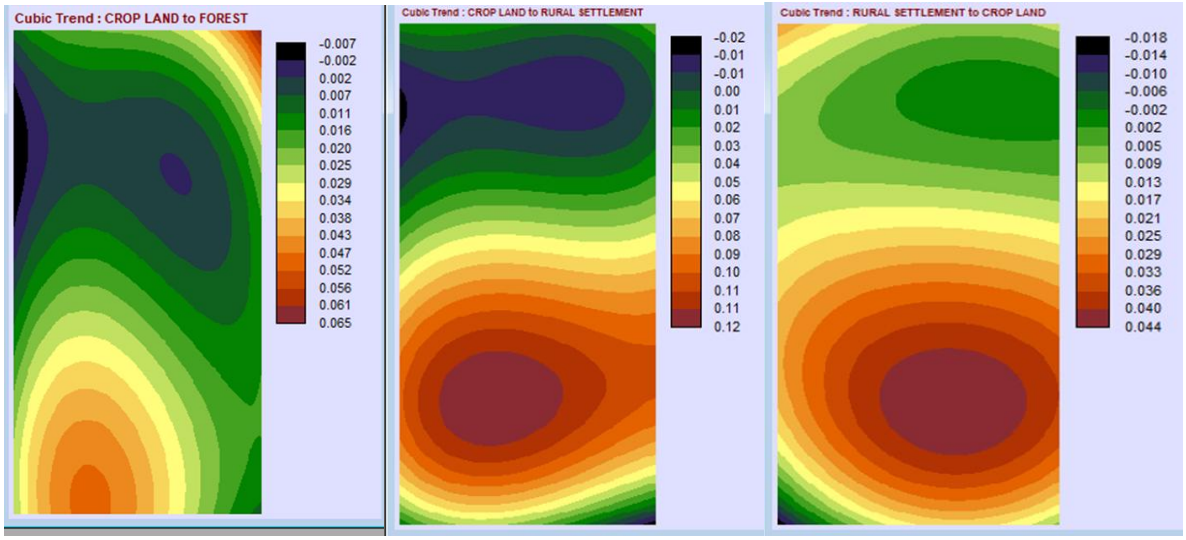
Cubic Trend : CROP LAND to FOREST
-0.007
-0.002
0.002
0.007
0.011
0.016
0.020
0.025
0.029
0.034
0.038
0.043
0.047
0.052
0.056
0.061
0.065
Cubic Trend : CROP LAND to RURAL SETTLEMENT
-0.02
-0.01
-0.01
0.00
0.01
0.02
0.03
0.04
0.05
0.06
0.07
0.08
0.09
0.10
0.11
0.11
0.12
Cubic Trend : RURAL SETTLEMENT to CROP LAND
-0.018
-0.014
-0.010
-0.006
-0.002
0.002
0.005
0.009
0.013
0.017
0.021
0.025
0.029
0.033
0.036
0.040
0.044

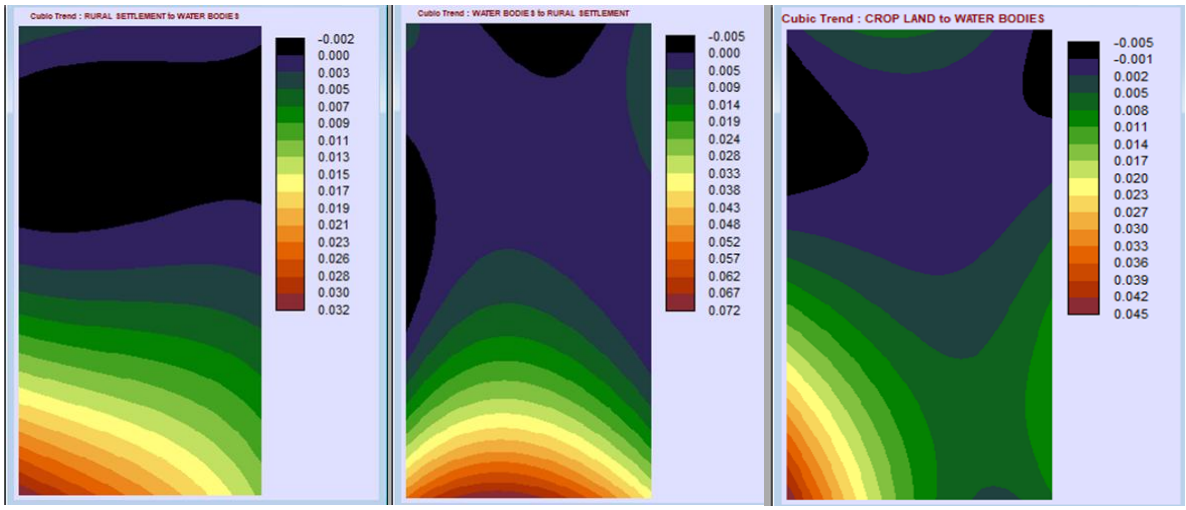
Cubic Trend : RURAL SETTLEMENT to WATER BODIES
-0.002
0.000
0.003
0.005
0.007
0.009
0.011
0.013
0.015
0.017
0.019
0.021
0.023
0.026
0.028
0.030
0.032
Cubic Trend : WATER BODIES to RURAL SETTLEMENT
-0.005
0.000
0.005
0.009
0.014
0.019
0.024
0.028
0.033
0.038
0.043
0.048
0.052
0.057
0.062
0.067
0.072
Cubic Trend : CROP LAND to WATER BODIES
-0.005
-0.001
0.002
0.005
0.008
0.011
0.014
0.017
0.020
0.023
0.027
0.030
0.033
0.036
0.039
0.042
0.045

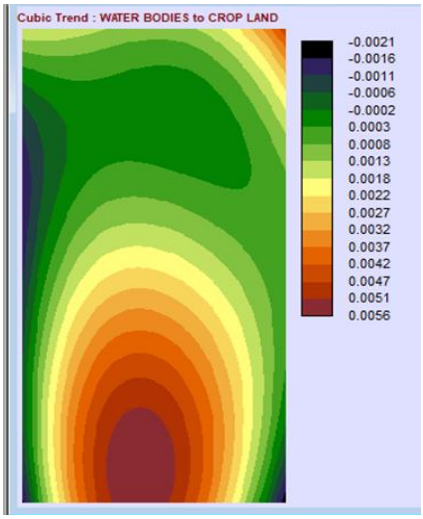

Fig.4.26: Spatial trends of change between different classes during 1999-2019

Fig. 4.27 shows the transition probability matrices for 2035, 2065 and 2085 respectively.

Given : Probability of changing to :

	Cl. 1	Cl. 2	Cl. 3	Cl. 4	Cl. 5
Class 1 :	0.7772	0.0518	0.1407	0.0151	0.0153
Class 2 :	0.0583	0.7042	0.1947	0.0190	0.0238
Class 3 :	0.1515	0.0687	0.7520	0.0207	0.0071
Class 4 :	0.4078	0.0216	0.2102	0.2530	0.1073
Class 5 :	0.1374	0.0467	0.1955	0.2071	0.4133

Transition probability matrix for 2035

Given : Probability of changing to :

	Cl. 1	Cl. 2	Cl. 3	Cl. 4	Cl. 5
Class 1 :	0.5529	0.1101	0.2859	0.0262	0.0249
Class 2 :	0.1834	0.3992	0.3537	0.0314	0.0323
Class 3 :	0.2980	0.1308	0.5243	0.0278	0.0191
Class 4 :	0.4650	0.0909	0.3327	0.0563	0.0552
Class 5 :	0.3525	0.0997	0.3474	0.0919	0.1085

Transition probability matrix for 2065

Given : Probability of changing to :

	Cl. 1	Cl. 2	Cl. 3	Cl. 4	Cl. 5
Class 1 :	0.4834	0.1307	0.3311	0.0284	0.0264
Class 2 :	0.2476	0.3030	0.3859	0.0323	0.0312
Class 3 :	0.3380	0.1473	0.4629	0.0290	0.0228
Class 4 :	0.4431	0.1191	0.3595	0.0397	0.0386
Class 5 :	0.3876	0.1232	0.3736	0.0560	0.0596

Transition probability matrix for 2085

Fig. 4.27: Transition probability matrices for 2035, 2065 and 2085

Based on the changes in LULC classes from 1999 to 2019, the LULC for the years 2035, 2065 and 2085 have been predicted using the CA-MARKOV model. Fig.4.28 shows the projected LULC maps for these three years.

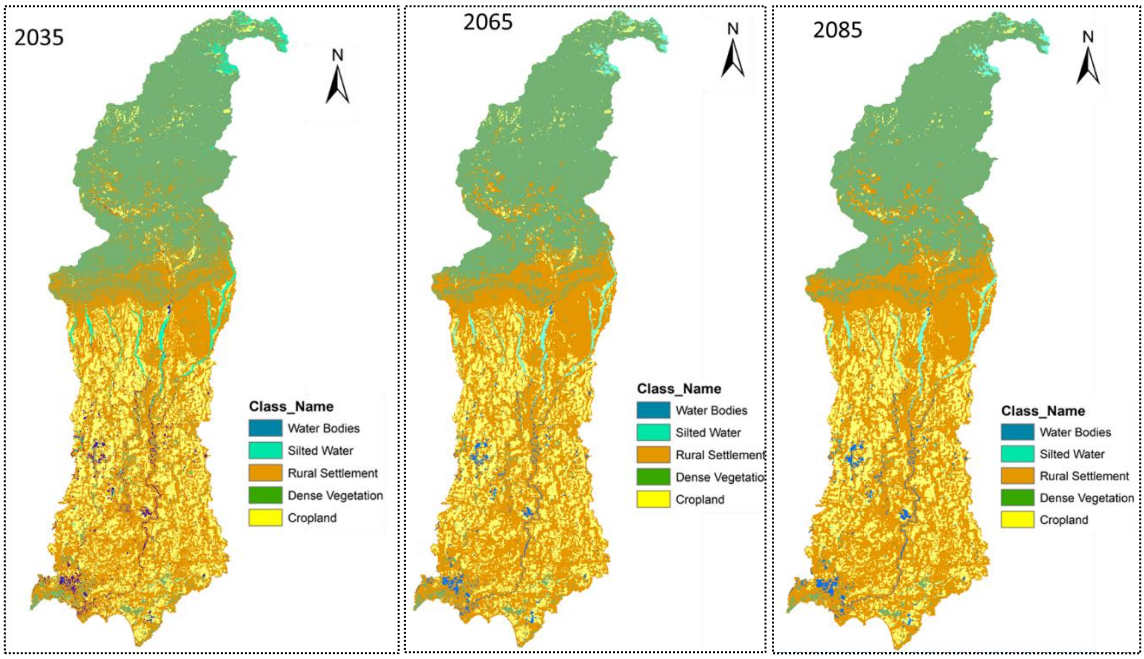

Fig. 4.28: Projected LULC maps for 2035, 2065 and 2085

The change analyses carried out in LCM for 2019-35, 2035-65 and 2065-85are shown in Fig. 4.29, 4.30 and 4.31 respectively.

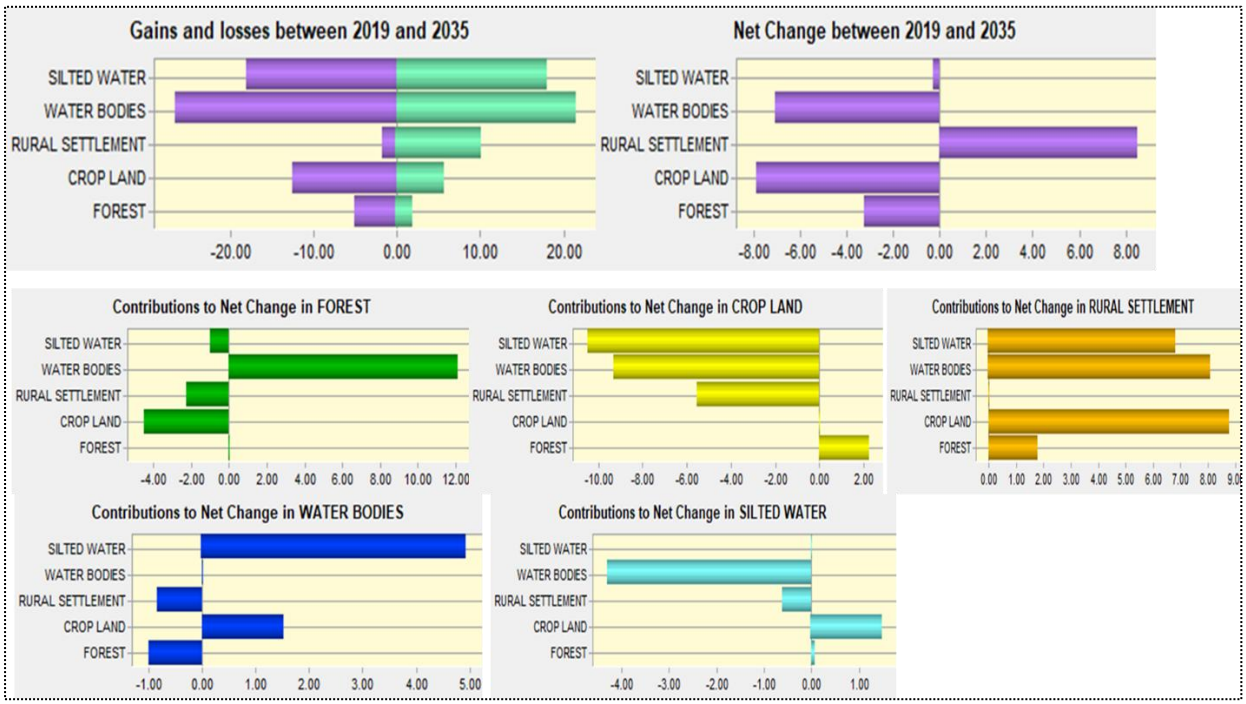

Fig.4.29: Change analysis carried out in LCM from 2019-35

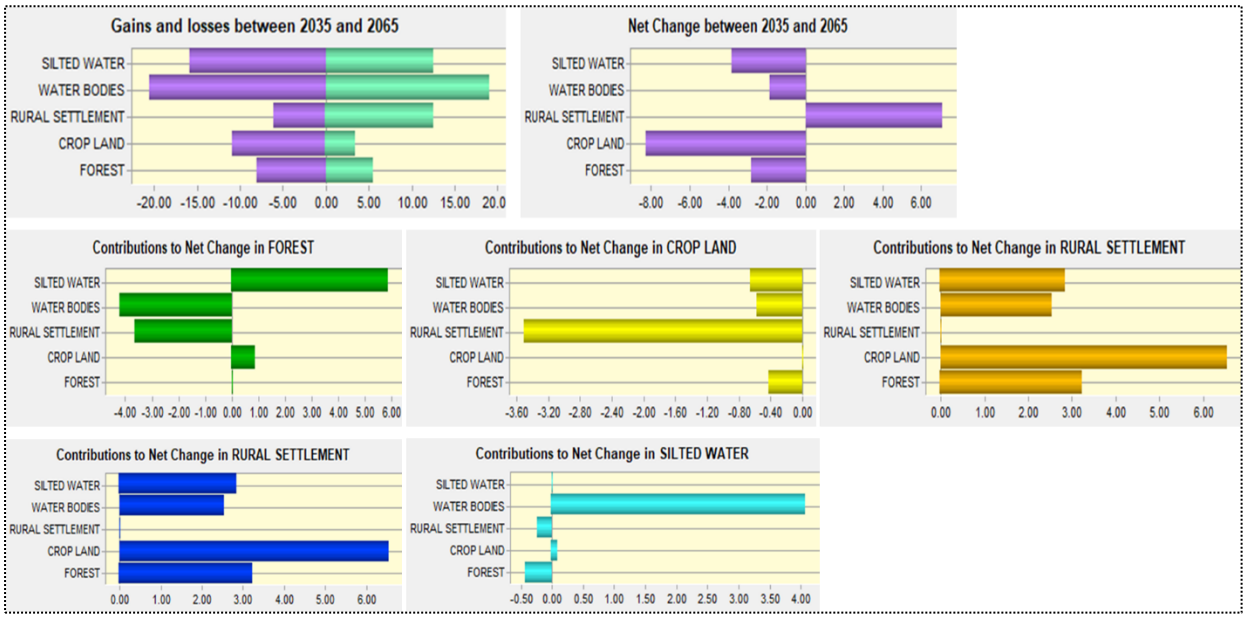

Fig.4.30: Change analysis carried out in LCM from 2035-65

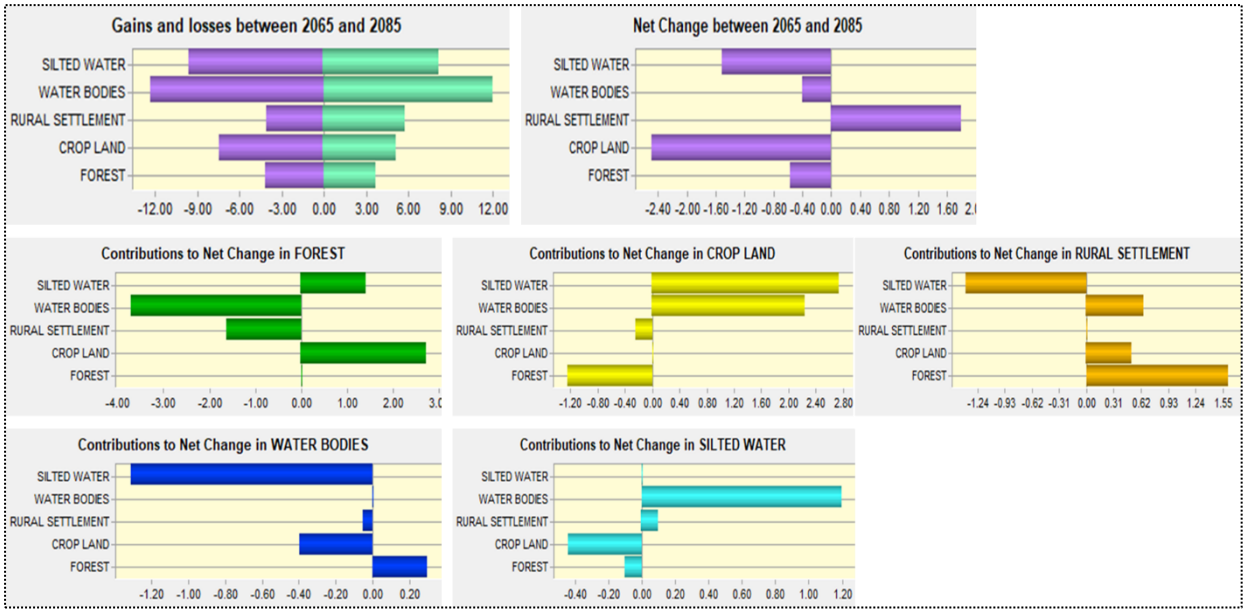

Fig.4.31: Change analysis carried out in LCM from 2065-85

From the above figures it is observed that between the time periods, the net change in rural settlement is positive in all the three cases, while for other classes, the net change is negative.

4.5 Runoff simulation using SWAT

4.5.1 Catchment chracteristics

The Puthimari basin has been divided into 9 sub-basins and 94 HRUs. The detail of land use, soil and slope as obtained from SWAT are given in Table 4.9, 4.10 and 4.11 respectively.

Table 4.9: Details of land use

LULC category	LULC class	Area (Ha)	Watershed area (%)
Forest- mixed	FRST	102725.88	65.94
Agricutural land- Generic	AGRL	14574.53	9.36
Residential- Low density	URLD	30792.59	19.77
Water	WATR	7696.98	4.94

Forest is the dominant land cover in the catchment covering 65.94% of the watershed followed by low density residential (19.77%), agricultural land (9.36%) and water (4.94%) respectively.

Table 4.10: Details of soil

Soil category	Soil class	Area (Ha)	Watershed area (%)
	Pt1	6437.19	4.13
	Pt2	117715.30	75.56
	Pt3	11419.97	7.33
	Pt4	949.72	0.61
	Pt5	3118.27	2.00
	Pt6	233.22	0.15
	Pt8	20.79	0.01
	Pt9	15895.51	10.20

Larger area of the catchment is covered by the Pt2 type of soil (75.56%) followed by Pt9(10.20%) and Pt3 (7.33%). Least area is covered by Pt8 type of soil.

Table 4.11: Details of slope

Slope category	Slope class	Area (Ha)	Watershed area (%)
1	0-10	37722.16	24.21
2	10-20	7262.40	4.66
3	20-30	11195.84	7.19
4	30-50	33065.82	21.22
5	50-9999	66543.76	42.71

The slope of the catchment ranges from 48-4493m. Most of the catchment area (42.71%) has higher slope.

The SWAT model was run on daily basis with two years of warm-up periods. The output hydrology obtained from SWAT simulation for the observed data is shown in Fig. 4.32.

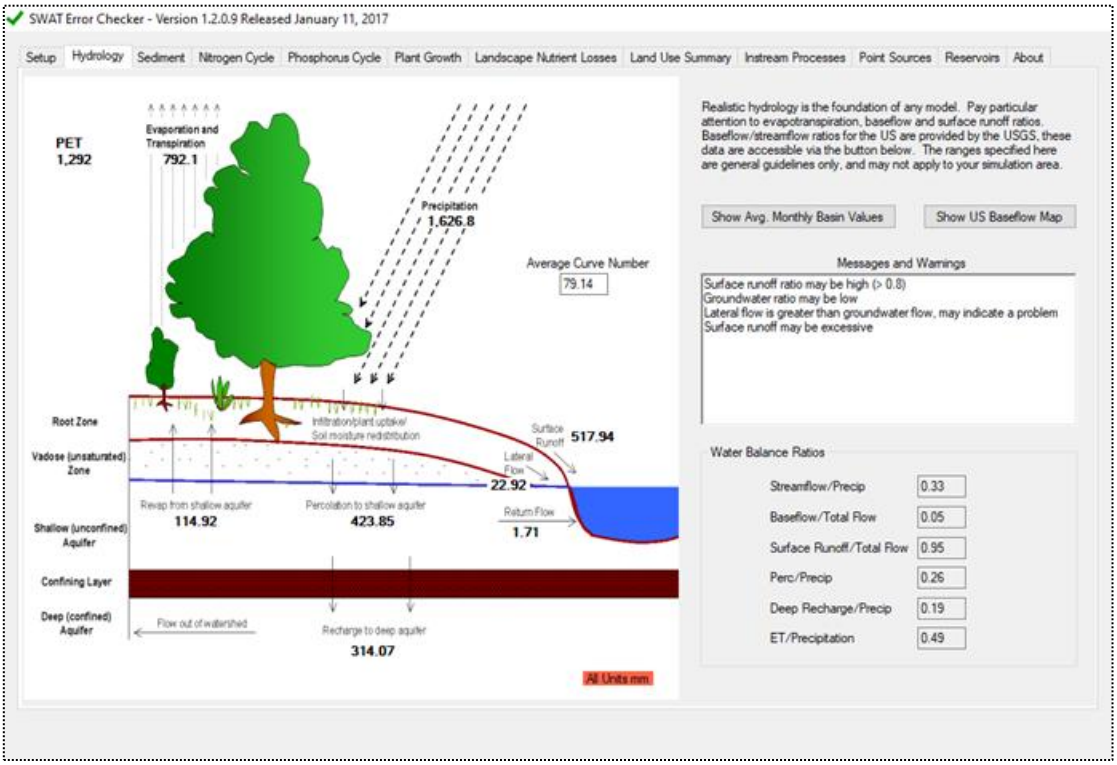

Fig.4.32: Output hydrology of SWAT simulation

4.5.2 Sensitive Parameters

Identifying sensitive parameters enables to focus only on those parameters which affect most the model output during calibration since SWAT model has a number of parameters to deal with. Some parameters do not have any influence on the model output while some may have little effect. Table 4.12 shows the parameters used for sensitivity analysis of flow calibration.

Table 4.12: List of parameters used in sensitivity analysis

Sl. No.	Description of parameter	Fitted value	Min value	Max Value
1.	R__CN2, moisture condition II of Initial SCS runoff curve number	0.018800	-0.2	0.2
2.	V__ALPHA_BF, Baseflow recession constant	0.073	0	1
3.	V__GW_DELAY, Delay time of groundwater	355.500	30	450
4.	V__GWQMN, Threshold depth of water in the shallow aquifer required for return flow to occur	637.00	0	1000
5.	V__SURLAG, Lag time of surface runoff	19.7910	1	24

6.	R__SOL_Z, Depth from soil surface to bottom of layer	-0.2562	-0.3	0.3
7.	R__SOL_AWC, Available water capacity of the soil layer	0.071400	-0.3	0.3
8.	R__SOL_K, Saturated hydraulic conductivity	-0.2814	-0.3	0.3
9.	V__CH_N2, Manning's "n" value for the main channel	0.22890	0	0.3
10.	V__CH_K2, Effective hydraulic conductivity in main channel alluvium	142.050003	0	150
11.	V__OV_N, Manning's "n" value for overland flow	0.099970	0.01	30
12.	R__SOL_BD, Moist bulk density	0.118200	-0.3	0.3
13.	V__EPCO, compensation of Plant uptake factor	0.812890	0.01	1
14.	V__ESCO, compensation of Soil evaporation factor	0.488170	0.01	1
15.	V__RCHRG_DP, Deep aquifer percolation fraction	0.741000	0	1
16.	R__SLSUBBSN, Average slope length	73.980003	10	150
17.	V__GW_REVAP, Groundwater "revap" coefficient	0.189380	0.02	0.2

The global sensitivity analysis for the parameters have been carried out and is summarized as shown in Table 4.13. According to the result from the global sensitivity analysis, the curve number (CN2) was found to be the most sensitive parameter followed by baseflow recession constant (ALPHA_BF), delay time of ground water (GW_DELAY), lag time of surface runoff (SURLAG), and depth from soil surface to bottom layer (SOL_Z) ranking up to fifth position as shown in Table 4.13 below.

Table 4.13: Global sensitivity of the parameters

Parameter Name	t-stat	p-value	sensitivity
R__CN2.mgt	-16.86	0.00	1
V__ALPHA_BF.gw	-15.98	0.00	2
V__GW_DELAY.gw	-2.44	0.01	3
V__SURLAG.bsn	-0.59	0.55	4
R__SOL_Z(..).sol	0.08	0.94	5

R__SLSUBBSN.hru	0.19	0.85	6
V__ESCO.hru	0.31	0.75	7
V__GWQMN.gw	0.38	0.71	8
V__RCHRG_DP.gw	0.58	0.56	9
V__GW_REVAP.gw	0.82	0.41	10
V__EPCO.hru	0.94	0.35	11
R__SOL_K(..).sol	1.55	0.12	12
R__SOL_AWC(..).sol	2.24	0.03	13
R__SOL_BD(..).sol	2.88	0.004	14
V__CH_N2.rte	5.25	0.00	15
V__CH_K2.rte	6.09	0.00	16
V__OV_N.hru	12.39	0.00	17

Each parameter was assigned the rank based on P-value and t-stat. P-value gives the significance of sensitivity and a parameter is more significant if its value is close to zero. Again, t-stat is the measure of sensitivity and larger values are more sensitive.

4.5.3 Model Calibration and Validation

The calibration of SWAT model for runoff was done by using the daily observed runoff data at the outlet of Puthimari watershed for the years 1999 and 2005. The observed and simuated daily discharge has been plotted as shown in Fig. 4.33. The model was calibrated using the sensitive parameters. The 95PPU plot is shown in Fig.4.34. The coefficient of determination (R^2) value for daily runoff for the calibration period was 0.75, the Nash- Sutcliffe coefficient of efficiency (NS) for the same period was found to be 0.74 and the PBIAS is -0.3. In general, the model performs well in predicting the runoff from Puthimari catchment.

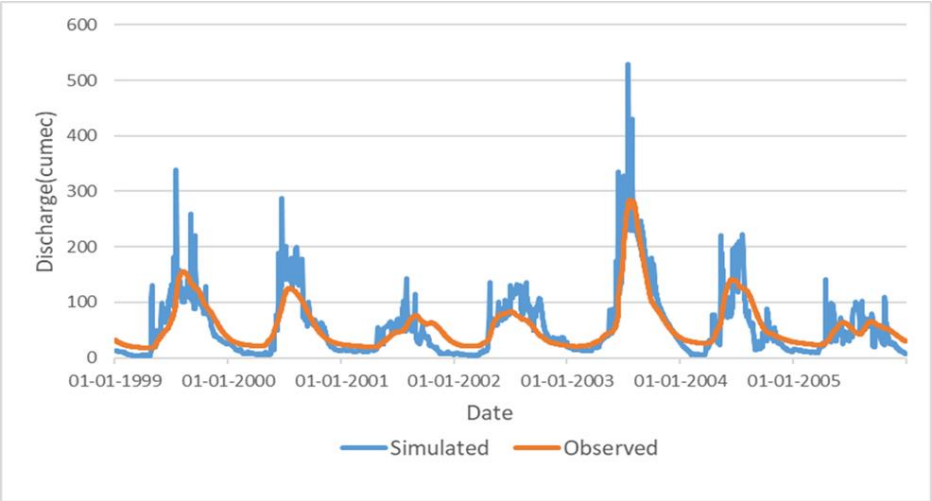

Fig.4.33: Model performance during the calibration period (1999-2005)

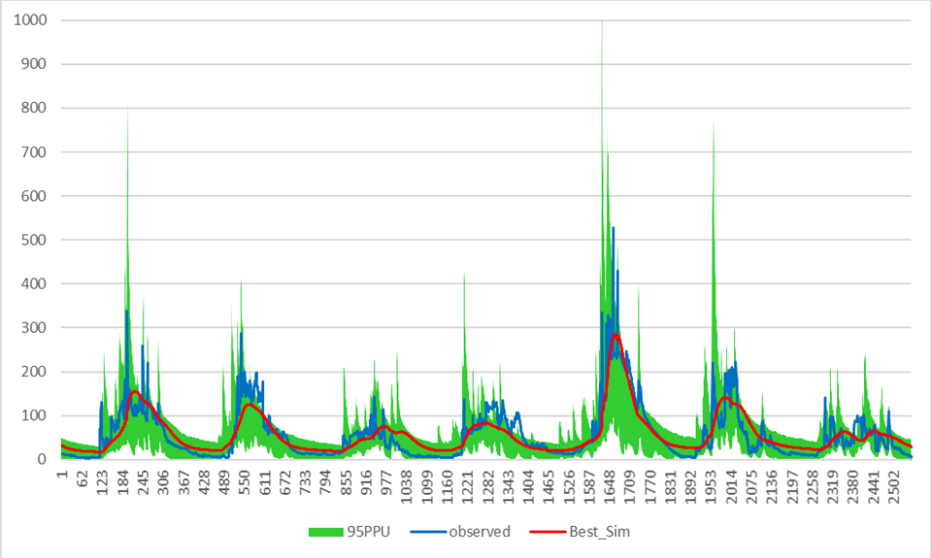

Fig.4.34: Observed and simulated hydrographs of daily streamflow at the Puthimari River Basin from 1999 to 2005 (calibration period). The green shaded part is the 95% prediction uncertainty

The model validation was carried out for daily runoff for the period 2006-2010. The value of R^2, NS and PBIAS for validation are 0.76, 0.77 and -0.27 respectively. The observed and simulated daily runoff for the validation period is shown in Fig. 4.35 and the 95PPU plot is shown in Fig. 4.36.

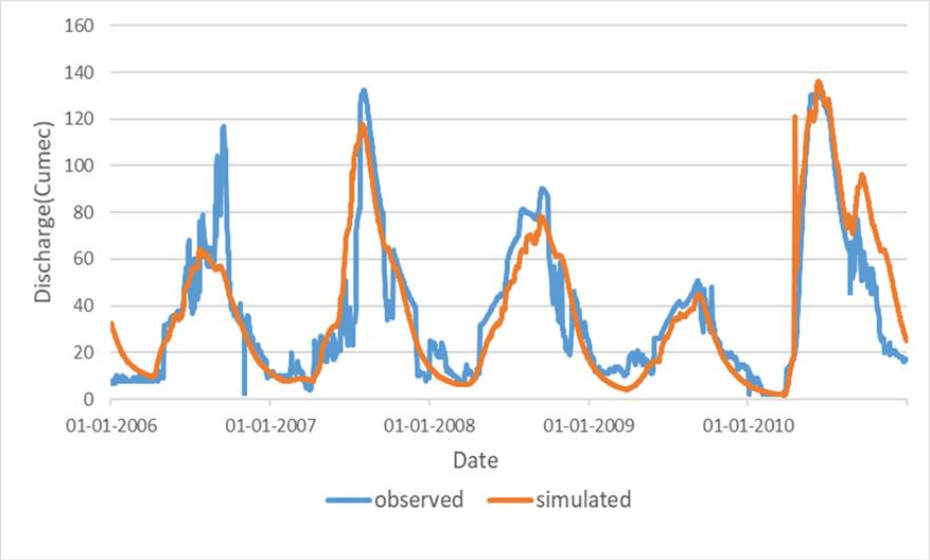

Fig.4.35: Model performance during the validation period (2006-2010)

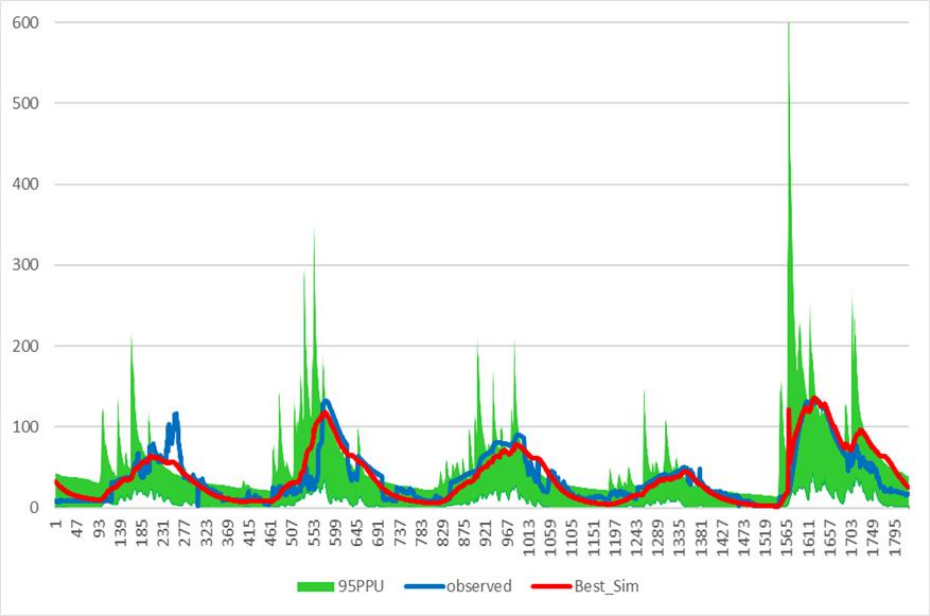

Fig.4.36: Observed and simulated hydrographs of daily streamflow at the Puthimari River Basin from 2006 to 2010 (validation period). The green shaded part is the 95% prediction uncertainty

The model evaluation result for calibration and validation are tabulated in Table 4.14.

Table 4.14: SWAT model performance statistics result

Performance Index	Calibration (1999-2005)	Validation (2006-2010)
NSE	0.74	0.77
R2	0.75	0.79

PBIAS	-3.0	-2.7
P-factor	0.79	0.93
R-factor	0.99	1.10

4.6 Streamflow simulation for different conditions of climate and LULC

4.6.1 Condition of change in both climate and LULC

After calibration and validation, SWAT model was run to analyze the impact of climate change on discharge for various models under both RCP4.5 and RCP8.5 for different time periods and a comparative study has been carried out. The LULC maps of 2035, 2065 and 2085 prepared from CA-Markov model have been used for the period 2025-39, 2050-74 and 2075-99 respectively. Future increase in discharge has been observed for the various models under both the climate scenarios. Fig.4.37 shows the comparative analysis of discharge under RCP4.5.

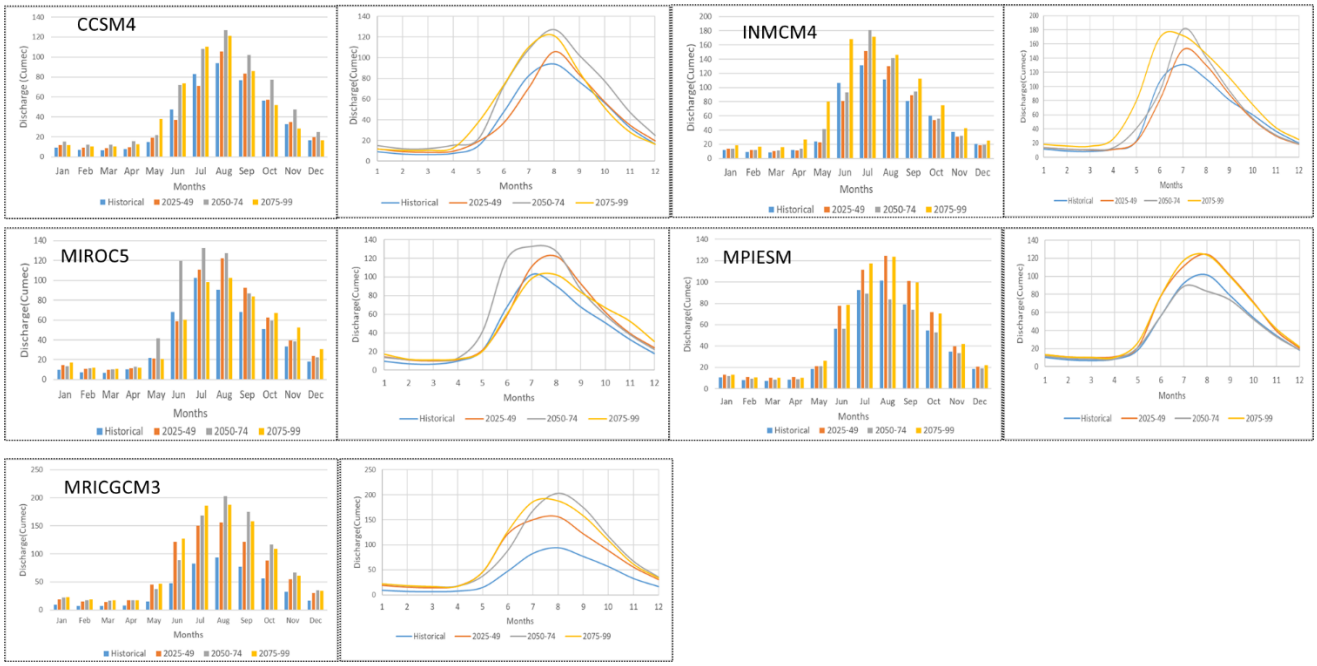

Fig. 4.37: Monthly discharge of different climate models under RCP4.5 for the condition of change in both climate and LULC

Except MPIESM, the maximum discharge for other four models are observed during the period 2050-74 either in the month of July or August. For MPIESM, the maximum discharge is observed in the month of August during 2024-49. Compared to the historical period, the discharge will increase towards the end of the century.

The percent change of discharge between different periods under RCP4.5 is shown in Fig.4.38.

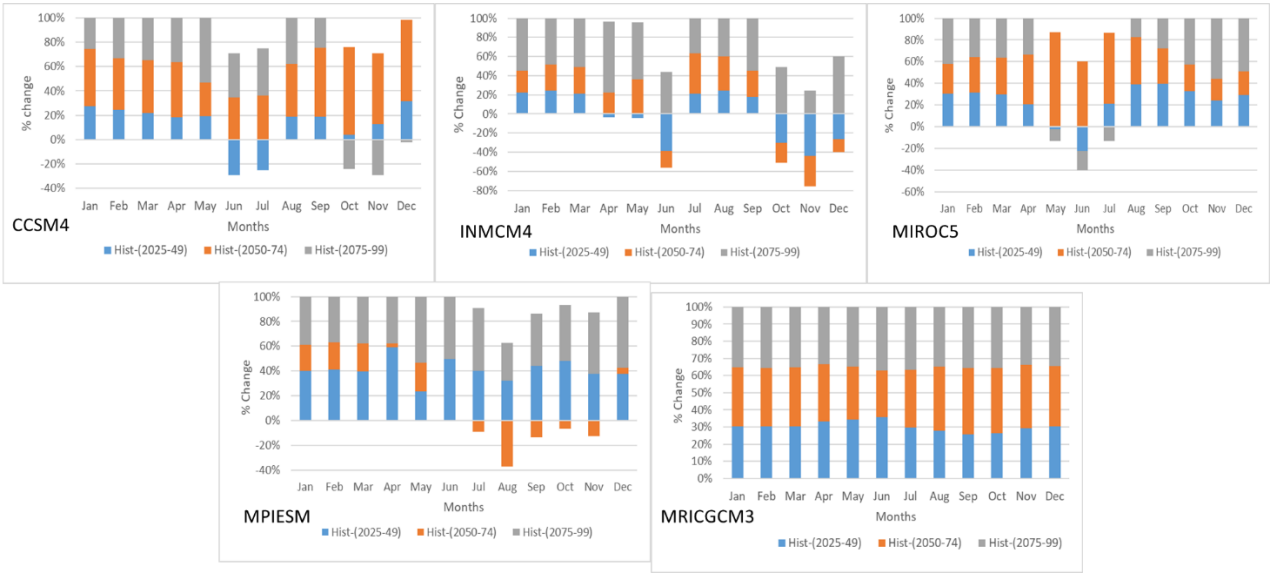

Fig.4.38: Percent change of discharge between different time periods under RCP4.5 for the condition of change in both climate and LULC

For almost all the models the percent increase from historical period is maximum for the period 2075-99 in the month of May. Exception is MIROC5, where discharge decreases in 2075-99 compared to the historical period.

The plots for rainfall vs discharge for the models are shown in Fig.4.39.

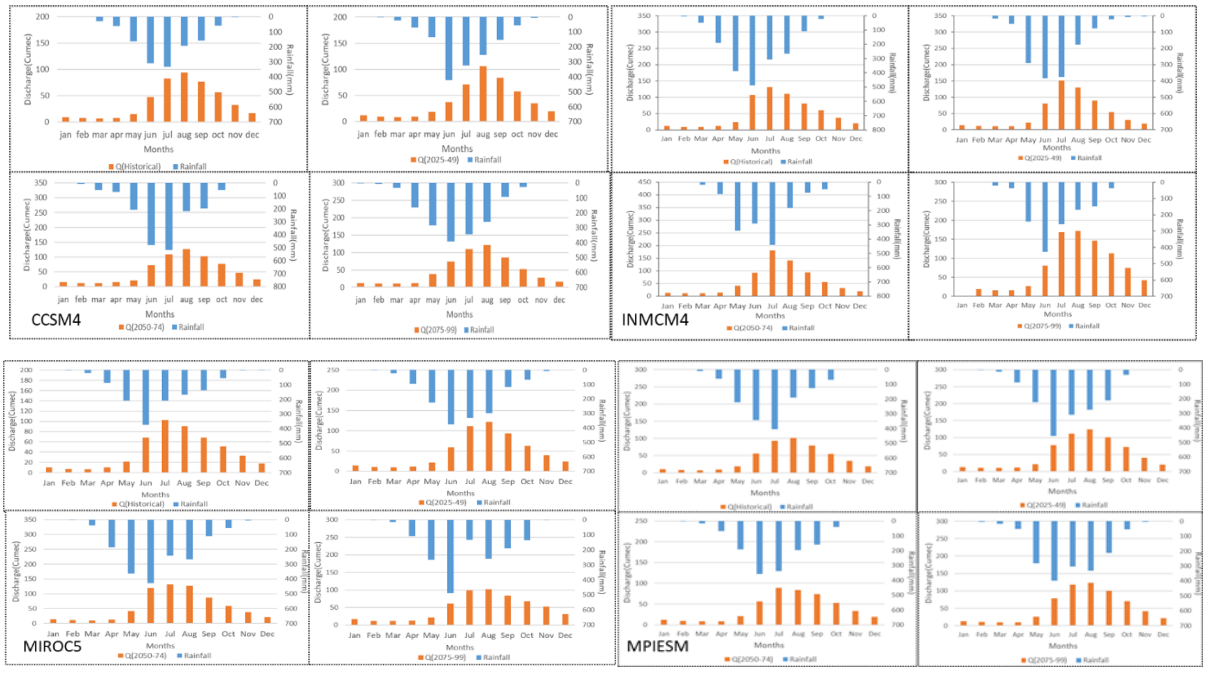

Fig.4.39: Rainfall vs. discharge for the climate models under RCP4.5

For each of the model it is observed that for each time period, more is the rainfall, more is the discharge and vice versa.

The similar analysis has also been performed for RCP8.5. Fig.4.40 shows the discharge variation for the models for different time periods.

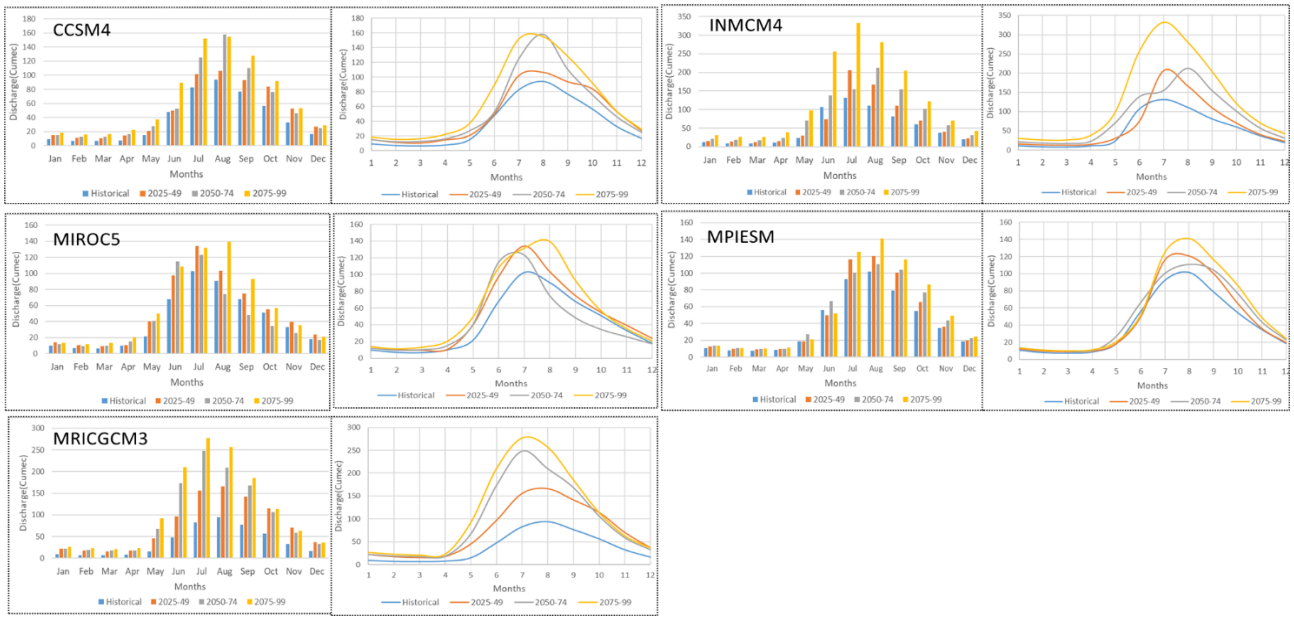

Fig. 4.40: Monthly discharge of different climate models under RCP8.5 for the condition of change in both climate and LULC

Similar to RCP4.5, under RCP8.5 also, the maximum discharge in future is observed in the months of July or August. Discharge is also more during the last two time periods compared to the previous time periods.

The percent change in discharge between different time periods for the models under RCP8.5 are shown in Fig. 4.41.

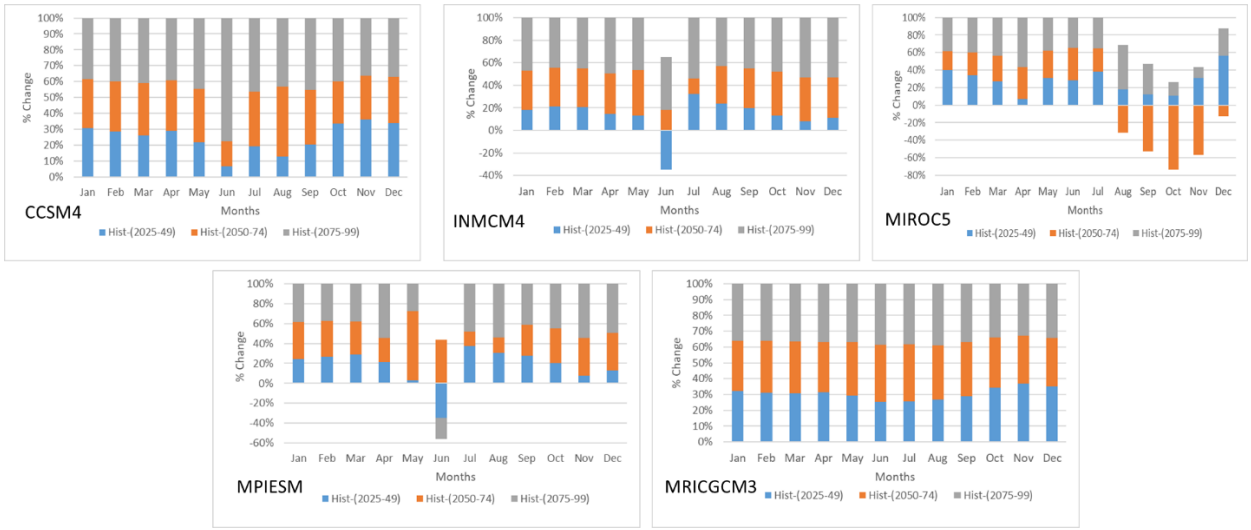

Fig.4.41: Percent change of discharge between different time periods under RCP8.5 for the condition of change in both climate and LULC

For almost all the models, except MPIESM, maximum increase in discharge compared to the historical period is observed during 2075-99 in the month of May.

Fig.4.42 shows the rainfall vs. discharge plots for the models under RCP8.5. The matching of the peaks of rainfall and discharge for the models indicate a direct relationship between them. That is, for more rainfall, increase in discharge for the models are observed in the plots.

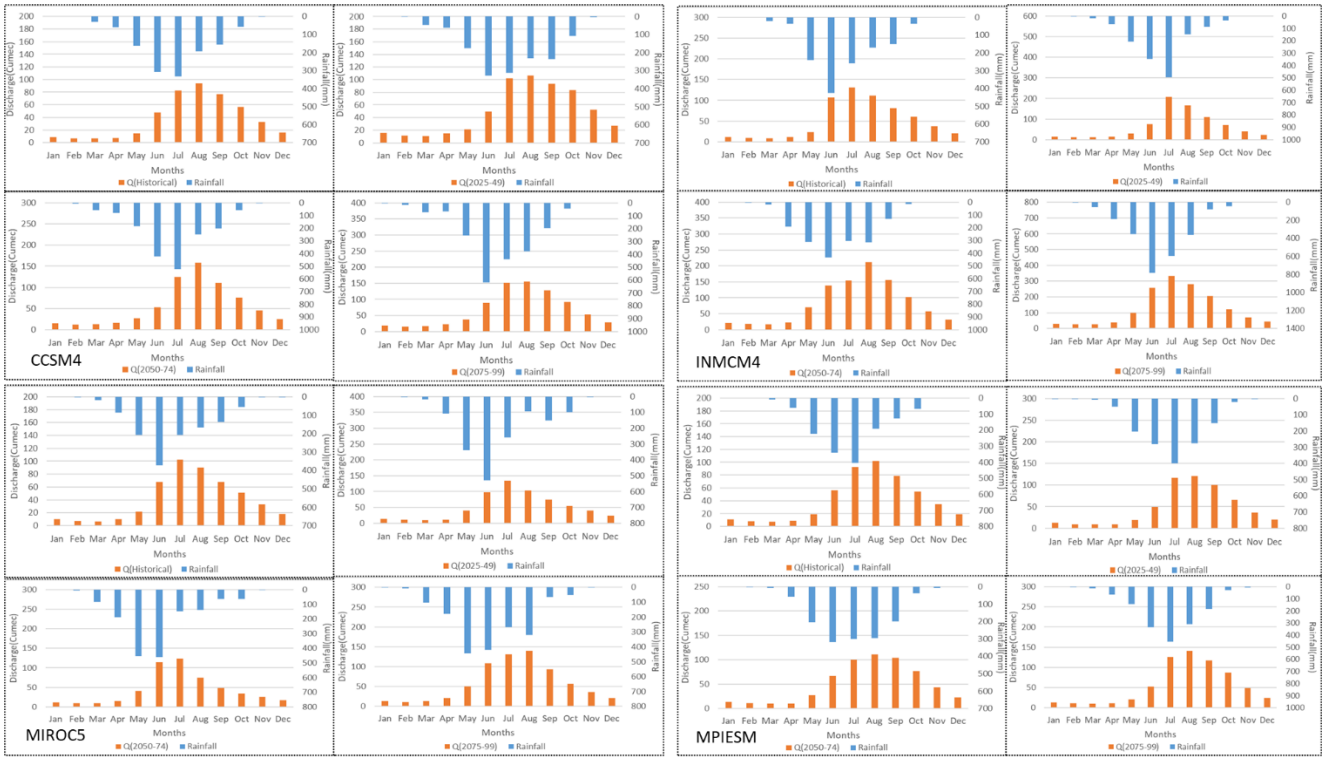

Fig.4.42: Rainfall vs. discharge for the climate models under RCP8.5

4.6.2 Analysis of discharge under the condition of changed climate and constant LULC

In the second condition, keeping the LULC up to 2099 as constant and considering change in climate, the runoff has been simulated for the different time periods for all the models under both RCP4.5 and RCP8.5. The LULC condition of 2019 has been kept constant for future runoff simulation. Fig.4.43 and Fig.4.44 shows the comparative analysis of discharge under this scenario for the climate models for RCP4.5 and RCP8.5 respectively.

Fig.4.43: Future discharge of the climate models under the condition of fixed LULC and change in climate under RCP4.5

For CCSM4, except for the month of May, for all other months, the peak discharge is observed during 2050-74. In case of INMCM4, MPIESM and MRICGCM3, however, the 2075-99 is the period of maximum discharge in all the months. For INMCM4, the maximum discharge from April till August can be observed during 2050-74, in September the maximum discharge is during 2025-49, and in October to December, maximum discharge seems to occur during 2075-99.

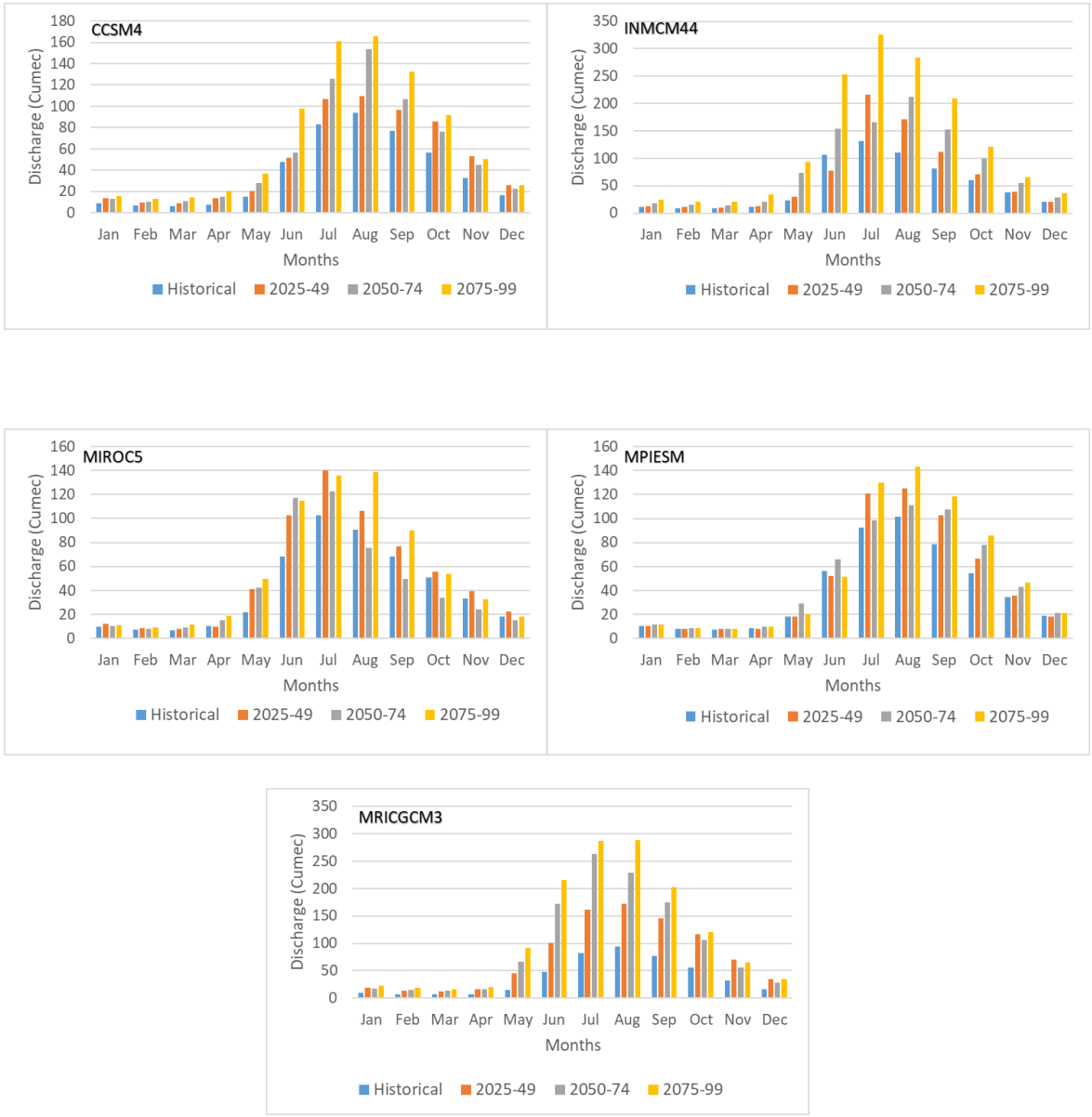

Fig.4.44: Future discharge of the climate models under the condition of fixed LULC and change in climate under RCP8.5

Under RCP8.5, for the condition of constant LULC and change in climate, for all the models, the maximum discharge is observed towards the end of the century, i.e., during 2075-99.

4.6.3 Analysis of discharge under the condition of changed LULC and constant climate

In the third scenario, the climate has been kept constant up to 2099, and the future change in LULC as projected from CA-MARKOV model for the years 2035, 2065 and 2085 have been considered for the periods 2025-49, 2050-74 and 2075-99 respectively to simulate the future

runoff. Fig. 4.45 shows the comparison of future discharge for different time periods for the models.

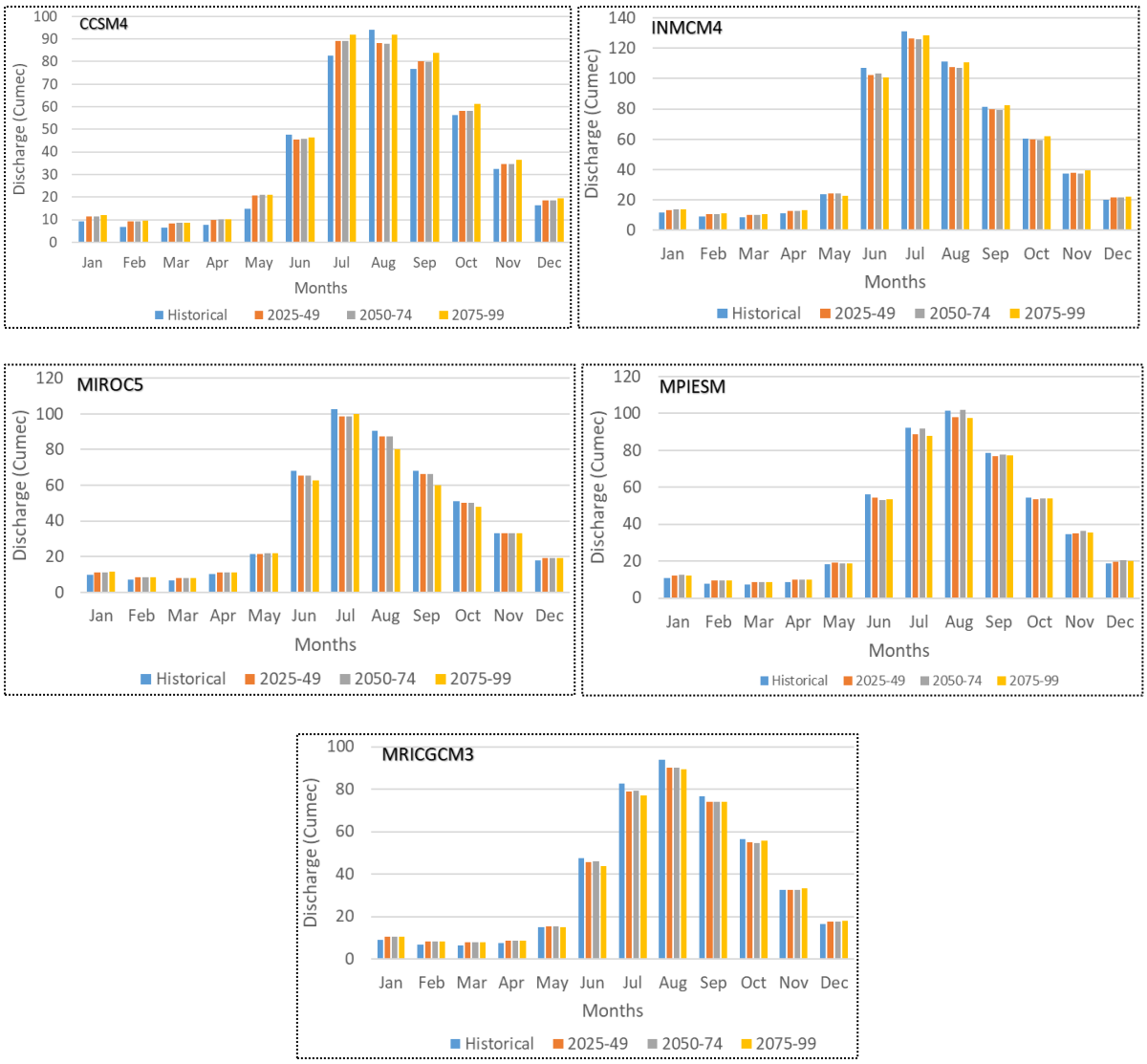

Fig.4.45: Future discharge comparison for different models under the condition of constant climate and changing LULC.

For CCSM4, for all the months, except in the month of August, the highest discharge can be seen during the end period. For other models, the variation in discharge during different time periods is minor. Maximum discharge for the models can be seen either during 2050-74 or during 2075-99.

The results from these conditions indicate that the impact of climate change on future discharge of river Puthimari is more compared to the solo impact of change in LULC.

4.7 Simulation of sediment yield for Puthimari basin using SWAT-ANN based hybrid model

As discussed in the previous chapter, the sediment yield for the Puthimari has been simulated by developing one hybrid SWAT-ANN approach. The runoff as simulated from SWAT and daily rainfall over the basin have been fed as input to the model to simulate the sediment yield.

Coefficient of correlation (R) values for training, validation and testing as obtained from the ANN model were 0.83, 0.94 and 0.91 respectively with and overall R of 0.85 for 15 nos. of neurons. The future sediment yield obtained for the Puthimari basin for the five climate models under RCP4.5 and RCP8.5 are shown in Fig4.46 and Fig4.47 respectively.

Fig.4.46: Future sediment yield for the climate models under RCP4.5

Under RCP4.5, for CCSM4, sediment yield is found to be maximum in June during 2050-74 and is minimum during 2025-49 in the month of February. For INMCM4, from May till October, a sudden rise in sediment yield is observed during the end period compared to the previous periods. The maximum is observed in the month of August during 2075-99 followed by the months July, September and June respectively during the same period. For MIROC5 however, though the sediment yield increases in each period chronologically till the month of May, the reverse could be seen from June to October where, sediment yield in future periods is less compared to the historical period. For MPIESM also, sediment yield in the historical period is more. In case of MRICGCM3, maximum sediment yield in future is observed either during 2050-74 or 2075-99.

Fig.4.47: Future sediment yield for the climate models under RCP8.5

Under RCP8.5, for CCSM4, a continuous increase in sediment yield can be seen till the end period. For INMCM4, sediment yield in the months of June and July are maximum during 2075-99. For other months, mostly a continuous decrease in yield can be seen from 2025 to 2099. For MIROC5, for January-May, and November and December sediment yield is observed to be maximum during 2075-99. For the rest of the months, sediment yield in future decreases compared to the historical period. In case of MPIESM, except July, August and September, for all other months, the historical sediment yield is more compared to future. For MRICGCM3, huge increase in sediment yield could be observed from May till September during 2075-99.

CHAPTER-5

SUMMARY AND CONCLUSIONS

The aim of the present study is to determine the impact of climate change on discharge and sediment yield of the Puthimari river which is a north bank tributary of the mighty river Brahmaputra. The Puthimari watershed has been delineated in ArcSWAT using ASTERGDEM of 30m resolution. The area of the catchment is 3225.47km^2. Taking the downscaled precipitation and temperature data from five different CMIP5 models, the rainfall and temperature over the basin has been analyzed for both historical (1980-2005) and future three different time periods (2024-49, 2050-74 and 2075-99) under RCP4.5 and RCP8.5. Under both the RCPs, maximum rainfall for different time periods were observed in the month of June and July. The Mann-Kendall test was performed for the trend analysis and the nature of the trends were determined based on the Z statistics for both monthly and seasonal rainfall. Different models resulted in different types of rainfall trends However, for almost all the models, trends for the months of January and December are insignificant and for remaining months it varies from model to model for different time periods. Apart from few exceptions, for most of the models, rainfall under RCP8.5 is more than that under RCP4.5. All the models agreed to the fact that the future temperature over the basin will increase under the two climate change scenarios. A linear trend analysis has been performed for maximum and minimum temperature under both the RCPs. Rising trends were observed in all the cases though the trends were not much significant. However, steeper trends were observed under RCP 8.5 compared to those under RCP 4.5.

The LULC maps of the basin have been prepared for 1999. 2009 and 2019 using supervised classification technique and maximum likelihood classifier algorithm. Five different LULC classes have been considered, viz., dense vegetation, water bodies, silted water, crop land and rural settlement. From change detection analysis, it has been found that the area covered by dense vegetation, water bodies and silted water gradually decreases and area covered by crop land and rural settlement gradually increases during this two-decades period. Using CA Markov model, the future LULC maps for 2035, 2065 and 2085 have been prepared and similar trend of change in future LULC has been observed for the Puthimari basin.

The SWAT hydrological model was successfully implemented in the Puthimari catchment to assess impact of climate change on discharge and sediment yield of the basin. The performance and applicability of SWAT model was successfully evaluated through model calibration and validation. The performance of the model was satisfactory with good statistical values of Nash-Sutcliffe (NSE > 0.7) and correlation coefficient (R^2 > 0.7). Three different conditions have been considered for assessing the future discharge of river Puthimari. First, change in both climate and LULC have been considered. In the second condition, the LULC was kept constant throughout the future and only future climate change was taken into consideration. In the third condition however, Climate was kept constant for the future and change in LULC in the basin was considered to analyse discharge. Not much difference can be seen between the first two conditions. However, for the third condition, where climate was kept constant, only little variation in resultant discharge between different time periods are observed for each month. This indicates more impact of climate change on future discharge of Puthimari compared to future LULC change.

To analyse the impact of climate change on future sediment yield of Puthimari basin, a SWAT-ANN base hybrid model was developed. The method adopted was non-linear autoregressive with exogeneous input (NARX). The output runoff from SWAT model and rainfall were fed as the input to the model. The model performed well with overall R value of 0.85. Except few models, for rest of the models, sediment yield increases towards the end of the century under both RCP4.5 and RCP8.5.

References

Adepoju, M.O., Millington, A.C. and Tansey, K.T. (2006). Land Use/ Land Cover Change Detection in Metropolitan Lagos (Nigeria): 1984–2002. American Society for Photogrammetry and Remote Sensing, Annual Conference, Reno, Nevada, May 1–5.

Akbari, S.and Singh, R. (2012). Hydrological modelling of catchments using MIKE SHE. *IEEE*-International Conference on Advances in Engineering, Science and Management, 335–340.

Arnell, N. W. (2004). Climate change and global water resources: SRES emission and socio-economic scenarios. Global Environ. Change, 14: 31–52.

Betts, R.A., Boucher, O., Collins, M., Cox, P.M., Falloon, P.D., Gedney, N., Hemming, D.L., Huntingford, C., Jones, C.D., Sexton, D.M.H., and Webb, M.J.(2007). Projected increase in continental runoff due to plant responses to increasing carbon dioxide. Nature,448: 1037-1041.

Bhagawat, R. (2011). Application of remote sensing and GIS, land use/land cover change in Kathmandu metropolitan city. Nepal. J. Theor. Appl. Inform. Technol., 23 (2): 80–86.

Chakrapani, G. J. (2005). Factors controlling variations in river sediment loads. Current Science, 88: 569–575.

Chander, G., Markham, B.L. and Helder, D.L. (2009). Summary of current radiometric calibration coefficients for Landsat MSS, TM, ETM+, and EO-1 ALI sensors. Rem. Sen. Envi., 113 (5): 893–903.

Chandralal, R., Arnold, K., Hedwig, D. et al. (2009). The dynamics of shifting cultivation captured in an extended constrained cellular automata land use model, Ecological Modelling 220: 2302–2309.

Changchun, X., Yaning, C. and Weihong, L. (2008). Potential impact of climate change on snow cover area in the Tarim River basin. Environ. Geol., 53: 1465-1474.

Cheng, H., Ouyang, W., Hao, F., Ren, X., and Yang, S. (2007). The nonpoint-source pollution in livestockbreeding areas of the Heihe River basin in Yellow River. Stochastic Environmental Research and Risk Assessment, 21: 213–221.

Cigizoglu, H.K. (2004) Estimation and forecasting of daily suspended sediment data by multi layer perceptrons. Advances Water Res,. 27 :185-195.

Das, L., Dutta, M., and Mezghani, A..(2018). Benestad, R.E. Use of observed temperature statistics in ranking CMIP5 model performance over the Western Himalayan Region of India. Int. J. Climatol., 38, 554–570.

Dash S. K., Sharma N., Pattnayak K. C., Gao, X. J. and Shi Y. (2012) 'Temperature and precipitation changes in the north-east India and their future projections', Global and Planetary Change, Vo. 98–99, pp. 31–44.

Demirel, M.C., and Moradkhani, H. (2016) Assessing the impact of CMIP5 climate multi-modeling on estimating the precipitation seasonality and timing', Climatic Change, 135(2):.357–372.

Dhar, O.N. and Nandargi, S. (2000). A study of floods in the Brahmaputra Basin in India. Int. J. Climatol., 20: 771-781.

Donat, M.G., Lowry, A.L., Alexander, L.V., O'Gorman, P.A., and Maher, N. (2016). More extreme precipitations in the world's dry and wet regions. Nature climate change, 6:508-513.

Dore, M.H.I. (2005). Climate change and changes in global precipitation pattern: What do we know? Environment International, 31(8): 1167-1181.

Dutta R. (2014) 'Climate change and its impact on tea in Northeast India', Journal of Water and Climate Change, Vol.5, No.4, pp. 625-632.

Dwarakish, G.S.and Ganasri, B.P. (2015). Impact of land use change on hydrological systems: A review of current modeling approaches. Cogent Geoscience, 1: 1115691.

Fohrer, N., Haverkamp, S., Eckhardt, K. and Frede, H. (2001). Hydrologic response to land use changes on the catchment scale. Physics and Chemistry of the Earth, Part B 26(7-8): 577-582.

Fu, G., Liu, Z., Charles, S.P., Xu, Z., and Yao, Z. (2013).A score-based method for assessing the performance of GCMs: A case study of southeastern Australia. J. Geophys. Res. Atmos., 118: 4154–4167.

Gaume, E. and Gosset, R. (2003). Over-parameterization, a major obstacle to the use of artificial neural networks in hydrology. Hydrology and Earth System Sciences, 7 (5): 693–706.

Ghosh, P., Mukhopadhyay, A., Chanda, A., Mondal, P., Akhand, A., Mukherjee, S., Nayak, S.K., Ghosh, S., Mitra, D., Ghosh, T., et al.(2017). Application of Cellular automata and Markov-chain model in geospatial environmental modeling—A review. Remote Sens. Appl. Soc. Environ., 5: 64–77.

Ghosh, S., Vittal, H., Sharma, T., Karmakar, S., Kasiviswanathan, K.S., Dhanesh, Y., Sudheer, K.P., and Gunthe, S.S. (2016). Indian summer monsoon rainfall: implecations of contrasting trends in the spatial variability of means and extremes. PLoS ONE, 11(7), e0158670.

Giri, C. and Jenkins, C. (2005). Land cover mapping of Greater Mesoamerica using MODIS data. Can. J. Remote Sensing, 31(4): 274-282.

Glymph, L.M. (1954). Water erosion problems and control on non-irrigated agricultural lands. Contribution to symposium on land erosion, Transactions, American Geophysical Union, 35: 246-252.

Goswami, D.C. (1998). Fluvial Regime and Flood Hydrology of the Brahmaputra River, Assam. Flood Studies in India, Kale V.S. (ed), Memoir 41, Geological Society of India, pp 53-75.

Guhathakrata, P., Rajeevan, M., Sikka, D.R., and Tyagi, A. (2015). Observed change in southwest monsoon rainfall over India during 1901-2011. International journal of climatology, 35(8): 1881-1898.

Guilbert, J. (2016). The Impacts of climate change on precipitation and hydrology in the Northeastern United States,Graduate College Dissertations and Theses, Paper 646, University of Vermont.

Hao, F. H., Zhang, X. S., and Yang, Z. F. (2004). A distributed nonpoint-source pollution model: Calibration and validation in the Yellow River basin. Journal of Environmental Sciences, 16: 646–650.

Intergovernmental Panel on Climate Change (IPCC). (2007a). The Physical Science Basis. Contribution of Working Group I to the Fourth Assessment Report of the IPCC, Geneva.

Intergovernmental Panel on Climate Change (IPCC). (2007b). Climate Change 2007: Mitigation of Climate Change. Contribution of working Group III to the Fourth Assessment Report of the IPCC. IPCC, Geneva.

Intergovernmental Panel on Climate Change (IPCC). (2013). IPCC Fifth Assessment Report - Climate Change 2013: The Physical Science Basis.

Jain S. K., Kumar V. and Saharia, M. (2013) 'Analysis of rainfall and temperature trends in northeast India', International Journal of Climatology, Vol. 33, pp.968–978.

Jones, I.D., Page, T., and Elliott, J.A. (2011). Increases in lake phytoplankton biomass caused by future climate driven changes to seasonal river flow. Global Change Biology, 17: 1809–1820.

Kadel, I., Yamazaki, T., Iwasaki, T., and Abdillah, M.R.(2018). Projection of future monsoon precipitation over the central Himalayas by CMIP5 models under warming scenarios. Clim. Res., 75, 1–21.

Kamga, F.M. (2001). Impact of greenhouses gas induced climate change on the runoff of the upper Benue River (Camernoon). J. Hydrol., 252:145–156.

Knutti, R., and Sedlavcek, J. (2012). Robustness and uncertainties in the new CMIP5climate model projections. Nature Climate Change.

Kothawale D. R. and Kumar, K. R. (2005) 'On the recent changes in surface temperature trends over India', Geophysical Research Letters, Vol. 32(L18714). doi:10.1029/2005GL023528.

Kuldeep, T. and Kamlesh, K. (2011). Land Use / Land cover change detection in Doon valley (Dehradun Tehsil), Uttarakhand: using GIS& Remote Sensing Technique. International Journal of Geomatics and Geosciences, 2(1): 34-41.

Kumar K. R., Kumar, K. K. and Pant G. B. (1994) 'Diurnal asymmetry of surface temperature trends over India', Geophys Res Lett., Vol. 21, pp.677–680.

Kumar R. and Gautam H. R. (2014) 'Climate Change and its Impact on Agricultural Productivity in India', Journal of Climatology & Weather Forecasting, Vo. 2, No.1, DOI: 10.4172/2332-2594.1000109.

Kumar, S., Merwade, V., Kinter, J.L.I., and Niyogi, D. (2013).Evaluation of Temperature and Precipitation Trends and Long-Term Persistence in CMIP5 Twentieth-Century Climate Simulations. J. Clim., 26:4168–4185.

Legesse, D., Vallet-Coulomb, C., and Gasse, F. (2003). Hydrological response of a catchment to climate and land use changes in Tropical Africa: Case study South Central Ethiopia. Journal of Hydrology, 275: 67–85.

Lehmann, J., Coumou, D., and Frieler, K. (2015). Increased record-breaking precipitation events under global warming. Climate change, 132(4):501-515.

Li, J., Liu, Z., Yao, Z., and Wang, R.(2019). Comprehensive assessment of Coupled Model Intercomparison Project Phase 5 global climate models using observed temperature and precipitation over mainland Southeast Asia. Int. J. Climatol., 39: 1–15.

Li, Z., Liu, W.Z., Zhang, X.C., and Zheng, F.L. (2009). Impacts of land use change and climate variability on hydrology in an agricultural catchment on the Loess Plateau of China. Journal of Hydrology, 377: 35-42.

Lin, Y. P., Verburg, H. P., Chang, C. R., Chen, H. Y. and Chen, M. H. (2009). Developing and comparing optimal and empirical land-use models for the development of an urbanized watershed forest in Taiwan.. Landscape and Urban Planning, 92: 242–254.

Lorup, J. K., Refsgaard, J. C. and Mazvimavi, D. (1998). Assessing the effect of land use change on catchment runoff by combined use of statistical tests and hydrological modelling: Case studies from Zimbabwe. Journal of Hydrology, 205: 147–163.

MacCracken, M. C., Barron, E. J., Easterling, D. R., Felzer, B. S., and Karl, T. R.(2003). Climate change scenarios for the U.S. national assessment. Bull. Am. Met. Soc., 84: 1711-1723.

Mahmood, R. and Babel, M.S. (2014) 'Future changes in extreme temperature events using the statistical downscaling model (SDSM) in the trans-boundary region of the Jhelum river basin', Weather and climate extremes, Vol. 5-6, pp.56-66.

Maria, C.M., Wenceslao, G.M., Manuel, F.B., Jose, M.P.S. and Roman, L.C.(2004). Modelling of the monthly and daily behaviour of the runoff of the Xallas River using Box-Jenkins and neural networks methods. Journal of Hydrology, 296: 38–58.

McMullen C.P. and Jabbour, J. (Eds.). (2009) 'Climate Change Science Compendium, UN Environmental Programme, Geneva, pp.72.

Meher, J.K., Das, L., Akhter, J., Benestad, R.E.;, and Mezghani, A.(2017). Performance of CMIP3 and CMIP5 GCMs to Simulate Observed Rainfall Characteristics over the Western Himalayan Region. J. Clim., 30: 7777–7799.

Mehta, A., Sinha, V.K. and Ayachit, G. (2012). Land use/land cover study using remote sensing and GIS in an arid environment. Bull. Envi. Sci. Res., 1 (3–4): 4–8.

Mengistu, A.G., Rensburg, L.D. and Woyessa, Y.E. (2019). Techniques for calibration and validation of SWAT model in data scarce arid and semi-arid catchments in South Africa. Journal of hydrology: Regional studies, 25(2019) 100621.

Mishra, V.N., Rai, P.K. and Mohan, K. (2014). Prediction of land use changes based on land change modeler (LCM) using remote sensing: A case study of Muzaffarpur (Bihar), India. J. Geogr. Inst. Jovan Cvijic SASA, 64: 111–127.

Mohapatra, G.N., Beham, A.R., Kavashree, C., Shree, K., Singh, L.M., and Vaishnavi, J. (2018). Study of Indian summer monsoon rainfall trend during the period 1901-2013 through data mining. International journal of research in applied science and engineering technology, 6: 1701-1705.

Mondal, A., Khare, D. and Kundu, S. (2015) 'Spatial and temporal analysis of rainfall and temperature trend of India', Theor. Appl. Climatol., Vol. 122, pp.143-158.

Moss, R. H., Edmonds, J. A., Hibbard, K. A., Manning, M. R., Rose, S. K., van Vuuren,D. P., and Kram, T. (2010). The next generation of scenarios for climate changeresearch and assessment. Nature, 463(7282), 747–756.

Mousavi, R.S., Ahmedizadeh, M., and Marofi, S. (2018). A multi-GCM assessment of the climate change impact on the hydrology and hydropower potential of a semi-arid basin (A Case Study of the Dez Dam Basin, Iran). Water, 10(1458). doi:10.3390/w10101458.

Mukherjee, S., Aadhar, S., Stone, D., and Mishra, V. (2018). Increase in extreme precipitation events under anthropogenic warming in India. Weather and climate extremes, 20:45-53.

Murthy, Y.K. (1981). Water resource potentials of the Himalaya. In The Himalayas- Aspects of Change. Lall, J.S., Moddi, A.D. (eds). India International Centre: New Delhi, 152–171.

Nandakumar, N. and Mein, R. G. (1997). Uncertainty in rainfall–runoff model simulations and the implications for predicting the hydrologic effects of land-use change. Journal of Hydrology, 192: 211–232.

Ozturk, M., Copty, N. K. and Saysel, A. K. (2013). Modeling the impact of land use change on the hydrology of a rural watershed.. Journal of Hydrology, 497: 97–109.

Pandy, A.C. and Nathawat, M.S. (2006). Land Use Land Cover Mapping Through Digital Image Processing of Satellite Data – A case study from Panchkula, Ambala and Yamunanagar Districts, Haryana State, India.

Pant G. B. and Kumar K. R. (1997) 'Climates of South Asia', John Wiley & Sons Ltd., West Sussex, UK, pp.320.

Postel, S.L., Daily, G.C. and Ehrlich, P.R. (1996. Human appropriation of renewable fresh water. Science, 271: 785–788.

Ramesh, K.V., and Goswami, P.(2014). Assessing reliability of regional climate projections: The case of Indian monsoon. Sci. Rep., 4: 4071.

Rawat, J.S. and Kumar, M. (2015). Monitoring land use/cover change using remote sensing and GIS techniques: A case study of Hawalbagh block, district Almora, Uttarakhand, India. The Egyptian Journal of Remote Sensing and Space Sciences, 18: 77–84.

Rehman, N., Adnan, M., and Ali, S. (2018). Assessment of CMIP5 climate models over South Asia and climate changeprojections over Pakistan under representative concentration pathways, Int. J. Global Warming, 16(4): 381-415.

Ruan, Y., Yao, Z., Wang, R., and Liu, Z.(2018). Ranking of CMIP5 GCM Skills in Simulating Observed Precipitation over the Lower Mekong Basin, Using an Improved Score-Based Method. Water, 10,:1868.

Rupp, D.E., Abatzoglou, J., Hegewisch, K., and Mote, P.(2013). Evaluation of CMIP5 20th century climate simulations for the PacificNorthwest US, Journal of Geophysical Research Atmospheres, 118(19),10884-10906.

Sarkar, A. and Kumar, R. (2012). Artificial neural networks for event based rainfall–runoff modeling. Journal of Water Resource and Protection, 04: 891–897.

Sarma K. and Kushwaha S.P.S.(2005).Coal mining impact on land use/land cover in Jaintia hills district of Meghalaya, India using Remote Sensing and GIS technique.

Sathaye J., Shukla P. R. and Ravindranath N. H. (2006) 'Climate change, sustainable development and India: Global and national concerns', Current Science, Vol.90, No. 3, pp. 314-325.

Sharma, L.K., Pandey, P.C. and Nathawat, M.S. (2012). Assessment of land consumption rate with urban dynamic changes using Geospatial approach. J. Land Use Sci., 7 (2): 131–148.

Shiu, C.J., Liu, S.C., Fu, C., Dai, A., and Sun, Y. (2012). How much do precipitation extremes change in a warming climate? Geophysical research letters, 39(17), L17707.

Singh, P., Gupta, P. and Singh, M. (2014). Hydrological inferences from watershed analysis for water resource management using remote sensing and GIS techniques. Egypt. J. Rem. Sens. Space Sci., 17: 111–121.

Srivastava, P., McNair, J. N., and Johnson, T. E. (2006). Comparison of process-based and artificial neural network approaches for streamflow modeling in an agricultural watershed. Journal of the American Water Resources Association, 42: 545–563.

Steffen, W., Rockstrom, J., Richardson, K., Lenton, T.M., Folke, K., Liverman, D., Summerhayes, C.P., Barnosky, A.D., Cornell, S.E., Crucifix, M., Dongos, J.F., Fetzer, I., Lade, S.J., Scheffer, M., Winklemann, R. and Schellnhuber, H.J. (2018) 'Trajectories of the Earth system in the Anthropocene', Proceedings of the National Academy of Sciences of the United States of America (PNAS), Vol.115, No.33, pp. 8252-8259.

Stern, N. (2006) 'The Stern Review: Economics of Climate Change', Cambridge University Press, ISBN- 13: 9780521700801,pp.700.

Stocker, T.F.Q., Dahe, G.K., Plattner, M.M.B., Tignor, S.K., Allen, J., Boschung, A., Nauels, X., Yu, V.B. and Midgley, P.M. (2013) 'Climate change 2013, the physical science basis', Contribution of working group I to the fifth assessment report of the Intergovernmental Panel on Climate Change, Univ. press, Cambridge, U.K., pp 1533.

Stonevicius, E., Rimkus, E., Stara, A., Kazys, J., and Valiukskevicius, G. (2016). Climate change impact on the Nemunas River basin hydrology in the 21st century. Boreal Environment Research, 22: 49-65.

Subedi, P., Subedi, K., and Thapa, B. (2013). Application of a hybrid cellular automaton-Markov (CA-Markov) Model in land-use change prediction: A case study of saddle creek drainage Basin, Florida. Appl. Ecol. Environ. Sci., 1: 126–132.

Sun, Q., Miao, C., amd Duan, Q.(2015). Comparative analysis of CMIP3 and CMIP5 global climate models for simulating the daily mean, maximum, and minimum temperatures and daily precipitation over China. J. Geophys. Res. Atmos., 120: 4806–4824.

Tadese, S., Soromessa, T. and Bekele, T. (2021). Analysis of the Current and Future Prediction of Land Use/Land Cover Change Using Remote Sensing and the CA-Markov Model in Majang Forest Biosphere Reserves of Gambella, Southwestern Ethiopia. The scientific world journal, vol. 2021, Article ID 6685045, 18 pages, 2021. https://doi.org/10.1155/2021/6685045.

Tayfur, G.(2002) Artificial neural networks for sheet sediment transport. Hydrol. Sci. J., 47 (6): 879-892.

Taylor, K.E., Stouffer, R.J., and Meehl, G.A. (2012). An overview of CMIP5 and the experiment design, American Meteorological Society, 485-498.

Tollan, A. (2002). Land use change and floods: what do we need most research or management? Water Science and technology, 45: 183-190.

Toprak, Z.F., Hamidi, N., Toprak, S. and Şen, Z. (2013) 'Climatic identity assessment of the climate change', International Journal of Global Warming, Vol. 5, No. 1, p.30 DOI: 10.1504/IJGW.2013.051480.

Turner, M.G. and Ruscher, C.L. (2004). Change in landscape patterns in Georgia. USA Land. Ecol., 1 (4): 251–421.

Usman, M., Liedl,R., Shahid, M.A. and Abbas, A. (2015). Land use/land cover classification and its change detection using multi-temporal MODIS NDVI data. J. Geogr. Sci., 25(12): 1479-1506.

Uzeika, T., Merten, G. H., Minella, J. P. G., and Moro, M. (2012). Use of the SWAT model for hydrosedimentologic simulating in a small rural watershed. Revista Brasileira de Ciência do Solo, 36,:557–565.

Valent, P., Szolgay, J. and Riverso, C. (2012). Assessment of the uncertainties of a conceptual hydrologic model by using artificially generated flows. Slovak Journal of Civil Engineering, 20: 35–43.

Viviroli, D., Zappa, M., Gurtz, J. and Weingartner, R. (2009). An introduction to the hydrological modelling system PREVAH and its pre- and post-processing-tools. Environmental Modelling and Software, 24: 1209–1222.

Walling, D. E. (2008.) The changing sediment load of the Mekong River. Ambio 37: 150–157.

Watterson, I.G. and Whetton, P.H. (2011). Distributions of decadal means of temperature and precipitation change under global warming. J. Geophys. Res., 116: D07101, doi:10.1029/2010JD014502.

Wayne, G.P. (2013). The Beginner's Guide to Representative Concentration Pathways (RCPs), 1.0:1–24, Skeptical Science [online] https://www.skepticalscience.com/docs/RCP_Guide.pdf.

Yesuf, H. M., Assen, M., Alamirew, T., and Melesse, A. M. (2015). Modeling of sediment yield in Maybar gauged watershed using SWAT, northeast Ethiopia. CATENA, 127: 191–205.

Yuan, F., Sawaya, K.E., Loeffelholz, B. and Bauer, M.E. (2005). Land cover classification and change analysis of the Twin Cities (Minnesota) Metropolitan Area by multitemporal Landsat remote sensing. Rem. Sen. Envi., 98: 317–328.

Zarandi, S.M., Navazi, A., Karbassi, A.R. and Monavari, S.M. (2017) . A modelling study for predicting temperature and precipitation variations. International Journal of Global Warming, 11(4): p.373, DOI:10.1504/IJGW.2017.083666.

Zhang, X.C., and Nearing M.A. (2005). Impact of climate change on soil erosion, runoff and wheat productivity in Central Oklahama. Catena, 61(2): 185-195.